NASA/TM—1999-209768

Strain Rate Dependent Deformation and Strength Modeling of a Polymer Matrix Composite Utilizing a Micromechanics Approach

Robert K. Goldberg
Glenn Research Center, Cleveland, Ohio

December 1999

The NASA STI Program Office . . . in Profile

Since its founding, NASA has been dedicated to the advancement of aeronautics and space science. The NASA Scientific and Technical Information (STI) Program Office plays a key part in helping NASA maintain this important role.

The NASA STI Program Office is operated by Langley Research Center, the Lead Center for NASA's scientific and technical information. The NASA STI Program Office provides access to the NASA STI Database, the largest collection of aeronautical and space science STI in the world. The Program Office is also NASA's institutional mechanism for disseminating the results of its research and development activities. These results are published by NASA in the NASA STI Report Series, which includes the following report types:

- TECHNICAL PUBLICATION. Reports of completed research or a major significant phase of research that present the results of NASA programs and include extensive data or theoretical analysis. Includes compilations of significant scientific and technical data and information deemed to be of continuing reference value. NASA's counterpart of peer-reviewed formal professional papers but has less stringent limitations on manuscript length and extent of graphic presentations.

- TECHNICAL MEMORANDUM. Scientific and technical findings that are preliminary or of specialized interest, e.g., quick release reports, working papers, and bibliographies that contain minimal annotation. Does not contain extensive analysis.

- CONTRACTOR REPORT. Scientific and technical findings by NASA-sponsored contractors and grantees.

- CONFERENCE PUBLICATION. Collected papers from scientific and technical conferences, symposia, seminars, or other meetings sponsored or cosponsored by NASA.

- SPECIAL PUBLICATION. Scientific, technical, or historical information from NASA programs, projects, and missions, often concerned with subjects having substantial public interest.

- TECHNICAL TRANSLATION. English-language translations of foreign scientific and technical material pertinent to NASA's mission.

Specialized services that complement the STI Program Office's diverse offerings include creating custom thesauri, building customized data bases, organizing and publishing research results . . . even providing videos.

For more information about the NASA STI Program Office, see the following:

- Access the NASA STI Program Home Page at ***http://www.sti.nasa.gov***

- E-mail your question via the Internet to help@sti.nasa.gov

- Fax your question to the NASA Access Help Desk at (301) 621-0134

- Telephone the NASA Access Help Desk at (301) 621-0390

- Write to:
  NASA Access Help Desk
  NASA Center for AeroSpace Information
  7121 Standard Drive
  Hanover, MD 21076

NASA/TM—1999-209768

Strain Rate Dependent Deformation and Strength Modeling of a Polymer Matrix Composite Utilizing a Micromechanics Approach

Robert K. Goldberg
Glenn Research Center, Cleveland, Ohio

National Aeronautics and
Space Administration

Glenn Research Center

December 1999

Acknowledgments

Fiberite, Inc. is to be acknowledged for providing the 977–2 resin and IM7/977–2 composite discussed in this report, along with information and data on the material. Cincinnati Testing Labs, Inc. of Cincinnati, Ohio is also acknowledged for conducting the tensile experiments on the above named materials discussed in this report. Livermore Software Technology Corporation of Livermore, California is acknowledged for providing assistance in the usage of the LS-DYNA computer code, as well as providing access to the version of the code required for implementing user defined material models. Dr. James Sherwood of the University of Massachusetts at Lowell is to be thanked for providing a great deal of assistance in the area of implementing state variable based constitutive models into the LS-DYNA computer code.

Available from

NASA Center for Aerospace Information
7121 Standard Drive
Hanover, MD 21076
Price Code: A05

National Technical Information Service
5285 Port Royal Road
Springfield, VA 22100
Price Code: A05

Table of Contents

List of Tables

List of Figures

CHAPTER 1
INTRODUCTION

In this chapter the motivation for the current research project will be given. Furthermore, a detailed description of the remaining chapters of this report will be presented.

1.1 Motivation

NASA Glenn Research Center has an ongoing research program to develop new technologies to improve aircraft engine fan containment systems. The program contains a feasibility study to replace metallic containment systems with hardwall containment systems composed of polymer matrix composites. In such an application, the composite would be loaded at strain rates up to several hundred per second. In designing a composite containment system, the ability to correctly model the deformation and failure behavior of the material under high strain rate loading conditions is of critical importance.

Experimental techniques to characterize the behavior of polymer matrix composites under low strain rate loading conditions have been well established for many years. Furthermore, numerous analytical methods have been developed to model the deformation and failure behavior of composites under quasi-static loads. However, test methods and analytical procedures for characterizing and modeling these materials under high strain rate conditions are still under development.

As will be discussed further in the background section of this report, experimental results to date indicate that the deformation and failure behavior of polymer matrix composites is strain rate dependent, particularly at higher strain rates. Furthermore, there are strong indications that for carbon fiber reinforced composites, the matrix constituent primarily is responsible for the rate dependence of the material. In addition, for high strain rate impact applications, ductile polymers are more likely to be used in the composite due to their energy absorbing capabilities. As a result, the deformation response of the composite as a whole is nonlinear. Analytical methods designed to predict the deformation and failure behavior of polymer matrix composites subject to impact loads must then have the capability of properly capturing the rate sensitivity and nonlinearities which are present in the material response.

1.2 Overview of Project

The goal of this project was to develop a nonlinear, strain rate dependent deformation and strength model for the analysis of polymer matrix composites. Since the polymer matrix drives both the nonlinearity and rate dependence of the composite, constitutive equations using state variables were developed to simulate the deformation response of the matrix constituent. The constitutive equations were then implemented into a mechanics of materials based micromechanics approach to predict the nonlinear, rate dependent deformation response of the composite as a whole. A quadratic failure model was utilized to predict ply ultimate strengths. Local failure mechanisms were approximated by appropriate combinations of macroscopic ply stresses. Finally, the deformation model was implemented in a transient dynamic finite element code to model the experimental results. This step provided the ability to analyze composite structures subject to impact loads.

Chapter 2 of this report gives a relatively complete general background describing previous investigations into characterizing and modeling the rate dependent response of polymers and polymer matrix composites. Specifically, experimental efforts to determine the effects of strain rate on the properties and response of polymer matrix composites will be described. Analytical methods that have been developed to predict the nonlinear deformation of polymers, including the effects of hydrostatic pressure, will be discussed. Macromechanical and micromechanical techniques that have been used to simulate the nonlinear, rate dependent deformation response of polymer matrix composites will be presented. Methods that have been developed to predict ply ultimate strengths, varying from very simple to more complex, will also be described. The correlation between the previous research and the current study will also be presented.

In Chapter 3, the constitutive equations that were used to model the nonlinear, rate dependent deformation response of the polymer matrix are described. First, an overview of the state variable modeling method will be given. The one-dimensional form of the constitutive equations will be presented, along with procedures for determining the material constants. The extension of the equations to three dimensions will be discussed, and the numerical techniques utilized to integrate the equations will be presented. Correlation studies conducted using two representative polymeric materials, Fiberite 977-2 (a toughened epoxy) and PEEK (a thermoplastic), will be discussed.

The implementation of the polymer constitutive equations into a mechanics of materials based composite micromechanics technique will be described in Chapter 4. An overview of the method, including assumptions, will be presented. The specific equations used to compute the local and ply level stresses based on total strains and fiber and matrix constitutive properties will be derived and discussed. Furthermore, equations to compute the effective inelastic strains in the composite ply will be given. The numerical techniques utilized to implement the equations will be presented. Verification studies conducted using two representative polymer matrix composites, IM7/977-2 (IM7 carbon fibers in a 977-2 toughened epoxy matrix) and AS4/PEEK (AS4 carbon fibers in a PEEK thermoplastic matrix), will be described.

In Chapter 5 the equations used to predict ply ultimate strengths will be discussed. An overview of the chosen failure criteria will be given. The ply level failure stresses for the same representative composites as above will then be predicted for a variety of fiber orientations and strain rates and compared to experimental values.

The implementation of the rate dependent, nonlinear deformation model into the LS-DYNA transient dynamic finite element code will be discussed in Chapter 6. An overview of the finite element code and the techniques required to implement a user defined material model will be presented. The transformation of the polymer constitutive equations into an incremental format, required for LS-DYNA, will be described. The implementation of the composite micromechanics equations into LS-DYNA will also be discussed. Verification studies conducted using the same materials used in earlier chapters will be presented and discussed.

CHAPTER 2
BACKGROUND

An overview is now given of the work by researchers in the topic areas investigated in this study. Specifically, previous work in determining the effects of strain rate on the material properties of polymer matrix composites will be described. Next, methods used to model the inelastic rate-dependent deformation response of polymers will be considered, including the effects of hydrostatic stresses on the yield response. Methods used to simulate the rate-dependent deformation of polymer matrix composites will be presented, and techniques used to predict the ultimate strength of composites will be discussed. Finally, the relationship between the previous work and the current research study will be stated.

2.1 Strain Rate Effect on Material Properties

Several experimental studies have been performed with the goal of determining the effects of strain rate on the material properties and response of polymer matrix composites. One method of performing such studies involved using the split Hopkinson bar technique, which was utilized by researchers such as Harding and Welsh [1], Staab and Gilat [2] and Choe, Finch and Vinson [3]. The technique has been extensively used in characterizing metals at high strain rates [4]. The basic technique involves propelling a striker bar into a pressure bar. The pressure bar transmits a compression stress wave that propagates through the specimen, which is sandwiched between the pressure bar and a transmission bar. Gages on the pressure and transmission bars are then used to compute the force and displacement in the specimen based on the wave propagation profiles.

Harding and Welsh [1] created a modified split Hopkinson bar to allow for the tensile testing of unidirectional graphite/epoxy composites at high strain rates. Tests were conducted at strain rates ranging from $5x10^{-4}$ /sec to 450 /sec on composites with a [0°] fiber orientation. The stress-strain curves obtained were nearly linear until failure, and there was minimal change in the elastic modulus and fracture strength with strain rate. Since the response of a [0°] composite is primarily fiber dominated, these results indicated that the graphite fibers in tension have minimal strain rate dependence. Harding also conducted split Hopkinson bar tests on glass/epoxy and glass/polyester woven composites loaded by using a punch [5]. For both types of materials tested, the study found that increasing the punch speed resulted in an increase in the maximum punch load present in the specimen, as well as an increase in the shear strength of the specimen.

In compressive split Hopkinson bar tests that Choe, Finch and Vinson [3] conducted, the ultimate stress and modulus were found to increase with strain rate for unidirectional [0°] graphite/epoxy specimens, which was different from what was observed by Harding for tensile loading [1]. The ultimate stress also increased with strain rate for quasi-isotropic graphite/epoxy specimens. These results indicated that strain rate dependence may also depend on whether tensile or compressive loads are being applied.

Staab and Gilat [2] conducted tensile split Hopkinson bar tests and static tests on glass/epoxy composites at strain rates ranging from $1x10^{-4}$ /sec to approximately 1000 /sec. Laminates with fiber orientations ranging from $[\pm 15]_s$ to $[\pm 75]_s$ were examined. For each of the laminate orientations considered, increasing the strain rate increased the initial modulus, maximum stress and failure strain. The difference between the static results and the high strain rate results increased significantly as the laminate orientation angle decreased. These results differed from

what was observed for graphite/epoxy composites, where the properties of laminates with fiber dominated orientations displayed minimal strain rate dependence. These results indicated that the properties of the glass fibers varied significantly with strain rate.

Another type of test technique utilized to determine the response of polymer matrix composites at high strain rates involved subjecting the composite to explosive pressure pulse loading. Such methods were utilized by Daniel, Hsaio and Cordes [6], Daniel, Hamilton and LaBedz [7] and Al-Salehi, Al-Hassani and Hinton [8]. Daniel, et. al. [6,7] utilized an expanding ring, where a thin composite ring was subjected to an explosive pulse loading. In combination with static tests, the effects of strain rate on the longitudinal, transverse and shear properties of a unidirectional graphite/epoxy composite system were determined. The experiments were conducted at strain rates ranging from $1x10^{-4}$ /sec to 500 /sec. In the longitudinal direction, the modulus increased slightly, but the strength and failure strain showed almost no variation with increasing strain rate. In the transverse direction, on the other hand, the modulus and strength increased significantly with increasing strain rate. When the shear properties were examined, the modulus and strength again increased noticeably with increasing strain rate. The results in the longitudinal direction were similar to what was found by Harding and Welsh [1], with the properties showing little variation with strain rate for a carbon fiber reinforced composite loaded along the fiber direction. However, since the transverse and shear properties are matrix dominated, the fact that these values varied with strain rate indicated that for a graphite/epoxy composite, the behavior of the epoxy matrix does vary with strain rate, and drives the rate dependence of the composite.

Using similar explosive pressure pulse testing techniques, Al-Salehi, et. al. [8] found that for a filament wound glass-epoxy tube, the burst strength and failure strain increased with increasing strain rate, while the elastic modulus displayed minimal variation with strain rate. These results, differing from what was observed for the unidirectional graphite/epoxy composites, indicated once again that material type and fiber layup can both have significant effects on the rate dependence of a composite.

The correlation between the strain rate dependence of the composite and the rate dependence of the matrix observed in graphite/epoxy composites was further explored by Groves, et. al. [9]. Tensile and compressive stress-strain curves were generated for an epoxy matrix over a variety of strain rates. For both tensile and compressive loads, the modulus was found to increase with strain rate, with particularly significant increases occurring at strain rates above 10 /sec. Both tensile and compressive strengths were also found to increase with strain rate. The results from these tests confirmed that strain rate has a significant effect on the properties of the matrix in a graphite/epoxy system.

The overall result from these experiments is that the material properties and response of polymer matrix composites were found to vary with strain rate. The fiber material and fiber layup affected the nature of the strain rate dependence. For graphite/epoxy composites under tensile loading, the strain rate dependence appeared to be primarily driven by the strain rate dependence of the polymer matrix. These results indicated that in modeling graphite fiber reinforced polymer matrix composites, simulating the rate dependence of the polymer matrix correctly is of critical importance.

2.2 Polymer Constitutive Modeling

Polymers are known to have a rate dependent deformation response. Traditionally, for very small strain analyses, linear viscoelasticity has been used to simulate the material behavior phenomelogically [10]. In linear viscoelastic models, combinations of springs and dashpots have been used to capture the rate dependent behavior. For cases where the strains are large enough that the response is no longer linear, nonlinear viscoelastic models have been developed. For example, in a model developed by Cessna and Sternstein [11], nonlinear dashpots were incorporated into the constitutive equations. The rate dependence observed in polymer deformation has also been modeled empirically by scaling the yield stress as a function of strain rate [12].

A more sophisticated technique in polymer constitutive modeling has taken a molecular approach. In this method [13], the polymer deformation was assumed to be due to the motion of molecular chains over potential energy barriers. The molecular flow was due to applied stress, and the internal viscosity was assumed to decrease with increasing stress. The yield stress (the point where permanent deformation begins) was defined as the point where the internal viscosity decreased to the point where the applied strain rate is equal to the plastic strain rate. Internal stresses were also defined [13,14]. These stresses represented the resistance to molecular flow that tends to drive the material back towards its original configuration. Another approach to polymer deformation assumed that the deformation was due to the unwinding of molecular kinks [15]. In both approaches, constitutive equations were developed [13-17]. In these equations, the polymer deformation was considered to be a function of parameters such as the activation energy, activation volume, molecular radius, molecular angle of rotation, and thermal constants. Furthermore, the deformation was assumed to be a function of state variables that represented the resistance to molecular flow caused by a variety of mechanisms. The state variable values evolved with stress, inelastic strain and inelastic strain rate.

An alternative approach to the constitutive modeling of polymers has utilized, either directly or with some modifications, viscoplastic constitutive equations which have been developed for metals. For example, Bordonaro [18] modified the Viscoplasticity Theory Based on Overstress developed by Krempl [19]. In Bordonaro's model, the original theory was modified to attempt to account for phenomena encountered in polymer deformation that are not present in metals. For example, polymers behave differently from metals under conditions such as creep, relaxation and unloading. Other authors, such as Valisetty and Teply [20] and Zhang and Moore [21], also utilized viscoplastic constitutive equations developed to model the deformation of metals to analyze polymers. However, in these studies, only uniaxial tensile behavior was analyzed, and no attempt was made to consider phenomena such as unloading, creep or relaxation.

The conclusion to be drawn from the work discussed above is that it is possible to analyze the rate dependent response of polymers by simulating the physical deformation mechanisms. Furthermore, the physical deformation mechanisms can be modeled by the use of state variables. This approach is very similar to what has been used in viscoplastic constitutive equations in the analysis of metals. The work completed to date indicates that modeling techniques developed for metals can be adapted for use with polymers. However, appropriate modifications must be made to the equations and consideration must be given to the range of applicability of the model.

2.3 Pressure Dependence of Polymer Inelastic Deformation

The hydrostatic stress state has been found to have a significant effect on the yield behavior of solid polymers [12,13,22,23]. Increasing the hydrostatic pressure has been found to increase the yield stress [13,22,23]. The effects of hydrostatic pressure also result in differences in the tensile and compressive yield stresses of a polymer. This effect has been incorporated into the Maximum Shear Stress (Tresca) and Maximum Distortion Energy (von Mises) yield theories to develop yield criteria that have been applied to polymers [12]. In the Maximum Shear Stress criteria, the shear yield stress is a linear function of the hydrostatic stress. In the Maximum Distortion Energy criteria, the octahedral shear stress at yield is a linear function of the mean stress. Ward [13,22,23] also incorporated these concepts into modifying the Eyring based yield criteria. Specifically, the hydrostatic pressure was included as an additional term in the equations relating the octahedral shear strain at yield to the octahedral shear stress at yield.

If the effects of hydrostatic pressure on the inelastic deformation of polymers are to be incorporated into a state variable constitutive model, appropriate effective stress definitions need to be developed. The effective stress is usually defined as being related to the second invariant of the deviatoric stress tensor [24]. Bordonaro [18] determined that the usual definition did not fit the multiaxial tensile and shear data obtained in their study for Nylon and PEEK. As a result, several alternative effective stress definitions were developed. One such modification involved utilizing total stresses instead of stress deviators in the effective stress terms. Another modification consisted of adding a multiple of the mean stress to the product of stress deviators. However, neither of these modifications yielded acceptable results when compared to the experimental data. These results indicated that the definition of effective stress might need to be modified for the analysis of polymers.

2.4 Rate Dependent Composite Constitutive Modeling

A variety of methods have been applied to model the rate dependent response of polymer matrix composites. As will be described below, models have been developed at both the macromechanical (ply) level and the micromechanical (constituent) level.

2.4.1 Macromechanical Approaches

In the macromechanical approach, the composite material is modeled as an anisotropic, homogeneous material, without any attention being paid to the individual constituents. For example, Weeks and Sun [25] developed a macromechanical, rate dependent constitutive model to analyze the nonlinear rate dependent response of thick composite laminates over a variety of strain rates. Building upon previous work conducted by Yoon and Sun [26] and Gates and Sun [27], the inelastic behavior of a carbon fiber reinforced thermoplastic was simulated through the use of a quadratic plastic potential function. A scaling function was defined to model the variation of the response due to varying fiber orientation of a single ply. The finite element method was utilized to analyze a composite laminate, where a layer of elements was used to simulate a single ply. The rate dependence of the deformation response was captured by varying the material properties as a function of strain rate. Thiruppukuzhi and Sun [28] later modified this technique in order to directly incorporate the rate dependence of the material response into the constitutive model. Espinosa, Lu, Dwivedi and Azvattieri [29] utilized a similar type of

approach. However, the finite element procedures were specifically reformulated to account for the dynamic, large deformation response often seen in high strain rate impact problems.

Other approaches have been used to model the high strain rate response of polymer matrix composites on the macromechanical scale. For instance, O'Donoghue, et. al. [30] assumed a linear elastic deformation response, but reformulated the constitutive equations to separate out the hydrostatic and deviatoric stresses. The stress separation facilitated implementation of the technique into a transient dynamic finite element code. A similar approach developed by Tay, Ang and Shim [31] utilized an empirical model that scaled the "dynamic" stresses (i.e. the stresses due to dynamic loading) as a function of strain rate.

2.4.2 Micromechanical Approaches

Research has also been conducted in simulating the high strain rate deformation response of polymer matrix composites through micromechanics approaches. In micromechanics, the effective properties and response of the composite are computed based on the properties and response of the individual constituents. Several different types of methodologies have been used in micromechanics analyses. These techniques have been thoroughly reviewed and discussed in works such as [32-36]. In general, three types of methodologies have been used. All of these approaches were based on analyzing the behavior of a unit cell of the composite. The unit cell is the smallest portion of the composite for which the behavior of the unit cell is considered to be representative of the response of the composite as a whole.

The simplest types of micromechanics techniques developed have been mechanics of materials based methods, in which various uniform stress and uniform strain assumptions were utilized within the composite unit cell to compute the effective properties and response of the material. Examples of this type of approach include the traditional "rule of mixtures" equations [33], and the simplified micromechanics equations developed by Murthy and Chamis [37]. While this approach involved a great deal of approximation and simplification, the resulting equations were very simple in form, were very easy to implement within a computer code, and were very computationally efficient.

A more sophisticated method to compute the effective properties of composite materials involved using continuum mechanics techniques. In this type of approach, the equations of continuum mechanics were solved in an average sense within the unit cell. Examples of this methodology include the Concentric Cylinders Model [35], the Self Consistent Method [35], the Mori-Tanaka Method [38], and the Method of Cells [32]. Continuum mechanics methods more completely satisfied the field equations of mechanics, resulting in a more accurate representation of the physics of the problem, in comparison to mechanics of materials techniques. However, these approaches still often resulted in closed form solutions, which permitted reasonable implementation and execution of these techniques within a computer code.

The most accurate micromechanics techniques have been the numerically based methods. In this approach, the fiber and matrix were explicitly modeled using either finite elements or boundary elements. The effective response of the unit cell was then computed by conducting a finite element or boundary element analysis. Examples of this approach can be found in [39,40]. A numerical technique was also developed by Walker, et. al. [41,42], in which integral equations were developed using Fourier series and Green's function approaches. The integral equations were then solved using numerical methods. This type of analysis yielded the greatest accuracy,

but the execution times required to conduct the analysis on a computer were often quite substantial.

In simulating the high strain rate deformation response of polymer matrix composites through micromechanics approaches, finite element and continuum mechanics methods have been used. For example, Espinosa, Emore and Xu [43] utilized a finite element approach in which the fibers and matrix were explicitly modeled in the finite element mesh. A molecular, state variable based polymer constitutive equation, similar to what was described earlier in this report, was used to model the inelastic, rate dependent deformation response of the polymer. Clements, et. al. [44] applied the Method of Cells [6] to account for the stress wave propagation at the constituent level seen in an impact problem. Aidun and Addessio [45] also used the Method of Cells to simulate a high strain rate impact problem. For their analysis, they developed a nonlinear elastic constitutive model to simulate the response of the polymer matrix. In addition, they reformulated the micromechanics equations to separate out the hydrostatic and deviatoric stress components to facilitate implementation of the technique into a transient dynamic finite element code.

2.4.3 Summary

The overall conclusion from this portion of the review is that the high strain rate deformation response of composite materials has been modeled using a variety of methods. Furthermore, the nonlinear response of the composite was accounted for within the constitutive equations. In macromechanical methods, the nonlinearity and rate dependence of the deformation response were accounted for at the ply level. In micromechanical approaches, the rate dependence and nonlinearity of the polymer matrix was modeled at the constituent level. The homogenization techniques then computed the effective deformation response of the composite based on the response of the individual constituents.

2.5 Ply Level Composite Failure Models

As indicated in reviews such as those conducted by Nahas [46], many failure criteria have been developed to predict the ply ultimate strength in polymer matrix composites. No one criterion has been found to be superior for all materials and loading conditions. Several “classic” criteria have been used, as detailed in texts such as those by Gibson [34] and Herakovich [47] and in review papers such as those by Reddy and Pandey [48]. Simple models such as the Maximum Stress and Maximum Strain criteria simply compared the stresses (or strains) in each coordinate direction to the ultimate values. The drawback to these models was that stress interaction was not accounted for to any significant extent. In the Tsai-Hill criteria, on the other hand, a quadratic combination of stresses and strengths in each coordinate direction was compared to a failure value. In this model, stress interaction was accounted for, but differences in tensile and compressive strengths were not considered. The Tsai-Wu equation utilized a tensor based failure criterion, which allowed for differences between tensile and compressive failure strengths. In general, the more sophisticated methods such as Tsai-Hill or Tsai-Wu provided improved failure predictions than simple models such as Maximum Stress or Maximum Strain. However, studies such as that conducted by Sun and Quinn [49] showed that this is not always the case.

In the models discussed above, composite failure was considered on purely a macromechanical scale, with no attention being paid to the specific mechanisms which cause failure. In reality, failure in a composite is a result of specific local mechanisms such as tensile fiber failure, matrix cracking or delamination [33]. While accurate modeling of these local failure mechanisms would require a detailed micromechanical analysis, several researchers have developed phenomenological failure criteria that predict local failure mechanisms based on ply level stresses.

Hashin [50] developed a failure model that predicts fiber failure or matrix failure (tensile or compressive) based on appropriate quadratic combinations of stresses and failure strengths. Chang and co-workers [51-53] developed similar quadratic failure criteria, but also accounted for nonlinearities in the stress-strain curve by using integrals of strain energy in the shear terms instead of shear stresses and shear strengths. While the Chang criteria assumed a plane stress condition, Yen [54] extended the Chang criteria to account for a three-dimensional stress state. Yen then utilized the modified criteria to predict composite damage and failure for a transient dynamic impact application. Banerjee [55] also successfully utilized the Hashin and Chang failure criteria to predict damage and failure for a polymer matrix composite subject to impact loads. Rotem [56] developed a quadratic failure criteria based on local failure mechanisms, but in the matrix failure equations the matrix failure strength and matrix stress were included along with the ply level stress and strength values. Tabiei et al. [57] utilized the Hashin criterion to predict the failure of a polymer matrix composite with a nonlinear deformation response. However, the nonlinear behavior was accounted for in the composite constitutive law instead of in the failure criteria. Langlie and Cheng [58] developed failure criteria based on local failure mechanisms to be used for composites subject to high strain rate impact. Their criteria used a maximum stress type of approach instead of a quadratic equation including stress interaction to predict the local failure modes. Pecknold and Rahman [59] applied a micromechanics model to predict the deformation response of the composite. The constituent level stresses computed using the micromechanics were then compared to the constituent strengths in order to predict failure. The research studies discussed here indicate that a failure criterion based on approximating local failure mechanisms might produce good predictions. A mechanism based failure criterion would also facilitate the development of a material degradation model when applied to the analysis of structures composed of composite materials.

2.6 Relationship of Literature Review to Current Project

The overall goal of the research study presented in this report was to conduct a preliminary investigation into some of the issues involved in modeling high strain rate impact of polymer matrix composites. Therefore, the goal was not to develop a refined, sophisticated set of analytical methods that could completely simulate an impact event. Instead, the goal was to investigate some of the relevant issues involved in the problem, and to see how the different pieces of the analysis would fit together to completely solve the problem. As a result, in this work, simplified methods, or modifications to previously existing methods, were used to conduct the analyses presented here. Once these preliminary investigations have been completed and the relevant issues identified, each of the aspects of the analytical model could then be refined and adjusted, eventually leading to the development of a complete deformation and failure model for simulating the impact of polymer matrix composites.

The first step in this process was the development of constitutive equations to model the rate-dependent, inelastic deformation response of ductile polymers, as the rate dependence of polymer matrix composites has been found to be driven by the matrix. As mentioned in Section 2.2, state variable methods have been successfully applied to the rate-dependant analysis of polymers. For this work, the Ramaswamy-Stouffer state variable constitutive equations, which have been used to model the viscoplastic response of metals, was modified to analyze the inelastic response of the polymers considered here.

Section 2.3 described a variety of methods that have been used to simulate the deformation response of polymer matrix composites. For this work, since the deformation response of the polymer matrix was to be explicitly modeled, micromechanics techniques were used to predict the effective composite response. As discussed earlier, a variety of techniques, from fairly simple to quite complex, have been developed to conduct micromechanical analyses. For this study, since the deformation model was implemented within a finite element code, the desire for this preliminary investigation was to keep the analysis method fairly simple while still capturing most of the physics of the problem. Utilization of a fairly simple micromechanics approach facilitated the finite element implementation. As will be discussed in Chapter 4, a previously developed mechanics of materials approach was modified to carry out the micromechanics calculations. As discussed in Chapter 6, the micromechanics equations, with the polymer constitutive equations embedded within them, were implemented into a commercially available, transient dynamic finite element code and the tensile response of representative composites was simulated.

In predicting the failure of polymer matrix composites subject to impact loads, an important first step is the prediction of the failure of the individual plies. However, in order to incorporate property degradation models into the finite element analysis, the particular mode of failure (fiber or matrix failure) must be identified. As will be discussed in Chapter 5, for this preliminary study the goal was to predict ply failure based on local failure mechanisms using ply level stresses and strengths. The Hashin failure criteria discussed in Section 2.5 appeared to meet the desired criteria and was used in this study.

CHAPTER 3
POLYMER CONSTITUTIVE EQUATIONS

In this chapter, a set of constitutive equations based on the state variable method are presented which allow for the analysis of the nonlinear, rate-dependent deformation response of ductile polymers. An overview of the state variable modeling method is discussed first. Next, the one-dimensional simplification of the constitutive equations is presented, along with the procedures for determining the material constants. The equations are then extended to three dimensions. The algorithm used to numerically implement the constitutive model is discussed, and the equations are characterized and correlated for two representative polymers: Fiberite 977-2 and PEEK.

3.1 State Variable Modeling Overview

As discussed previously, the rate dependence of a polymer matrix is primarily a function of the rate dependence of the matrix constituent. Furthermore, the stress-strain response of polymers is nonlinear above one or two percent strain [10]. Consequently, a need exists for constitutive equations that capture the nonlinear, rate dependent deformation response of the matrix material.

Constitutive equations for polymers that incorporate the deformation mechanisms of the material have been developed. For polymers, deformation is due to the motion of the molecular chains [13]. At small deformation levels, prior to yield, there is also a resistance to the molecular flow. In constitutive equations, a state variable approach has been utilized to model the mechanisms that cause material deformation [24]. In this methodology, the specific changes in the local details of the material microstructure were not considered. Alternatively, variables were defined which were meant to represent the average effects of the deformation mechanisms that were present. These variables evolved as a function of external parameters such as the stress, inelastic strain, and the current value of the state variable. Furthermore, the inelastic strain rate was defined to be a function of the state variables and external variables such as the current stress level.

The state variable approach to constitutive modeling has been fairly extensively utilized to model the inelastic deformation response of metals, which exhibit a viscoplastic response above about one-half of the melting temperature. An important characteristic of this method was that there was no defined yield stress or onset of inelasticity [24]. Alternatively, inelastic strain was assumed to be present at all values of stress. The inelastic strain was just assumed to be very small compared to the elastic strain at low stress levels. When the inelastic strain evolved to a more significant value, the stress-strain curve began to exhibit a nonlinear response. Furthermore, a single, unified variable was utilized to represent all inelastic strains. The effects of viscoelasticity, plasticity and creep were not separated in this type of approach, but were combined into one unified strain variable.

There is some physical motivation to utilize state variable models that were developed for metals to simulate the nonlinear deformation response of polymers. For polymers, while the nonlinear deformation response is due to the nonlinear response of long chain molecules as opposed to the propagation of dislocations for metals, a unified inelastic strain variable can still be utilized to simulate the nonlinear behavior. In addition, the “saturation stress” in metals and

the "yield stress" in polymers (the point where the stress-strain curve becomes flat) have both been defined as the stress level at which the inelastic strain rate equals the applied strain rate in constant strain rate tensile tests [13, 24].

In metals, the inelastic strain rate has often been modeled as being proportional to the difference between the deviatoric stress and "back stress" tensors. The back stress was defined as a resistance to slip resulting from the interaction of dislocations under a shear stress with a barrier. As dislocations pile up at a barrier, atomic forces will cause additional dislocations approaching the barrier to be repelled. This repelling force was referred to as the back stress. The back stress is in the direction opposite to the local shear stress in uniaxial loading (and thus will be orientation dependent in three-dimensional loading). The net stress producing slip or inelastic strain is related to the difference between the shear stress and the back stress [24]. An isotropic initial resistance to slip is also present in metals due to the presence of obstacles such as precipitates, grains and point defects. This initial resistance to slip has often been referred to as a "drag stress". Similar concepts have been used in the deformation modeling of polymers. Ward [13] discussed how creep strain and plastic strain could be defined as being proportional to the difference between the applied stress and an "internal stress". The internal stress was defined as evolving with increasing strain.

It is important to note several significant limitations in using equations developed for metals to simulate the nonlinear deformation response of polymers. Polymers exhibit nonlinear strain recovery on unloading, while metals display linear elastic strain recovery. The unloading behavior of polymers may not be represented accurately with a constitutive equation that was developed for metals. Furthermore, phenomena such as creep, relaxation and high cycle fatigue may not be simulated correctly in polymers with a metals based constitutive model. However, for predicting failure in high velocity impact loading, the ultimate future goal of this research, none of these phenomena were considered to be extremely significant. Furthermore, in the analyses described in this report, only uniaxial tensile loading was considered.

The constitutive equations utilized here will most likely only be valid for relatively ductile polymers with at least some level of crystallinity, such as thermoplastics or toughened epoxies (with thermoplastic tougheners), where the correlation between the polymer deformation response and the deformation response of metals is strongest. However, it is not clear at this time exactly how the level of crystallinity in the polymer will affect the applicability of the equations. To fully simulate the complete range of polymer deformation response, a combined viscoelastic-viscoplastic model would most likely be required. A combined viscoelastic-viscoplastic model would have the ability to completely represent all of the mechanisms present in polymer deformation. Efforts have been made by several researchers to develop such a model [16,17,60]. However, such a combined model, which could be very complex, was not considered for this study.

3.2 One-Dimensional Constitutive Equation

A state variable based constitutive model was utilized to simulate the rate dependent, nonlinear deformation behavior of the polymer matrix. For the purposes of determining material constants and model correlation, one-dimensional uniaxial versions of the equations were considered first. An important point to note is that the flow equation, in its three-dimensional form, was based on deviatoric stresses and stress invariants, which are the primary drivers for the inelastic deformation of both polymers and metals [12,24]. Only the equations for the inelastic

strain rate are presented. The total strain rate is the sum of the elastic and inelastic strain rates. The total strain rate for uniaxial loading was defined as follows:

$$\dot{\varepsilon} = \frac{\dot{\sigma}}{E} + \dot{\varepsilon}^I \tag{3.1}$$

where $\dot{\varepsilon}$ was the total strain rate, $\dot{\sigma}$ was the stress rate, $\dot{\varepsilon}^I$ was the inelastic strain rate, and E was the elastic modulus of the material.

Several key assumptions were made in the constitutive model. First, even though in high strain rate impact situations adiabatic heating may be a significant issue, for this study temperature effects have been neglected, and all of the results were obtained for room temperature. Second, small strain conditions have been assumed. In reality polymers, particularly in compression, can be subject to very large strains. Furthermore, structures undergoing high strain rate impact are subject to large deformations and rotations. However, incorporating large deformation and rotation effects into the constitutive equations would add a level of complexity that is beyond the scope of this study. For the purposes of this modeling effort, therefore, all large deformation effects have been neglected. Future efforts will include modifying the constitutive equations to account for large deformation effects.

For this study, constitutive equations developed by Ramaswamy and Stouffer [24] were used to compute the inelastic strain rate in the polymer. These equations were originally developed to compute the high temperature, inelastic deformation of metals. However, variations of these equations and the similar set of equations developed by Bodner [61] have been used to model the inelastic response of polymers [21,62]. A tensorial state variable was used to represent an "internal stress" which represented the resistance to inelastic deformation. As discussed earlier, in metals this "internal stress" was defined as the "back stress". In the analysis of polymers, the "internal stress" represented the resistance to molecular flow. The tensorial state variable is orientation dependent. The state variable was assumed to be equal to zero when the material is in its virgin state, and evolved towards a maximum value at saturation. As a reminder, the "saturation stress" in metals and the "yield stress" in polymers have similar definitions. In this report, when the terms "saturation" or "saturation stress" are used in relation to polymers, the "yield stress" is the physical mechanism that is being referred to. However, in order to maintain consistent terminology with the original development of the equations, the term "saturation" will be used.

The inelastic strain rate was defined as being proportional to the exponential of the overstress, the difference between the applied stress and the internal stress. This type of relationship was similar in form to the molecular based constitutive equations for polymers discussed by Ward [13]. In these equations, the inelastic strain rate (equal to the total strain rate at yield) was defined as being proportional to the exponential of the yield stress.

In the uniaxial simplification of the Ramaswamy-Stouffer constitutive model, the inelastic strain rate was defined by the following equation:

$$\dot{\varepsilon}^I = \frac{2}{\sqrt{3}} D_0 \exp\left[-\frac{1}{2}\left(\frac{Z_0}{|\sigma - \Omega|} \right)^{2n} \right] * \frac{\sigma - \Omega}{|\sigma - \Omega|} \tag{3.2}$$

where $\dot{\varepsilon}^I$ was the inelastic strain rate, σ was the stress, and Ω was the state variable ("internal stress") which represented the resistance to molecular flow. Material constants included D_o, a scale factor which represented the maximum inelastic strain rate; n, a variable which controlled the rate dependence of the deformation response; and Z_0, which represented the isotropic, initial "hardness" of the material before any load was applied. The value of the state variable Ω was assumed to be zero when the material was in its virgin state. While not apparent from the uniaxial form of the flow equation, Ω was a tensorial, not a scalar, variable.

The evolution of the state variable Ω was described by the following expression,

$$\dot{\Omega} = q\Omega_m \dot{\varepsilon}^I - q\Omega\left|\dot{\varepsilon}^I\right| \tag{3.3}$$

where $\dot{\Omega}$ was the state variable rate, $\dot{\varepsilon}^I$ was the inelastic strain rate, and Ω was the current value of the state variable. Material constants included q, which was the "hardening" rate, and Ω_m, which was the maximum value of the "internal stress" at saturation. This equation is slightly different from the evolution law developed by Ramaswamy and Stouffer [24]. The original equation included an additional stress rate term that was not used here. The stress rate term was included in order to provide for additional hardening at low stress levels. This additional hardening was found not to be required for the materials analyzed in this study. For tensile loading, where the absolute value of the inelastic strain rate equaled the inelastic strain rate, Equation (3.3) was integrated to obtain the following form:

$$\Omega = \Omega_m - \Omega_m \exp(-q\varepsilon^I) \tag{3.4}$$

where ε^I was the inelastic strain and all other parameters were as defined for Equation (3.3).

3.3 Material Constant Determination

A summary of the procedure for determining the material constants for the Ramaswamy-Stouffer model will be described here. Detailed discussions of the methods for finding the constants can be found in [24,61,63]. D_0 was assumed to be equal to a value 10^4 times the maximum applied total strain rate, and was considered to be the limiting value of the inelastic strain rate. Future investigations may be conducted to investigate whether a relationship between D_o and the shear wave speed can be determined.

To determine the values of n, Z_0 and Ω_m, the following procedure was utilized. First, the natural logarithm of both sides of Equation (3.2) was taken. The values of the inelastic strain rate, stress, and state variable Ω at "saturation" were substituted into the resulting expression. The following equation was obtained:

$$\ln\left[-2\ln\left(\frac{\sqrt{3}\dot{\varepsilon}_0}{2D_0}\right)\right] = 2n\ln(Z_0) - 2n\ln(\sigma_s - \Omega_m) \tag{3.5}$$

where σ_s equaled the "saturation" stress, $\dot{\varepsilon}_o$ was the constant applied total strain rate, and the remaining terms were as defined in Equations (3.2) and (3.3).

The required constants were determined from a set of tensile curves obtained from constant strain rate tests. Each curve in this set was obtained at a different constant strain rate. Data pairs of the total strain rate and saturation stress values from each curve were taken. Values for Ω_m were estimated for the material, with initial estimates ranging from 50% to 75% of the highest saturation stress found to work well. These estimates were similar to the values used for large-grain metals. For each strain rate, the data values were substituted into Equation (3.5), and represented a point on a master curve. The number of points in the master curve equaled the number of strain rates at which tensile tests were conducted. A least squares regression analysis was then performed on the master curve. As suggested by Equation (3.5), the slope of the best fit line was equal to -2*n. The intercept of the best fit line was equal to $2*n*\ln(Z_o)$. The value for Ω_m was then adjusted until an optimal fit to the data was obtained.

To determine the value for q, Equation (3.4) was utilized. At saturation, the value of the internal stress was assumed to approach the maximum value, resulting in the exponential term approaching zero. Assuming that saturation occurred when the following condition was satisfied:

$$\exp(-q\varepsilon_s^I) = 0.01 \tag{3.6}$$

the equation was solved for q, where ε_s^I was the inelastic strain at saturation. The inelastic strain at saturation was estimated by determining the total strain at saturation from a constant strain rate tensile curve, and subtracting the elastic strain. The elastic strain was computed by dividing the saturation stress by the elastic modulus, as suggested by Equation (3.1). The computed inelastic strain was substituted into Equation (3.6), which was solved for q. If the inelastic strain at saturation was found to vary with strain rate, the parameter q was computed at each strain rate and regression techniques utilized to determine an expression for the variation of q.

An important point to note is that the meaning and ranges of the material constants when these equations were used to model polymer deformation were not the same as when they were applied to metals. For example, when analyzing metals using the Ramaswamy-Stouffer model, a value of n greater than or equal to 3.0 indicated that the deformation response was relatively rate insensitive [24]. However, when the equations were applied to polymers, this rule of thumb did not necessarily apply due to the differences in deformation mechanisms and strain rate sensitivity between the two types of materials. Similarly, other rules of thumb utilized in estimating and interpreting the material constants for metals most likely would not apply to polymers.

3.4 Three-Dimensional Extension of Constitutive Equations

This section describes the extension of the one-dimensional constitutive equations (Equations (3.2)-(3.4)) to three dimensions. To account for the effect of hydrostatic stresses on the response, the effective stress term in the flow equation was appropriately modified. A discussion of the nature of the tensorial state variable is presented, and the procedure for determining the material constants for the three-dimensional version of the equations is discussed.

3.4.1 Original Flow Equation

The three-dimensional extension of the Ramaswamy-Stouffer flow equation given in Equation (3.2) was as follows [24]:

$$\dot{\varepsilon}_{ij}^{I} = D_o \exp\left[-\frac{1}{2}\left(\frac{Z_o^2}{3K_2}\right)^n\right] * \frac{S_{ij} - \Omega_{ij}}{\sqrt{K_2}} \tag{3.7}$$

where S_{ij} was the deviatoric stress component, Ω_{ij} was the component of the state variable, $\dot{\varepsilon}_{ij}^{I}$ was the component of inelastic strain, n and Z_o were as defined in Equation (3.2), and K_2 was defined as follows:

$$K_2 = \frac{1}{2}\left(S_{ij} - \Omega_{ij}\right)\left(S_{ij} - \Omega_{ij}\right) \tag{3.8}$$

where repeated indices indicated summation using the standard indicial notation definitions [24].

3.4.2 Modified Flow Equation with Shear Correction Factor

When the flow law described in Equations (3.7) and (3.8) was implemented into the composite micromechanics method described later in this report, the nonlinear deformation response and component stresses for laminates with shear dominated fiber orientation angles were predicted incorrectly. These results indicated that the nonlinear shear stresses in the matrix constituent were not being computed properly. For this work, the cause of the discrepancy was assumed to be due to the effects of the hydrostatic stresses on the inelastic response. As described earlier in this report, hydrostatic stresses have been found to affect the yield behavior of polymers. Furthermore, earlier work has indicated that the effective stress terms may need to be modified for the multiaxial analysis of polymers [18].

The effect of the hydrostatic stresses on the inelastic response of the polymer was accounted for by modifying the effective stress term K_2 in the flow law (Equations (3.7) and (3.8)). Specifically, since the shear response of the polymer required modification, the shear terms in the effective stress were adjusted to account for the effects of hydrostatic stresses. Equation (3.8) was rewritten as follows:

$$K_2 = \frac{1}{2}\left[K_{11} + K_{22} + K_{33} + 2\left(K_{12} + K_{13} + K_{23}\right)\right] \tag{3.9}$$

The normal terms (11,22,33) in this expression maintained their original definition as suggested by Equation (3.8) as follows:

$$K_{11} = \left(S_{11} - \Omega_{11}\right)\left(S_{11} - \Omega_{11}\right) \tag{3.10}$$

$$K_{22} = \left(S_{22} - \Omega_{22}\right)\left(S_{22} - \Omega_{22}\right) \tag{3.11}$$

$$K_{33} = (S_{33} - \Omega_{33})(S_{33} - \Omega_{33}) \tag{3.12}$$

However, the shear terms in the effective stress definition were modified as follows:

$$K_{12} = \alpha(S_{12} - \Omega_{12})(S_{12} - \Omega_{12}) \tag{3.13}$$

$$K_{13} = \alpha(S_{13} - \Omega_{13})(S_{13} - \Omega_{13}) \tag{3.14}$$

$$K_{23} = \alpha(S_{23} - \Omega_{23})(S_{23} - \Omega_{23}) \tag{3.15}$$

where:

$$\alpha = \left(\frac{\sigma_m}{\sqrt{J_2}} \right)^{\beta} \tag{3.16}$$

$$\sigma_m = \frac{1}{3}(\sigma_{11} + \sigma_{22} + \sigma_{33}) \tag{3.17}$$

$$J_2 = \frac{1}{2} S_{ij} S_{ij} \tag{3.18}$$

The primary modification to these equations was the multiplication of the shear terms in the effective stress by the parameter α. In Equation (3.16), σ_m was the mean stress, J_2 was the second invariant of the deviatoric stress tensor, and β was a rate independent material constant. While this formulation was somewhat phenomenological in nature, it was based on actual observed physical mechanisms. When the parameter β is set equal to zero (0), the value of α in Equation (3.16) is equal to one (1), and Equation (3.9) is equivalent to Equation (3.8). Therefore, the modification to the constitutive equations was implemented through the use of the correlation coefficient α.

Since only uniaxial tensile data were available for the polymers considered in this study, the value of the parameter β was determined empirically by fitting composite data with shear dominated fiber orientation angles, such as [10°] or [15°]. Analyses of [45°] laminates, in which the magnitudes of the normal and shear stresses were relatively close, were then conducted in order to verify that the determined constant value was reasonable. Ideally, the polymer model would be characterized by using a combination of tension, torsion, and tension-torsion tests done on the bulk polymer. Since composite data were utilized to characterize the model, simplified, consistent techniques to characterize the polymer using bulk polymer data have not yet been determined. Future work will involve obtaining multiaxial test data, and determining structured, consistent means of determining the effects of hydrostatic stresses on the polymer deformation.

3.4.3 Three-Dimensional Extension of Internal Stress Evolution Law

The internal stress rate, $\dot{\Omega}_{ij}$, was defined by the following relation:

$$\dot{\Omega}_{ij} = \frac{2}{3} q \Omega_m \dot{\varepsilon}^I_{ij} - q \Omega_{ij} \dot{\varepsilon}^I_e \tag{3.19}$$

where $\dot{\varepsilon}^I_e$ was the effective inelastic strain rate, defined as follows:

$$\dot{\varepsilon}^I_e = \sqrt{\frac{2}{3} \dot{\varepsilon}^I_{ij} \dot{\varepsilon}^I_{ij}} \tag{3.20}$$

and repeated indices again indicated summation using the standard indicial notation definitions [24]. The remainder of the terms were as defined in Equations (3.2) and (3.3).

3.4.4 Tensorial Definition of Internal Stress State Variable

A key difference between the three dimensional Ramaswamy-Stouffer equations, and other equations that use tensorial state variables, such as the Walker model [64], lies in the definition of the tensorial state variable. In the Ramaswamy-Stouffer model, the back stress (or internal stress for polymers) was defined in the same manner as the stress deviator. Under uniaxial loading, the tensorial state variable tensor had the following format:

$$[\Omega_{ij}] = \begin{bmatrix} \frac{2}{3}\Omega & 0 & 0 \\ 0 & -\frac{1}{3}\Omega & 0 \\ 0 & 0 & -\frac{1}{3}\Omega \end{bmatrix} \tag{3.21}$$

where Ω represented the uniaxial value of the state variable. In the Walker model, the state variable tensor under uniaxial loading was defined as follows. This definition was similar to the definition of the plastic strain tensor in standard plasticity theory [24]:

$$[\Omega_{ij}] = \begin{bmatrix} \Omega & 0 & 0 \\ 0 & -\frac{1}{2}\Omega & 0 \\ 0 & 0 & -\frac{1}{2}\Omega \end{bmatrix} \tag{3.22}$$

While both tensors were deviatoric tensors, the varying definition of the state variable resulted in two definitions of the K_2 term. Using the definition of Ω_{ij} specified in Equation (3.22), K_2 would be defined as follows:

$$K_2 = \frac{2}{3}\left(\frac{3}{2}S_{ij} - \Omega_{ij}\right)\left(\frac{3}{2}S_{ij} - \Omega_{ij}\right) \tag{3.23}$$

which was what was used in the Walker equation. Note that these expressions were based on the original definitions of the effective stress K_2, without the shear correction factor discussed above.

3.4.5 Material Constants for Three-Dimensional Extension of Constitutive Equations

As discussed by Stouffer and Dame [24], the values of the material constants for the three-dimensional formulation of the equations were identical to those obtained using the uniaxial representation of the equations. However, since the shear correction factor was not utilized for uniaxial tensile loads, the value of the material constant β associated with this term would have to be determined through multiaxial tests of the polymer. Alternatively, as discussed above β could be determined empirically through examination of tensile curves obtained from off-axis loading of composite laminates containing the polymer under consideration.

3.5 Numerical Implementation of Constitutive Equations

To test and correlate the constitutive equations, a stand-alone computer code was developed. To integrate the flow and evolution laws, the standard fourth order Runge-Kutta explicit integration routine was used [65]. For this class of equations, implicit integration routines have often been used because of their inherent numerical stability [24]. However, in this case, the equations were ultimately implemented into a transient dynamic finite element code, which used explicit integration schemes. Therefore, in developing the stand-alone computer code, an explicit integration scheme was used in order to facilitate the eventual finite element implementation. The Runge-Kutta method was employed for this study due to its simplicity and ease of implementation. Future efforts might include investigating more robust numerical techniques such as semi-implicit algorithms, which provide the stability of implicit methods while still maintaining the appearance of an explicit technique.

To compute the value of a set of variables y_n at time step $t+\Delta t$, where t is the current time and Δt is the time increment, the following equation was used:

$$y_n(t+\Delta t) = y_n(t) + \frac{1}{6}\left(k_1 + 2k_2 + 2k_3 + k_4\right) \tag{3.24}$$

$$k_1 = \Delta t * y_n'\left(t, y_n\right) \tag{3.25}$$

$$k_2 = \Delta t * y_n'\left(t + \frac{1}{2}\Delta t, y_n + \frac{1}{2}k_1\right) \tag{3.26}$$

$$k_3 = \Delta t * y_n'\left(t + \frac{1}{2}\Delta t, y_n + \frac{1}{2}k_2\right) \tag{3.27}$$

$$k_4 = \Delta t * y_n'\left(t + \frac{1}{2}\Delta t, y_n + \frac{1}{2}k_3\right) \tag{3.28}$$

where y_n' was the time derivative of variable y_n.

For the stand-alone code developed to correlate and test the constitutive equations, strain controlled loading was assumed. This condition was applied for two reasons. First, in a finite element application, strains and/or strain increments were passed from the main code into a user developed material subroutine. The routine then computed the stresses based on the supplied strains. Since the equations utilized here were implemented within a transient dynamic finite element code, similar conditions were assumed here to assure compatibility. Second, the tensile tests that were used to correlate the model were conducted at constant strain rate. Utilizing strain controlled loading in the stand-alone computer code simplified the simulation of these tests.

To determine the value of the total strain, inelastic strain, and internal stress at time $t+\Delta t$, the following algorithm was utilized for each step of the Runge-Kutta integration. The strains at time t (or strain estimate at time $t+0.5\Delta t$) were passed into the integration routine. The stresses were computed using the elastic constants and the current value of the inelastic strains. The effective stress K_2 was then computed using Equations (3.9)-(3.18). The inelastic strain rate was computed using Equation (3.7), and the internal stress rate was computed using Equations (3.19) and (3.20). The elastic Poisson's ratio and the inelastic strain rates were then used to compute the total strain rates. The total strain, inelastic strain and internal stress were computed by integrating the corresponding rate equations using Equations (3.24)-(3.28).

3.6 Model Correlation Analyses

In this section, the correlation and characterization of the constitutive equations for two materials, Fiberite 977-2 and PEEK, is described.

3.6.1 Fiberite 977-2 Toughened Epoxy

Consider first Fiberite 977-2, a toughened epoxy. Since toughening the polymer makes it more ductile and damage resistant [66] than traditional epoxy resins, a material of this type would be more likely to be used in applications where impact resistance is required.

Tensile tests at low strain rates, ranging from $1x10^{-4}$ /sec to 0.1 /sec, were conducted on the Fiberite 977-2 material by Cincinnati Testing Labs, Inc. [67]. Although the ultimate application of this research is the study of high strain rate impact problems, good high strain rate tensile data were not obtainable at this time. However, the polymer under consideration was rate dependent even at relatively low strain rates. Therefore, the ability of the constitutive equations to capture rate dependent, inelastic deformation was capable of being examined even by using low strain rate data. Furthermore, even though these initial correlation studies were conducted at low strain rates, there is no reason, once appropriate data are obtained, that the methodology cannot be extended to high strain rate applications.

Axial tensile tests at constant strain rate were conducted to obtain the test data. Engineering stress and engineering strain were measured due to the small strain assumptions that were made. Stress-strain curves obtained at constant strain rates of $1x10^{-4}$ /sec, 0.01 /sec and 0.1 /sec are shown in Figure 3.1. As can be seen in the figure, the tensile response was rate dependent. An important point to note is that the unusual results observed at low strains for the results obtained at strain rates of 0.01 /sec and 0.1 /sec were most likely due to difficulties that were encountered in ramping up to the desired strain rate during the experimental tests.

To obtain the tensile material constants, the stress-strain curves had to be extrapolated since the tensile specimens failed before "saturation" occurred. To obtain an estimate of the saturation stress and strain, the curves for the strain rates of $1x10^{-4}$ /sec and 0.1 /sec were extrapolated using a quadratic curve fit. Since the specimens failed in tension before the saturation level was reached, it was assumed that matching the actual saturation stress would not be critical. By extrapolating, estimates of the saturation stress and strain were obtained and are shown in Table 3.1. The elastic and inelastic material constants for this material are shown in Table 3.2. Note that the constant β, related to the shear correction factor, was not obtained using the uniaxial tensile data, but is included here for completeness. The procedures used to determine the value of this constant will be discussed in a later section of this report.

Tensile stress-strain curves were computed for constant strain rates of $1x10^{-4}$ /sec, 0.01 /sec, and 0.1 /sec using Equations (3.7)-(3.20). The computed results, along with the experimental data, are shown in Figures 3.2-3.4. As can be seen in the figures, the computed results correlated reasonably well with the experimental values. In particular, the nonlinearity of the stress-strain curves was captured for all three strain rates. Any discrepancies between the experimental and computed results were most likely due to the approximations that were made in estimating the saturation stress and strain. The constants used in the constitutive equations were strongly dependent on these parameters. Therefore, any inaccuracies in these values could significantly affect the computed results. Furthermore, for the experiments conducted at strain rates of 0.01 /sec and 0.1 /sec, as mentioned earlier difficulties were encountered during the tests in ramping up to the desired strain rate. These difficulties could be the cause of the discrepancies between the experimental and computed results observed at the lower strain levels.

3.6.2 PEEK Thermoplastic

To further examine the capabilities of the constitutive equations, a PEEK (polyetheretherketone) thermoplastic was characterized and modeled. Tensile stress strain curves were obtained by Bordonaro and Krempl [68] at constant strain rates ranging from $1x10^{-6}$ /sec to $1x10^{-3}$ /sec. The experimental results are shown in Figure 3.5. As can be seen in the figure, the tensile curves for this material exhibited a distinct "saturation", or flattening out, unlike the tensile curves for the Fiberite 977-2 epoxy. This result was expected since a thermoplastic like PEEK is more ductile than the toughened epoxy Fiberite 977-2. Due to the fact that the tensile curves flatten out, the inelastic material constants were determined directly, with no approximation (beyond those standard to the constitutive equations) required. The inelastic material constants for this polymer were determined using the procedures described earlier, and are shown in Table 3.2 along with the elastic modulus and Poisson's ratio.

Tensile stress-strain curves were computed under strain controlled loading at constant strain rates of $1x10^{-6}$ /sec, $1x10^{-4}$ /sec and $1x10^{-3}$ /sec. The computed curves and the corresponding experimental results are shown in Figures 3.6-3.8. As can be seen from the figures, the computed values correlated with the experimental results extremely well. Furthermore, the constitutive equations appeared to capture the tensile response of this polymer more accurately than was seen for the Fiberite 977-2. The quality of the simulations for the PEEK was most likely due to the fact that the measured stress-strain curves for this material displayed a distinct saturation, allowing for a more accurate determination of the material constants. These results indicated that if the polymer under consideration was appropriately characterized, the constitutive equations described here could do a good job in computing the polymer deformation response.

3.7 Summary

Rate dependent, inelastic constitutive equations based on the state variable method have been used to model the deformation response of ductile polymers under small strain conditions. Two representative polymers were characterized, and their uniaxial tensile deformation response was computed using the constitutive equations. The computed results correlated reasonably well to the experimental values for both polymers, indicating that the equations adequately captured the material response. The constitutive model can thus be used in micromechanics equations to predict the rate dependent, nonlinear deformation response of polymer matrix composites.

Table 3.1
Extrapolated Saturation Stress and Saturation Strain Values for Fiberite 977-2

Strain Rate (/sec)	Saturation Stress (MPa)	Saturation Strain
$1x10^{-4}$	97	0.055
0.1	110	0.053

Table 3.2
Material Properties for Fiberite 977-2 and PEEK

	E (GPa)	ν	D_o (1/sec)	N	Z_o (MPa)	q	Ω_m (MPa)	β
977-2	3.65	0.40	1E+04	0.50	1030	100	69	1.2
PEEK	4.00	0.40	1E+04	0.70	630	310	52	0.45

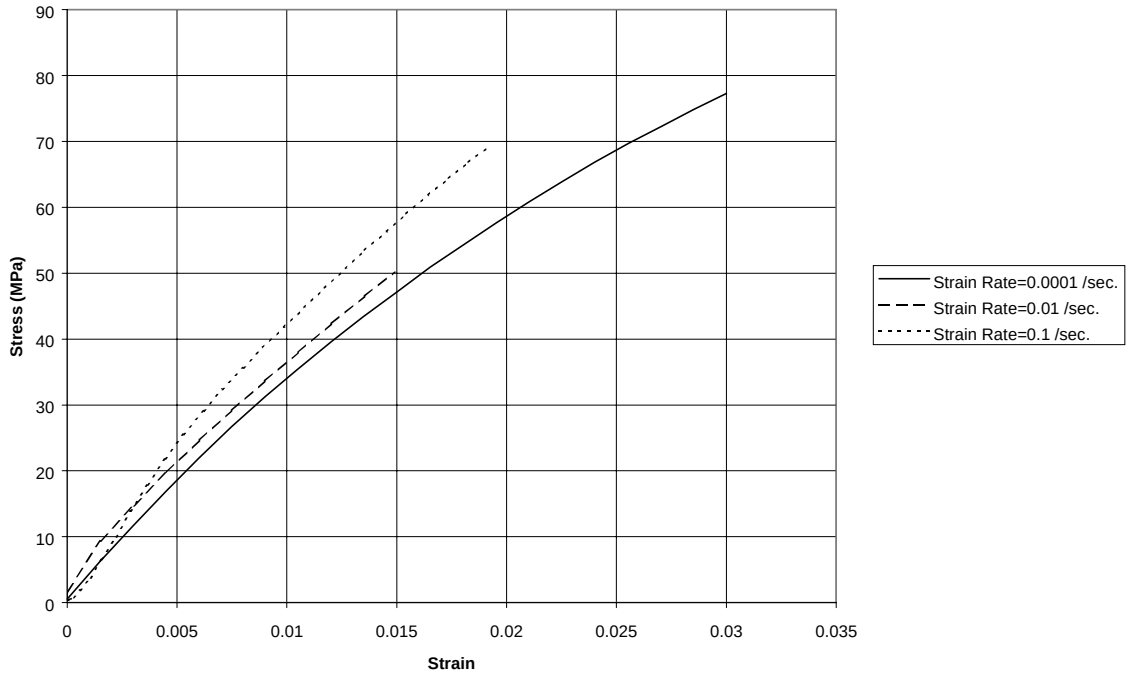

Figure 3.1: Tensile Curves for Fiberite 977-2 Toughened Epoxy

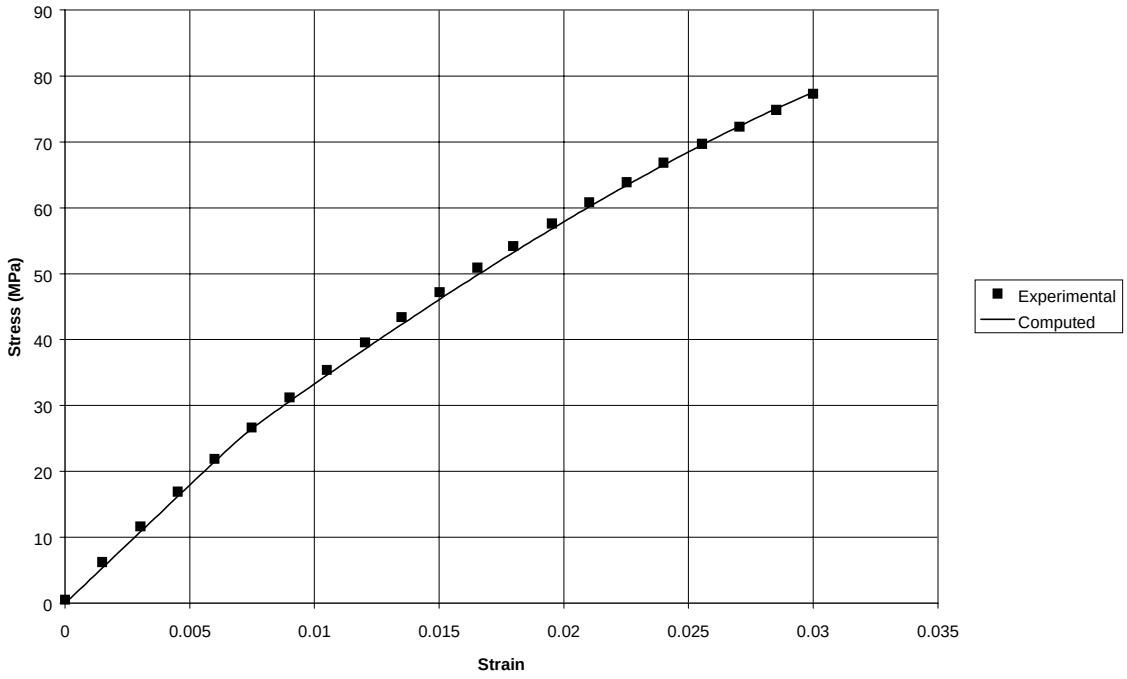

Figure 3.2: Model Correlation for 977-2 Resin at Strain Rate of $1x10^{-4}$ /sec

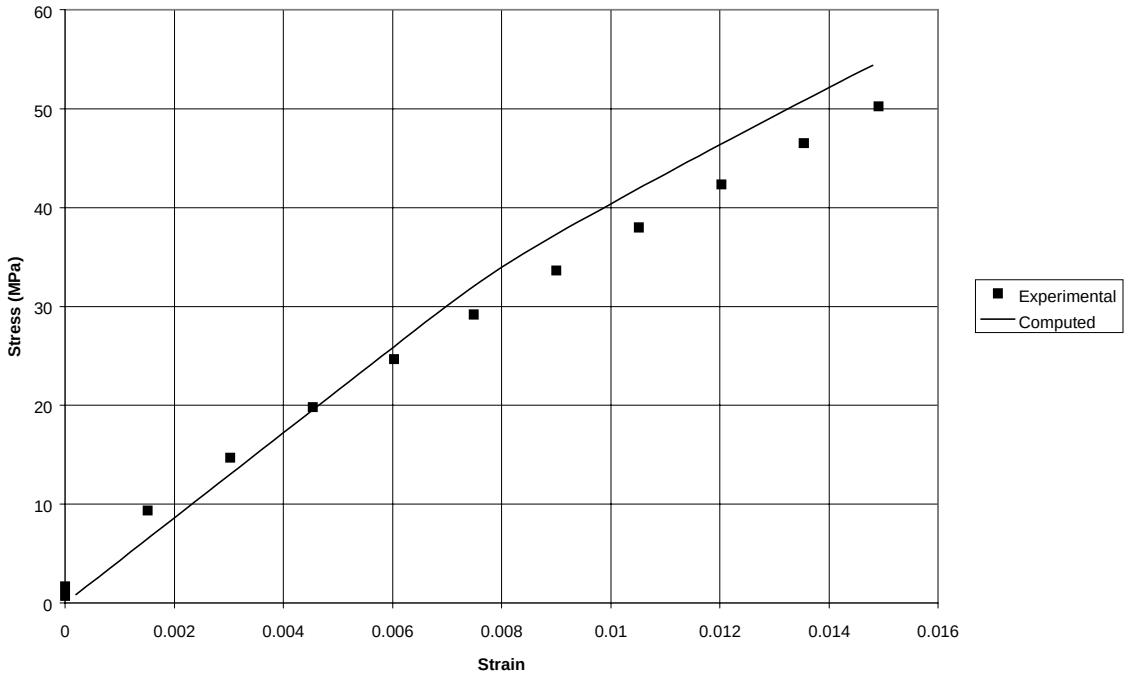

Figure 3.3: Model Correlation for 977-2 Resin at Strain Rate of 0.01 /sec

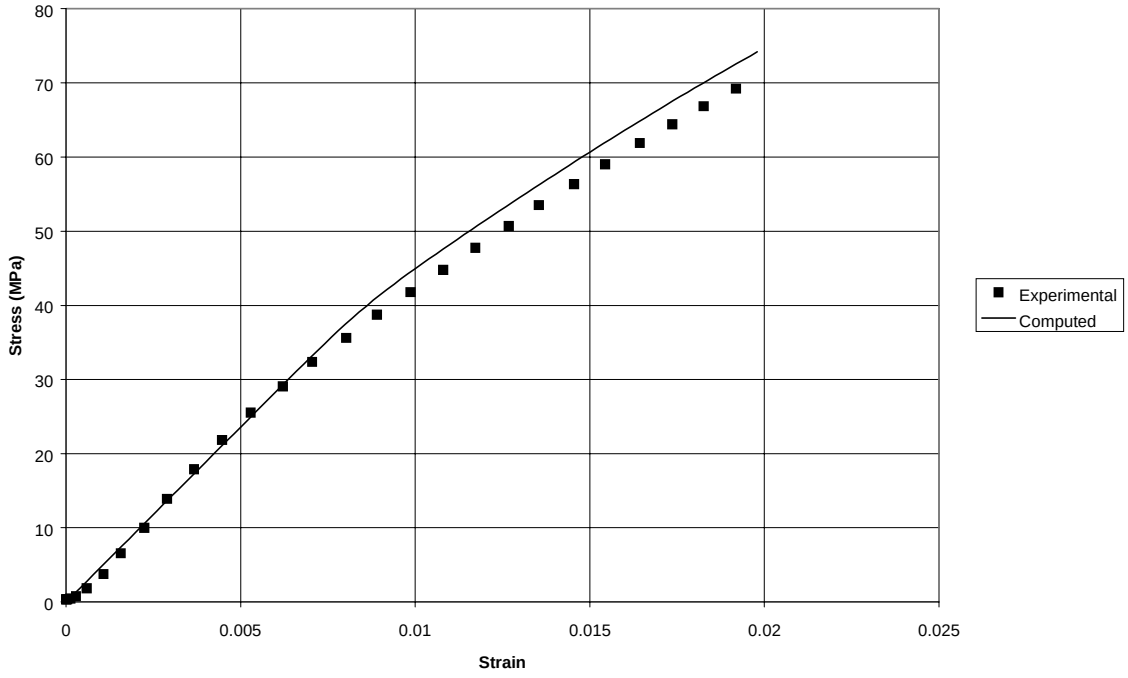

Figure 3.4: Model Correlation for 977-2 Resin at Strain Rate of 0.1 /sec

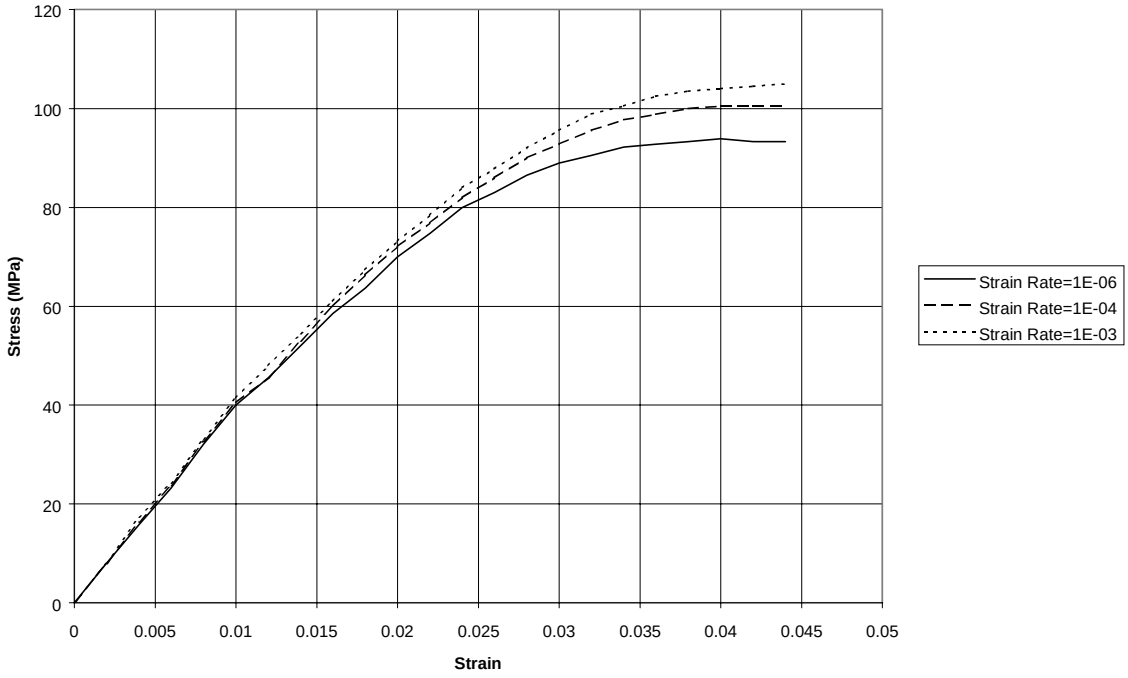

Figure 3.5: Tensile Curves for PEEK

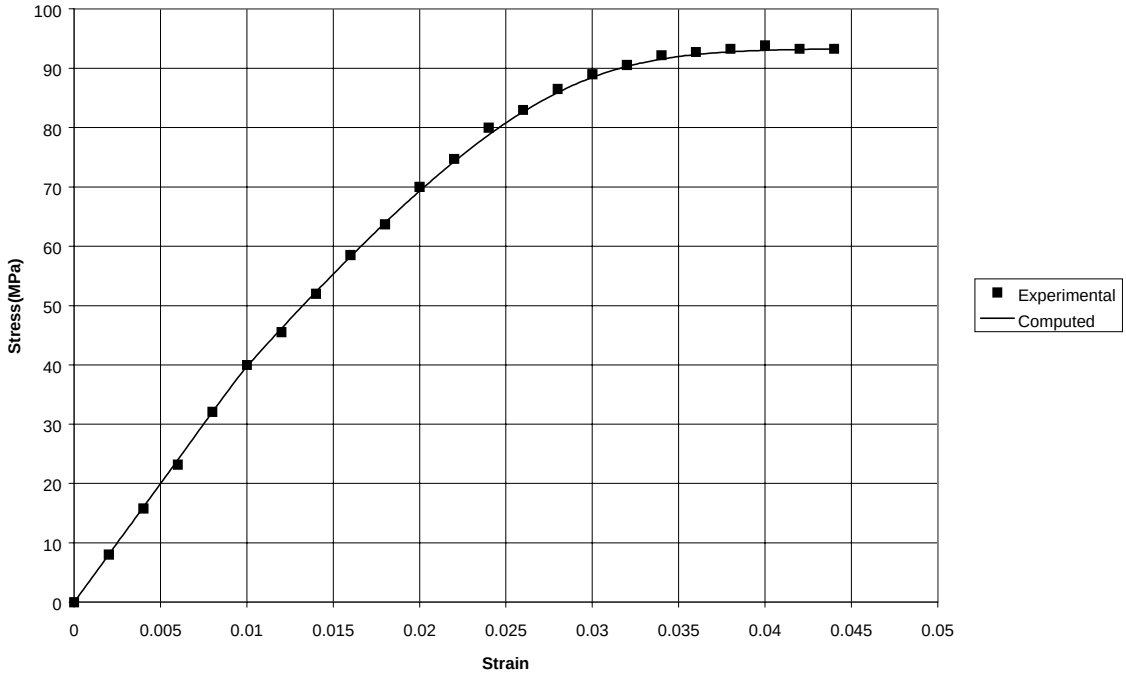

Figure 3.6: Model Correlation for PEEK at Strain Rate of $1x10^{-6}$ /sec

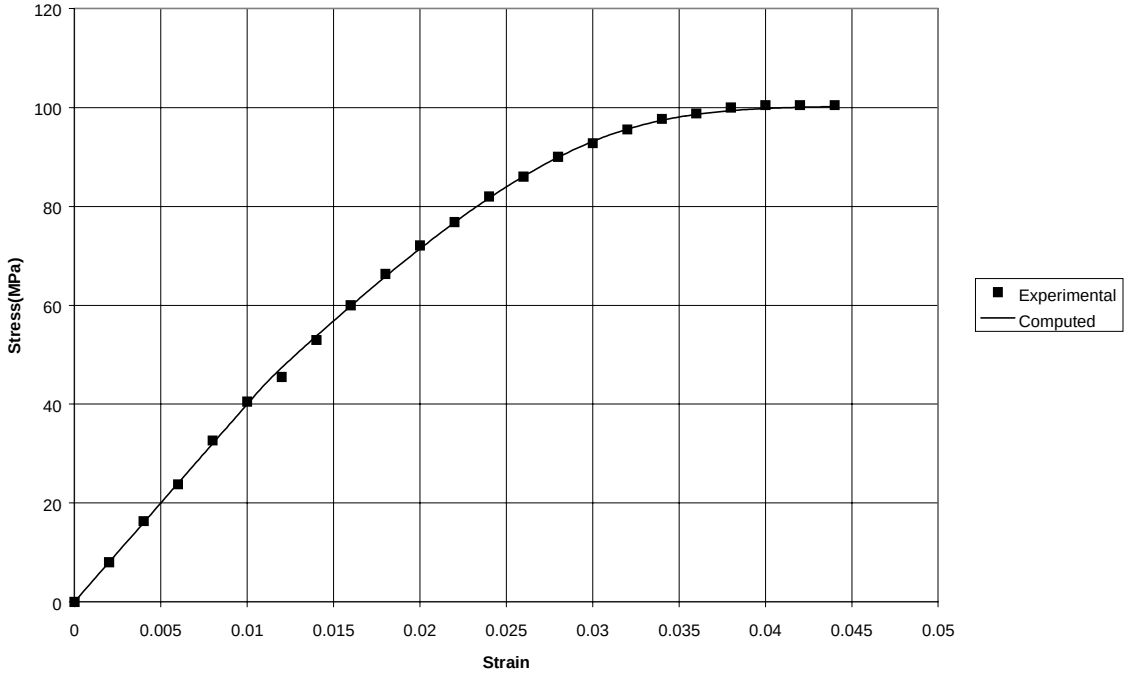

Figure 3.7: Model Correlation for PEEK at Strain Rate of $1x10^{-4}$ /sec

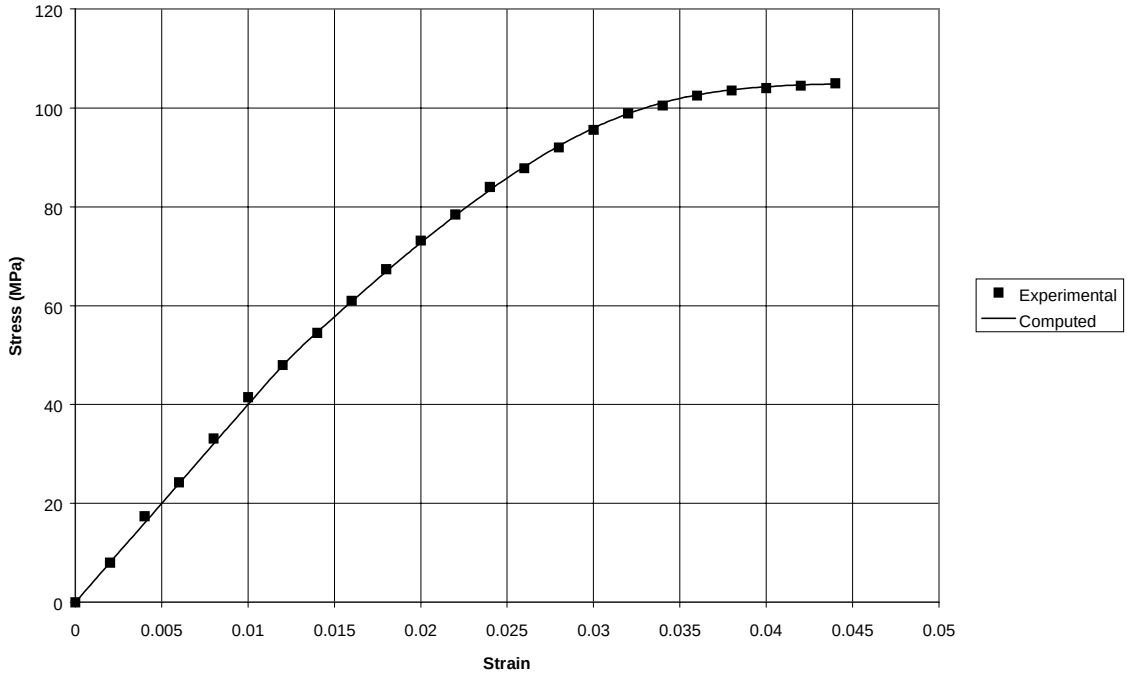

Figure 3.8: Model Correlation for PEEK at Strain Rate of $1x10^{-3}$ /sec

CHAPTER 4
COMPOSITE MICROMECHANICAL MODEL

The implementation of the polymer constitutive equations described above into a mechanics of materials based micromechanics model will now be described. In this manner, the nonlinearity and rate dependence of the deformation response of a polymer matrix composite were accounted for by computing the inelastic response of the polymer matrix. In this chapter, the assumptions of the micromechanics model will be presented, along with an overview of the method. The equations used to compute local and effective stresses as a function of total strains will be derived, and the equations used to compute the effective inelastic strains will be given. The numerical techniques used to implement the micromechanics equations into a stand-alone computer code will be discussed. Finally, verification studies conducted using two representative polymer matrix composites will be described.

4.1 Model Assumptions

Micromechanics techniques were used to predict the effective properties and deformation response of the polymer matrix composites examined in this study. As mentioned previously, in micromechanics methods the effective properties of a composite material unit cell are predicted based on the properties of the individual constituents. As was discussed earlier in this report, micromechanics techniques were utilized for this study since the inelastic, rate dependent deformation response of the polymer was explicitly modeled using the constitutive equations described in the previous chapter. Furthermore, a fairly simple mechanics of materials based composite micromechanics model was utilized in order to facilitate implementation of the model within a transient dynamic finite element computer code.

For this study, the composite unit cell was defined as consisting of a single continuous fiber and its surrounding matrix. Only laminated composites were analyzed; woven composites were not considered at the present time. The matrix constituent and the composite as a whole were assumed to have a sufficient degree of ductility for nontrivial inelastic strains to be present.

The composites were assumed to have a periodic, square, fiber packing arrangement, with perfect bonding between the fiber and the matrix. These assumptions are common in the micromechanical analysis of composite materials [33-36]. While actual composites often have more complicated fiber architectures [69], for this study the fiber packing arrangement utilized was chosen in order to simplify the development of the micromechanics equations and to minimize the computational effort required. If future analytical results indicate that fiber packing plays a significant role in the application under consideration, modifications to the micromechanical models could be made. Alternatively, selected detailed finite element analyses might be performed in order to quantify the fiber packing effects. The assumption of perfect bonding, a common assumption for polymer matrix composites, was also made in order to simplify the development of the micromechanics equations. If fiber/matrix debonding turns out to play a significant role in the strength and failure analyses of the materials under consideration, once again appropriate modifications could be made to the equations.

Only unidirectional composites at various fiber orientation angles were analyzed with the micromechanics equations presented in this study. The finite element method could be used to model laminated composites with varying fiber orientation through the thickness. In such an

analysis, two approaches would be possible. First, a layer of elements could be used to model a single ply of the composite at a specified orientation angle. Multiple layers of elements would then be used to simulate the composite laminate. Alternatively, if the finite element code under consideration permitted laminated shell elements, the micromechanics equations presented in this section would be used to calculate the stresses for a single layer of the laminated element.

As discussed earlier, some efforts have been made by previous researchers to apply equations of state on the micromechanical level in modeling the high strain rate response of polymer matrix composites [44]. Equations of state were used to model the effects of changing density on the hydrostatic stresses in the material. These equations are usually only required for very high strain rate loading conditions. The strain rates encountered in fan containment problems should be low enough that equation of state considerations on the micromechanical level will not be required.

The deformation response of the polymer matrix was simulated using the modified Ramaswamy-Stouffer constitutive equations described above. The fibers of the composite were assumed to be linear elastic, with rate independent properties. Temperature effects were not considered, and small strain conditions were assumed. These assumptions were also applied in the development of the matrix constitutive equations.

4.2 Overview of Micromechanics Method

The micromechanics method utilized in this study was based on a method proposed by Sun and Chen [70]. In this approach, the composite unit cell was broken up into three subcells. One subcell represented the fiber while the remaining two subcells represented the matrix. This approach was similar to the Method of Cells approach utilized by Aboudi [32]. However, in the Method of Cells a displacement field was assumed for each subcell. The effective displacements and stresses were then determined using the equations of continuity and equilibrium. As part of this process, the stresses in the individual subcells were also computed. In the Sun and Chen approach, on the other hand, uniform stress and uniform strain assumptions, in combination with the material constitutive equations, were utilized to solve for the stresses and strains for each subcell and for the overall composite. Furthermore, in the Sun and Chen model out of plane stresses were neglected (plane stress), and classical plasticity theory was used to account for any inelastic strains which might be present. In the Sun and Chen model, stresses were assumed to be given, and the strains were determined by the constitutive model.

Robertson and Mall revised and expanded the Sun and Chen model [71-73]. In this approach, the plane stress assumption was removed, and the full three-dimensional stresses and strains were computed for each subcell and for the overall composite. Since the model was fully three-dimensional, four subcells were used to represent the unit cell. One subcell represented the fiber, and the remaining three subcells represented the surrounding matrix material. The Robertson and Mall model applied unified state variable constitutive equations to compute the inelastic strains in the matrix material. The micromechanics equations were formulated assuming stress controlled loading, in which the subcell stresses and strains were computed based on a defined effective stress condition. Since Robertson and Mall concentrated on analyzing metal matrix composites, where fiber/matrix debonding is significant, the equations were also modified to allow for the presence of a weak fiber/matrix interface.

Pindera and Bednarcyk [74] utilized a similar approach in reformulating the Generalized Method of Cells [75]. The Generalized Method of Cells was a reformulation of the original Method of Cells [32] that allowed for an unrestricted number of subcells in the unit cell. In this latest reformulation by Pindera and Bednarcyk, the subcell stresses were computed based on the macroscopic strains. The reformulation significantly improved the computational efficiency of the method.

The micromechanics model developed for this study was similar to the method utilized by Robertson and Mall. Uniform stress and uniform strain assumptions were applied to a four subcell unit cell, which is displayed in Figure 4.1. In the unit cell, subcell "Af" represented the fiber and subcells "Am", "B1", and "B2" were composed of matrix material. The material axis system was as shown in the figure. The "1" coordinate direction was along the fiber direction, the "2" coordinate direction was perpendicular to the fiber in the plane of the composite, and the "3" coordinate direction was perpendicular to the fiber in the out of plane direction. The fiber was idealized as having a square shape, with the side length equal to the square root of the fiber volume fraction (k_f). Assuming a square fiber shape would result in an incorrect prediction of the interfacial stresses. However, due to the perfect bonding assumption, as well as the expected failure modes in the chosen application, the accurate prediction of interfacial stresses was assumed not to be critical.

The full three-dimensional stresses and strains were computed for each subcell and for the unit cell as a whole. By removing the plane stress assumption, thick composites could be analyzed. Furthermore, through the thickness stresses could be more accurately computed, which would most likely be important in modeling high strain rate impact normal to the plane of the laminate.

In the equations developed here, the subcell stresses and equivalent unit cell stresses were computed based on the applied macroscopic strains. The loading condition was the primary difference between this method and the Robertson and Mall technique. Utilization of strain controlled loading simplified the implementation of this model into a finite element code. In a user defined material subroutine in a finite element code, strains were passed into the routine, and stresses were computed and passed back to the calling routines. Furthermore, the equations presented here were to some extent a specialization of the reformulation of the Generalized Method of Cells (GMC) described above. Specifically, if the GMC equations were explicitly solved for a four subcell model, equations very similar to those presented in this report would result. However, while GMC was designed to allow for a variable number of subcells, the equations given in this report were limited to a four subcell unit cell model, which simplified the equations significantly.

4.3 Derivation of Micromechanics Equations

The unit cell used in the development of the micromechanics equations is shown in Figure 4.1. The bottom layer of subcells, with subcells "Af" and "Am", was referred to as Row 1 (R1). The top layer of subcells, with subcells "B1" and "B2", was referred to as Row 2 (R2). Column 1 (C1) was defined as consisting of subcells "Af" and "B1", and Column 2 (C2) was defined as consisting of subcells "Am" and "B2". The subscript "f" was used to denote fiber related properties, and the subscript "m" was used to denote matrix related properties. Subscripts "Af", "Am", "B1" and "B2" were used to denote stresses and strains of the individual subcells. Subscripts "R1", "R2", "C1", and "C2" were used to denote stresses and strains in the

corresponding regions as defined above. Stresses and strains with no region identifying subscript were assumed to represent the total effective stresses and strains for the unit cell. A superscript "I" was used to denote inelastic strains. The subscripts "11", "22" and "33" were used to define normal stresses, strains and material properties, with the coordinate directions as defined in Figure 1. The subscripts "12", "13" and "23" were used to define shear stresses, strains, and material properties.

The symbol "E" represented the elastic modulus, the symbol "G" represented the shear modulus, and the symbol "ν" represented the Poisson's ratio. Subscripts were attached to these terms as noted above. The symbol "σ_{ij}" represented stress tensor components, the symbol "ε_{ij}" represented strain tensor components, and the symbol "γ_{ij}" represented engineering shear strain components, all assigned in a Cartesian frame of reference. The symbol "k_f" represented the fiber volume ratio of the composite.

The stress and strain in each subcell were assumed to be the effective stress and strain, equal to the average stress or strain over the volume of the subcell, and were assumed to be uniform over the volume of the subcell. The effective stress and strain in Row 1, Row 2, Column 1 and Column 2 were defined as the volume average of the stresses and strains in the component subcells. The effective stress and strain in the unit cell were defined as the volume average of the stresses and strains in Row 1 and Row 2 (or Column 1 and Column 2). To determine the volume average, a weighted sum was computed where the value (stress or strain) in each subcell or combination of subcells was weighted by the volume ratio of the subcell or combination of subcells.

The fibers were assumed to be transversely isotropic. The components in the transversely isotropic compliance matrix (the inverse of the stiffness matrix) for the fiber were defined as follows. Note that the symbol S_{ijf}, which was used to denote the terms in the compliance matrix for the fibers, should not be confused with the symbol S_{ij}, which was used in the previous chapter to represent the components of deviatoric stress in the polymer constitutive equations.

$$S_{11f} = \frac{1}{E_{11f}}, S_{22f} = \frac{1}{E_{22f}}, S_{12f} = \frac{-\nu_{12f}}{E_{11f}}, S_{23f} = \frac{-\nu_{23f}}{E_{22f}}, S_{44f} = \frac{1}{G_{23f}}, S_{66f} = \frac{1}{G_{12f}} \qquad (4.1)$$

where E_{11f} represented the longitudinal elastic modulus of the fiber (along the 1 direction axis in Figure 4.1), E_{22f} represented the transverse elastic modulus of the fiber, ν_{12f} represented the axial Poisson's ratio of the fiber, ν_{23f} represented the transverse Poisson's ratio of the fiber, G_{12f} represented the in-plane shear modulus of the fiber, and G_{23f} represented the transverse shear modulus of the fiber.

The matrix was assumed to be an isotropic material, with compliance matrix terms S_{ijm} defined as follows.

$$S_{11m} = \frac{1}{E_m}, S_{12m} = \frac{-\nu_m}{E_m}, S_{66m} = \frac{1}{G_m} \qquad (4.2)$$

where E_m represented the elastic modulus of the matrix, ν_m represented the Poisson's ratio of the matrix, and G_m represented the shear modulus of the matrix.

The transversely isotropic compliance matrix was used to relate the strains to the stresses, using the following relations. Again, note that in these equations S_{ij} represented the components of the compliance matrix, not the components of the deviatoric stress tensor as in the previous chapter.

$$\begin{Bmatrix} \varepsilon_{11} \\ \varepsilon_{22} \\ \varepsilon_{33} \end{Bmatrix} = \begin{bmatrix} S_{11} & S_{12} & S_{12} \\ S_{12} & S_{22} & S_{23} \\ S_{12} & S_{23} & S_{22} \end{bmatrix} \begin{Bmatrix} \sigma_{11} \\ \sigma_{22} \\ \sigma_{33} \end{Bmatrix} + \begin{Bmatrix} \varepsilon_{11}^{I} \\ \varepsilon_{22}^{I} \\ \varepsilon_{33}^{I} \end{Bmatrix} \tag{4.3}$$

$$\gamma_{12} = S_{66} * \sigma_{12} + 2 * \varepsilon_{12}^{I} \tag{4.4}$$

$$\gamma_{13} = S_{66} * \sigma_{13} + 2 * \varepsilon_{13}^{I} \tag{4.5}$$

$$\gamma_{23} = S_{44} * \sigma_{23} + 2 * \varepsilon_{23}^{I} \tag{4.6}$$

The addition of the inelastic strain components to the standard transversely isotropic elastic constitutive law was how inelasticity was incorporated into the constitutive relations. For the fiber, which was assumed to be linear elastic, these components were neglected. For the matrix material, which was assumed to be isotropic, S_{23} was set equal to S_{12}, S_{22} was set equal to S_{11}, and S_{44} was set equal to S_{66}.

The effective total strains in the composite unit cell were assumed to be known in the micromechanics equations. Furthermore, the inelastic strains in each subcell were assumed to be given. Also, the MATHCAD software package [76] was utilized to assist in carrying out the algebraic computations presented in this derivation.

4.3.1 Normal Stresses and Strains

For the normal stresses and strains (11, 22 and 33), the following uniform stress and uniform strain assumptions were made:

In the fiber direction:

$$\begin{aligned} \varepsilon_{11Af} &= \varepsilon_{11Am} = \varepsilon_{11R1} \\ \varepsilon_{11B1} &= \varepsilon_{11B2} = \varepsilon_{11R2} \\ \varepsilon_{11R1} &= \varepsilon_{11R2} = \varepsilon_{11} \end{aligned} \tag{4.7}$$

Normal to the fiber, in the plane of the ply:

$$\begin{aligned} \sigma_{22Af} &= \sigma_{22Am} = \sigma_{22R1} \\ \sigma_{22B1} &= \sigma_{22B2} = \sigma_{22R2} \end{aligned} \tag{4.8}$$

$$\varepsilon_{22R1} = \varepsilon_{22R2} = \varepsilon_{22} \tag{4.9}$$

Normal to the fiber, normal to the plane of the ply:

$$\sigma_{33Af} = \sigma_{33B1} = \sigma_{33C1}$$
$$\sigma_{33Am} = \sigma_{33B2} = \sigma_{33C2} \tag{4.10}$$

$$\varepsilon_{33C1} = \varepsilon_{33C2} = \varepsilon_{33} \tag{4.11}$$

The effective stresses and strains in Row 1, Row 2, Column 1 and Column 2, as well as for the composite unit cell, were computed using volume averaging, yielding the following expressions:

$$\varepsilon_{22R1} = \sqrt{k_f} * \varepsilon_{22Af} + (1 - \sqrt{k_f}) * \varepsilon_{22Am} \tag{4.12}$$

$$\varepsilon_{22R2} = \sqrt{k_f} * \varepsilon_{22B1} + (1 - \sqrt{k_f}) * \varepsilon_{22B2} \tag{4.13}$$

$$\varepsilon_{33C1} = \sqrt{k_f} * \varepsilon_{33Af} + (1 - \sqrt{k_f}) * \varepsilon_{33B1} \tag{4.14}$$

$$\varepsilon_{33C2} = \sqrt{k_f} * \varepsilon_{33Am} + (1 - \sqrt{k_f}) * \varepsilon_{33B2} \tag{4.15}$$

$$\sigma_{11R1} = \sqrt{k_f} * \sigma_{11Af} + (1 - \sqrt{k_f}) * \sigma_{11Am} \tag{4.16}$$

$$\sigma_{11R2} = \sqrt{k_f} * \sigma_{11B1} + (1 - \sqrt{k_f}) * \sigma_{11B2} \tag{4.17}$$

$$\sigma_{11} = \sqrt{k_f} * \sigma_{11R1} + (1 - \sqrt{k_f}) * \sigma_{11R2} \tag{4.18}$$

$$\sigma_{22} = \sqrt{k_f} * \sigma_{22R1} + (1 - \sqrt{k_f}) * \sigma_{22R2} \tag{4.19}$$

$$\sigma_{33} = \sqrt{k_f} * \sigma_{33C1} + (1 - \sqrt{k_f}) * \sigma_{33C2} \tag{4.20}$$

The constitutive relations for the fiber and matrix were defined as follows, using Equation (4.3):

$$\varepsilon_{11f} = S_{11f} * \sigma_{11f} + S_{12f} * \sigma_{22f} + S_{12f} * \sigma_{33f} \tag{4.21}$$

$$\varepsilon_{22f} = S_{12f} * \sigma_{11f} + S_{22f} * \sigma_{22f} + S_{23f} * \sigma_{33f} \tag{4.22}$$

$$\varepsilon_{33f} = S_{12f} * \sigma_{11f} + S_{23f} * \sigma_{22f} + S_{22f} * \sigma_{33f} \tag{4.23}$$

$$\varepsilon_{11m} = S_{11m} * \sigma_{11m} + S_{12m} * \sigma_{22m} + S_{12m} * \sigma_{33m} + \varepsilon_{11m}^{I} \tag{4.24}$$

$$\varepsilon_{22m} = S_{12m} * \sigma_{11m} + S_{11m} * \sigma_{22m} + S_{12m} * \sigma_{33m} + \varepsilon^{I}_{22m} \tag{4.25}$$

$$\varepsilon_{33m} = S_{12m} * \sigma_{11m} + S_{12m} * \sigma_{22m} + S_{11m} * \sigma_{33m} + \varepsilon^{I}_{33m} \tag{4.26}$$

By solving Equations (4.21) and (4.24) for each subcell, and by utilizing the appropriate uniform stress and uniform strain assumptions, the following expressions were obtained.

$$\sigma_{11Af} = \frac{1}{S_{11f}}\left(\varepsilon_{11} - S_{12f} * \sigma_{22R1} - S_{12f} * \sigma_{33C1}\right) \tag{4.27}$$

$$\sigma_{11Am} = \frac{1}{S_{11m}}\left(\varepsilon_{11} - S_{12m} * \sigma_{22R1} - S_{12m} * \sigma_{33C2} - \varepsilon^{I}_{11Am}\right) \tag{4.28}$$

$$\sigma_{11B1} = \frac{1}{S_{11m}}\left(\varepsilon_{11} - S_{12m} * \sigma_{22R2} - S_{12m} * \sigma_{33C1} - \varepsilon^{I}_{11B1}\right) \tag{4.29}$$

$$\sigma_{11B2} = \frac{1}{S_{11m}}\left(\varepsilon_{11} - S_{12m} * \sigma_{22R2} - S_{12m} * \sigma_{33C2} - \varepsilon^{I}_{11B2}\right) \tag{4.30}$$

Equations (4.27)-(4.30) were then substituted into Equations (4.22), (4.23), (4.25), and (4.26) for each subcell, applying the appropriate uniform stress and uniform strain assumptions. By inserting the resulting expressions into Equations (4.12)-(4.15), the following system of equations resulted:

$$\begin{aligned}
&\varepsilon_{22R1} - \left(\sqrt{k_f}\,\frac{S_{12f}}{S_{11f}} + (1-\sqrt{k_f})\frac{S_{12m}}{S_{11m}}\right)\varepsilon_{11} + (1-\sqrt{k_f})\frac{S_{12m}}{S_{11m}}\varepsilon^{I}_{11Am} \\
&-(1-\sqrt{k_f})\varepsilon^{I}_{22Am} = \left(\sqrt{k_f}\left(S_{22f} - \frac{S^2_{12f}}{S_{11f}}\right) + (1-\sqrt{k_f})\left(S_{11m} - \frac{S^2_{12m}}{S_{11m}}\right)\right)\sigma_{22R1} \\
&+\left(\sqrt{k_f}\left(S_{23f} - \frac{S^2_{12f}}{S_{11f}}\right)\right)\sigma_{33C1} + \left(\left(1-\sqrt{k_f}\right)\left(S_{12m} - \frac{S^2_{12m}}{S_{11m}}\right)\right)\sigma_{33C2}
\end{aligned} \tag{4.31}$$

$$\begin{aligned}
&\varepsilon_{22R2} - \frac{S_{12m}}{S_{11m}}\varepsilon_{11} + \sqrt{k_f}\,\frac{S_{12m}}{S_{11m}}\varepsilon^{I}_{11B1} - \sqrt{k_f}\,\varepsilon^{I}_{22B1} + (1-\sqrt{k_f})\frac{S_{12m}}{S_{11m}}\varepsilon^{I}_{11B2} \\
&-(1-\sqrt{k_f})\varepsilon^{I}_{22B2} = \left(S_{11m} - \frac{S^2_{12m}}{S_{11m}}\right)\sigma_{22R2} + \left(\sqrt{k_f}\left(S_{12m} - \frac{S^2_{12m}}{S_{11m}}\right)\right)\sigma_{33C1} \\
&+\left((1-\sqrt{k_f})\left(S_{12m} - \frac{S^2_{12m}}{S_{11m}}\right)\right)\sigma_{33C2}
\end{aligned} \tag{4.32}$$

$$\varepsilon_{33C1} - \left(\sqrt{k_f}\,\frac{S_{12f}}{S_{11f}} + (1-\sqrt{k_f})\frac{S_{12m}}{S_{11m}} \right)\varepsilon_{11} + (1-\sqrt{k_f})\frac{S_{12m}}{S_{11m}}\varepsilon^{I}_{11B1}$$
$$-(1-\sqrt{k_f})\varepsilon^{I}_{33B1} = \left(\sqrt{k_f}\left(S_{22f} - \frac{S^2_{12f}}{S_{11f}} \right) + (1-\sqrt{k_f})\left(S_{11m} - \frac{S^2_{12m}}{S_{11m}} \right) \right)\sigma_{33C1} \qquad (4.33)$$
$$+\left(\sqrt{k_f}\left(S_{23f} - \frac{S^2_{12f}}{S_{11f}} \right) \right)\sigma_{22R1} + \left((1-\sqrt{k_f})\left(S_{12m} - \frac{S^2_{12m}}{S_{11m}} \right) \right)\sigma_{22R2}$$

$$\varepsilon_{33C2} - \frac{S_{12m}}{S_{11m}}\varepsilon_{11} + \sqrt{k_f}\,\frac{S_{12m}}{S_{11m}}\varepsilon^{I}_{11Am} - \sqrt{k_f}\,\varepsilon^{I}_{33Am} + (1-\sqrt{k_f})\frac{S_{12m}}{S_{11m}}\varepsilon^{I}_{11B2}$$
$$-(1-\sqrt{k_f})\varepsilon^{I}_{33B2} = \left(S_{11m} - \frac{S^2_{12m}}{S_{11m}} \right)\sigma_{33C2} + \left(\sqrt{k_f}\left(S_{12m} - \frac{S^2_{12m}}{S_{11m}} \right) \right)\sigma_{22R1} \qquad (4.34)$$
$$+\left((1-\sqrt{k_f})\left(S_{12m} - \frac{S^2_{12m}}{S_{11m}} \right) \right)\sigma_{22R2}$$

Equations (4.31)-(4.34), together with Equations (4.27)-(4.30), were solved for the required subcell stresses. Equations (4.8), (4.9), and (4.16)-(4.20) were then used to compute the effective stress state in the unit cell.

4.3.2 In-Plane Shear Stresses and Strains

For the in-plane shear (1-2 direction) stresses and strains, the following uniform stress and uniform strain assumptions were made:

<u>In the plane of the ply:</u>

$$\gamma_{12R1} = \gamma_{12R2} = \gamma_{12} \qquad (4.35)$$

$$\begin{aligned} \sigma_{12Af} &= \sigma_{12Am} = \sigma_{12R1} \\ \sigma_{12B1} &= \sigma_{12B2} = \sigma_{12R2} \end{aligned} \qquad (4.36)$$

By applying volume averaging, the effective in-plane shear stresses and strains for Row 1, Row 2, and the composite unit cell were defined as follows:

$$\begin{aligned} \gamma_{12R1} &= \sqrt{k_f} * \gamma_{12Af} + (1-\sqrt{k_f}) * \gamma_{12Am} \\ \gamma_{12R2} &= \sqrt{k_f} * \gamma_{12B1} + (1-\sqrt{k_f}) * \gamma_{12B2} \end{aligned} \qquad (4.37)$$

$$\sigma_{12} = \sqrt{k_f} * \sigma_{12R1} + (1-\sqrt{k_f}) * \sigma_{12R2} \qquad (4.38)$$

The constitutive relations for the fiber and matrix were defined by the following expressions, using Equation (4.4):

$$\gamma_{12f} = S_{66f} * \sigma_{12f} \tag{4.39}$$

$$\gamma_{12m} = S_{66m} * \sigma_{12m} + 2 * \varepsilon^{I}_{12m} \tag{4.40}$$

By substituting Equations (4.39) and (4.40) into Equation (4.37), and using the appropriate uniform stress and uniform strain assumptions, the following expressions were obtained, from which the subcell in-plane shear stresses were computed.

$$\gamma_{12} = [\sqrt{k_f} * S_{66f} + (1-\sqrt{k_f}) * S_{66m}] * \sigma_{12R1} + 2 * (1-\sqrt{k_f}) * \varepsilon^{I}_{12Am} \tag{4.41}$$

$$\gamma_{12} = S_{66m} * \sigma_{12R2} + 2 * \sqrt{k_f} * \varepsilon^{I}_{12B1} + 2 * (1-\sqrt{k_f}) * \varepsilon^{I}_{12B2} \tag{4.42}$$

4.3.3 Transverse Shear Stresses and Strains: 1-3 Direction

The computation of the subcell shear stresses in the 1-3 direction was very similar to the computation of the subcell shear stresses in the 1-2 direction. The only difference was that Column 1 and Column 2 were used instead of Row 1 and Row 2. The uniform stress and uniform strain assumptions shown in Equations (4.35) and (4.36) were transformed as follows:

<u>In the fiber/normal direction:</u>

$$\gamma_{13C1} = \gamma_{13C2} = \gamma_{13} \tag{4.43}$$

$$\begin{aligned} \sigma_{13Af} &= \sigma_{13B1} = \sigma_{13C1} \\ \sigma_{13Am} &= \sigma_{13B2} = \sigma_{13C2} \end{aligned} \tag{4.44}$$

The volume averaged stresses and strains in Column 1 and Column 2 were computed using the expressions:

$$\begin{aligned} \gamma_{13C1} &= \sqrt{k_f} * \gamma_{13Af} + (1-\sqrt{k_f}) * \gamma_{13B1} \\ \gamma_{13C2} &= \sqrt{k_f} * \gamma_{13Am} + (1-\sqrt{k_f}) * \gamma_{13B2} \end{aligned} \tag{4.45}$$

$$\sigma_{13} = \sqrt{k_f} * \sigma_{13C1} + (1-\sqrt{k_f}) * \sigma_{13C2} \tag{4.46}$$

By substituting Equations (4.39) and (4.40) (replacing the subscript “12” with “13” as indicated by Equation (4.5)) into Equation (4.45), the transverse 1-3 direction shear stresses in the individual subcells were computed from the following equations:

$$\gamma_{13} = [\sqrt{k_f} * S_{66f} + (1-\sqrt{k_f}) * S_{66m}] * \sigma_{13C1} + 2 * (1-\sqrt{k_f}) * \varepsilon^{I}_{13B1} \tag{4.47}$$

$$\gamma_{13} = S_{66m} * \sigma_{13B'} + 2 * \sqrt{kf} * \varepsilon^{I}_{13Am} + 2 * (1 - \sqrt{kf}) * \varepsilon^{I}_{13B2} \tag{4.48}$$

4.3.4 Transverse Shear Stresses and Strains: 2-3 Direction

To compute the transverse 2-3 direction shear stresses in the subcells of the composite unit cell, the following uniform stress assumptions were made:

In the transverse ply-normal direction:

$$\sigma_{23R1} = \sigma_{23R2} = \sigma_{23} \tag{4.49}$$

$$\begin{aligned} \sigma_{23Af} &= \sigma_{23Am} = \sigma_{23R1} \\ \sigma_{23B1} &= \sigma_{23B2} = \sigma_{23R2} \end{aligned} \tag{4.50}$$

The volume averaged shear strains in Row 1, Row 2 and the composite unit cell were then defined as follows:

$$\begin{aligned} \gamma_{23R1} &= \sqrt{k_f} * \gamma_{23Af} + (1 - \sqrt{k_f}) * \gamma_{23Am} \\ \gamma_{23R2} &= \sqrt{k_f} * \gamma_{23B1} + (1 - \sqrt{k_f}) * \gamma_{23B2} \end{aligned} \tag{4.51}$$

$$\gamma_{23} = \sqrt{kf} * \gamma_{23R1} + (1 - \sqrt{kf}) * \gamma_{23R2} \tag{4.52}$$

The constitutive relations for the fiber and matrix were defined by using Equation (4.6):

$$\gamma_{23f} = S_{44f} * \sigma_{23f} \tag{4.53}$$

$$\gamma_{23m} = S_{66m} * \sigma_{23m} + 2 * \varepsilon^{I}_{23m} \tag{4.54}$$

By substituting Equations (4.53) and (4.54) into Equations (4.51) and (4.52), and by using the uniform stress assumptions, the following expression was obtained which was used to compute the subcell shear stresses in the transverse 2-3 direction:

$$\begin{aligned} \gamma_{23} &= [k_f * S_{44f} + (1 - k_f) * S_{66m}] * \sigma_{23} \\ &+ 2 * (1 - \sqrt{k_f}) * [\sqrt{k_f} * (\varepsilon^{I}_{23Am} + \varepsilon^{I}_{23B1}) + (1 - \sqrt{k_f}) * \varepsilon^{I}_{23B2}] \end{aligned} \tag{4.55}$$

4.4 Effective Inelastic Strains

In applying a strain controlled load to a composite unit cell, accurate determination of the Poisson strains was required. To compute the Poisson strains based on an applied total strain in a particular coordinate direction, the effective inelastic strains in each coordinate direction were required. To compute the effective inelastic strains for the unit cell, the same uniform stress and uniform strain assumptions that were used in the previous section were applied again.

The constitutive relations (Equations (4.3)-(4.6)) for the fiber and matrix were modified for these calculations. By making these simplifications, the complexity of the mathematics was reduced considerably. However, the accuracy of the results was not significantly affected. The modified constitutive equations for the normal and in-plane shear stresses were given by the following expressions:

$$\sigma_{11} = E_{11}(\varepsilon_{11} - \varepsilon_{11}^{I}) \tag{4.56}$$

$$\sigma_{22} = E_{22}(\varepsilon_{22} - \varepsilon_{22}^{I}) \tag{4.57}$$

$$\sigma_{12} = G_{12}(\gamma_{12} - 2*\varepsilon_{12}^{I}) \tag{4.58}$$

where all symbols were as defined previously. The equations for the transverse shear stresses were very similar to Equation (4.58), replacing the subscript "12" with "13" or "23" as appropriate. The equation for the stress in the 3-3 coordinate direction was very similar to Equations (4.56) and (4.57), replacing the subscript "11" or "22" with "33". Note, as before, the inelastic strain values were only used when the matrix material was considered. Furthermore, for the isotropic matrix material, E_m replaced E_{11} and E_{22}, and G_m replaced G_{12}.

By utilizing the constitutive equations for the fiber and matrix (Equations (4.56)-(4.57)), along with the uniform stress and uniform strain assumptions (Equations (4.7)-(4.20)), the following expressions were obtained for the effective inelastic normal strains:

$$\varepsilon_{11}^{I} = \frac{(1-\sqrt{k_f})E_m\left(\sqrt{k_f}(\varepsilon_{11Am}^{I} + \varepsilon_{11B1}^{I}) + (1-\sqrt{k_f})\varepsilon_{11B2}^{I}\right)}{(k_f)E_{11f} + (1-k_f)E_m} \tag{4.59}$$

$$\varepsilon_{22}^{I} = \frac{\left(1-\sqrt{k_f}\right)E'\varepsilon_{22Am}^{I} + E_m\left(1-\sqrt{k_f}\right)\left(\sqrt{k_f}\,\varepsilon_{22B1}^{I} + \left(1-\sqrt{k_f}\right)\varepsilon_{22B2}^{I}\right)}{E' + \left(1-\sqrt{k_f}\right)E_m} \tag{4.60}$$

where:

$$E' = \frac{\sqrt{k_f}\,E_{22f}E_m}{E_m\sqrt{k_f} + E_{22f}\left(1-\sqrt{k_f}\right)} \tag{4.61}$$

The effective inelastic strain in the 3-3 direction was also computed by using Equation (4.60). In this case, the inelastic strains in subcells "Am" and "B1" were switched in the expression.

By utilizing the constitutive equations for the fiber and matrix (Equation (4.58)), along with the uniform stress and uniform strain assumptions (Equations (4.35)-(4.38)), the following expression was obtained for the effective inelastic in-plane shear strain:

$$\varepsilon_{12}^{I} = \frac{\left(1-\sqrt{k_f}\right)G'\varepsilon_{12Am}^{I} + G_m\left(1-\sqrt{k_f}\right)\left(\sqrt{k_f}\,\varepsilon_{12B1}^{I} + \left(1-\sqrt{k_f}\right)\varepsilon_{12B2}^{I}\right)}{G' + \left(1-\sqrt{k_f}\right)G_m} \tag{4.62}$$

where:

$$G' = \frac{\sqrt{k_f}\, G_{12f}\, G_m}{G_m \sqrt{k_f} + G_{12f}\left(1-\sqrt{k_f}\right)} \tag{4.63}$$

The effective inelastic strain in the 1-3 out-of-plane shear direction was computed by using Equation (4.62) and switching the inelastic strains in subcells "Am" and "B1". The effective inelastic strain in the 2-3 out-of-plane shear direction followed automatically from Equation (4.55), and is presented without further comment.

$$\varepsilon_{23}^{I} = (1-\sqrt{k_f}) * \left(\sqrt{k_f} * (\varepsilon_{23Am}^{I} + \varepsilon_{23B1}^{I}) + (1-\sqrt{k_f}) * \varepsilon_{23B2}^{I}\right) \tag{4.64}$$

4.5 Numerical Implementation of Micromechanics Equations

For the current study, a stand-alone computer code was developed in order to implement and test the micromechanics equations. A standard fourth order Runge-Kutta explicit integration scheme was again utilized to integrate the rate dependent constitutive equations. The details of the method can be found in Section 3.5.

As mentioned in the development of the micromechanics equations, strain controlled loading was assumed in the formulation. In the computer algorithm, strains were specified in a particular coordinate direction. To impose the required Poisson and axial-shear coupling strains, effective elastic properties for the composite at a specified fiber orientation angle were utilized. First, the elastic constants in the material axis system were computed using equations developed by Murthy and Chamis [37]. The elastic constants in the structural axis system were then computed using standard techniques and equations described in references such as [33], [36] and [47]. The material axis system was the coordinate system shown in Figure 4.1. The structural axis system was the axis system along which the loads are applied. The material coordinate system was obtained by rotating the structural axis system about the "3" coordinate axis by an amount equal to the fiber orientation angle.

For the computer code execution, first the required geometric data (fiber volume ratio and fiber orientation angle), constituent properties and load history data were read in from an input file. The required elastic constants in both material and structural coordinate systems were computed, along with the required tensor transformation matrices. For each time step, the total strain rate in the load direction was determined. The Runge-Kutta integration procedure was then carried out to compute the total strains in the structural axis system, as well as the inelastic strains and internal stresses in each subcell. The total stresses in structural coordinates were calculated using the total strains, appropriate tensor transformations, and the micromechanics equations. At this point, the code moved on to the next time step.

The Runge-Kutta integration algorithm involved the computation of several intermediate estimates of the total strains, subcell inelastic strains and subcell internal stresses. To calculate the intermediate estimates, first the total strain estimate was converted from the structural axis system to the material axis system. The stresses in each of the subcells were then determined using the micromechanics equations. Using the computed stresses, the inelastic strain rates and internal stress rates in each matrix subcell were computed using the polymer constitutive equations. The effective inelastic strain rate tensor for the composite unit cell in the material axis

system was computed, and the values were then transformed into the structural axis system. Using the ply level Poisson's ratios and axial-shear coupling coefficients, the total strain rate tensor in structural coordinates was calculated. The intermediate values required for the Runge-Kutta integration routine were then determined.

4.6 Model Verification Analyses

To verify the micromechanics equations, a series of analyses were carried out using two material systems. Both material systems exhibited a nonlinear deformation response for off-axis fiber orientation angles.

4.6.1 Material Properties

The first material system examined, supplied by Fiberite, Inc., consisted of carbon IM-7 fibers in a 977-2 toughened epoxy matrix. Unidirectional laminates with fiber orientations of [0°], [10°], [45°], and [90°] were tested. Tensile tests were conducted by Cincinnati Testing Labs of Cincinnati, Ohio at a strain rate of $1x10^{-4}$ /sec on each of the composites [67]. As mentioned before in the discussion of the polymer constitutive equations, good high strain rate tensile data have not been obtained at this time. However, the equations will be characterized and validated at high strain rates once appropriate data are obtained.

The IM7/977-2 composite had a fiber volume ratio of 0.60. The material properties of the IM-7 fibers, as determined from Reference [77], are shown in Table 4.1. The material properties of the 977-2 matrix, discussed in Chapter 3, are listed in Table 3.2. As mentioned in Section 3.4.2, the constant β for the shear correction factor was determined empirically using composite data. For the IM7/977-2 system, the constant was determined using the [10°] off-axis composite data. This orientation was chosen as it is shear dominated [78]. The value of β was determined to be 1.2.

The second material that was studied consisted of carbon AS-4 fibers in a PEEK thermoplastic matrix. Tensile stress-strain curves were obtained by Weeks and Sun [25] for unidirectional composites with fiber orientations of [14°], [30°], [45°] and [90°] at a strain rate of $1x10^{-5}$ /sec, and composites with fiber orientations of [15°], [30°], [45°] and [90°] at a strain rate of 0.1 /sec. Only the low strain rate data were examined since the PEEK material was only characterized for relatively low strain rates. However, by conducting verification studies using this data, the ability of the micromechanics equations to capture the rate dependent deformation response of a polymer matrix composite was determined.

The fiber volume ratio used for the AS4/PEEK material was 0.62 (a typical value for this material based on representative manufacturer information). The elastic properties of the AS-4 fibers, as listed in Reference [79], are shown in Table 4.1. For the PEEK matrix, the material properties are shown in Table 3.2. The value of the constant β was determined empirically by fitting data from the [14°] and [15°] laminates, which were shear dominated. By examining the data, the constant β was determined to be rate independent, and equal to a value of 0.45. Note that since there was currently no good explanation for the physical explanation for the physical meaning of the parameter β, the significance of the value of this parameter and its variation for the two materials examined in this study could not be quantified at this time.

4.6.2 Analysis Results

Analyses were conducted using the micromechanics equations described above. The modified Ramaswamy-Stouffer constitutive equations described in Chapter 3 were used to compute the rate dependent, inelastic response of the polymer matrix. The predicted results were compared to experimentally obtained values. Stress-strain curves for the IM7/977-2 laminates are shown in Figures 4.2-4.5. Stress-strain curves for the AS4/PEEK composite are shown in Figures 4.6-4.9 for a strain rate of $1x10^{-5}$ /sec, and in Figures 4.10-13 for a strain rate of 0.1 /sec. The calculations for the [10°] IM7/977-2 laminate shown in Figure 4.3, and the [14°] and [15°] AS4/PEEK laminates shown in Figures 4.6 and 4.10 were correlations, while the remaining calculations were "true" predictions.

As can be seen in the figures, for both materials, and for both strain rates for the AS4/PEEK system, the analytical results matched the experimental values quite well in general for all fiber orientation angles examined. For the shear dominated fiber orientation angles ([10°], [14°], and [15°]), the inelastic portion of the predicted stress-strain curves were flatter than the experimental results. Furthermore, the strain level at which significant inelasticity begins was somewhat overpredicted. However, the predicted stresses at the end of the stress-strain curves matched the experimental values reasonably well. For predicting ply strength, which will be discussed in the next chapter of this report, correctly predicting the stress levels at the end of the stress-strain curve was most critical.

For the AS4/PEEK system, the elastic response of the [30°] and [45°] laminates was slightly underpredicted. As the elastic response of the other laminates was predicted reasonably well, these results indicated that the transverse Poisson's ratio or shear moduli used for the AS-4 fiber may not have been correct. As these values are often just approximated instead of experimentally measured, inaccuracies in these values were not surprising.

Overall, the comparison between the experimental and predicted values was quite good. In particular, the rate dependence and nonlinearity of the deformation response of the composites was captured. To emphasize the ability of the analytical model to capture the rate dependence of the deformation response, the results for the [30°] AS4/PEEK laminate shown in Figures 4.7 and 4.11 are superimposed in Figure 4.14. In this figure, the curves labeled "1E-05" are results obtained at a strain rate of $1x10^{-5}$ /sec, and the curves labeled 0.1 are results obtained at a strain rate of 0.1 /sec. The results in this figure show that the response of the AS4/PEEK system was rate dependent for this fiber orientation. Furthermore, the predicted curves show that the micromechanics equations and the polymer constitutive model captured the rate dependence. The rate dependence of the composite deformation response should be even more dramatic once high strain rate experiments and analyses are considered.

4.7 Summary

A mechanics of materials based composite micromechanics model was developed to predict the effective properties and deformation response of rate dependent, inelastic, polymer matrix composites based on the constituent properties and applied strains. The modified Ramswamy-Stouffer equations were used to model the polymer matrix constituent. The effective inelastic strains of the composite unit cell have also been computed. The model has been implemented into a stand-alone computer code, and was verified for two representative polymer matrix composites. The analytical predictions compared favorably to experimentally obtained values.

As discussed in the next chapter, the micromechanics model was used in combination with selected failure criteria to predict the failure of a composite ply based on the macroscopic stresses.

Table 4.1
Material Properties for IM-7 and AS-4 Fibers

	Longitudinal Modulus (GPa)	Transverse Modulus (GPa)	Poisson's Ratio	In-Plane Shear Modulus (GPa)
IM-7	276	13.8	0.25	20.0
AS-4	214	14.0	0.20	14.0

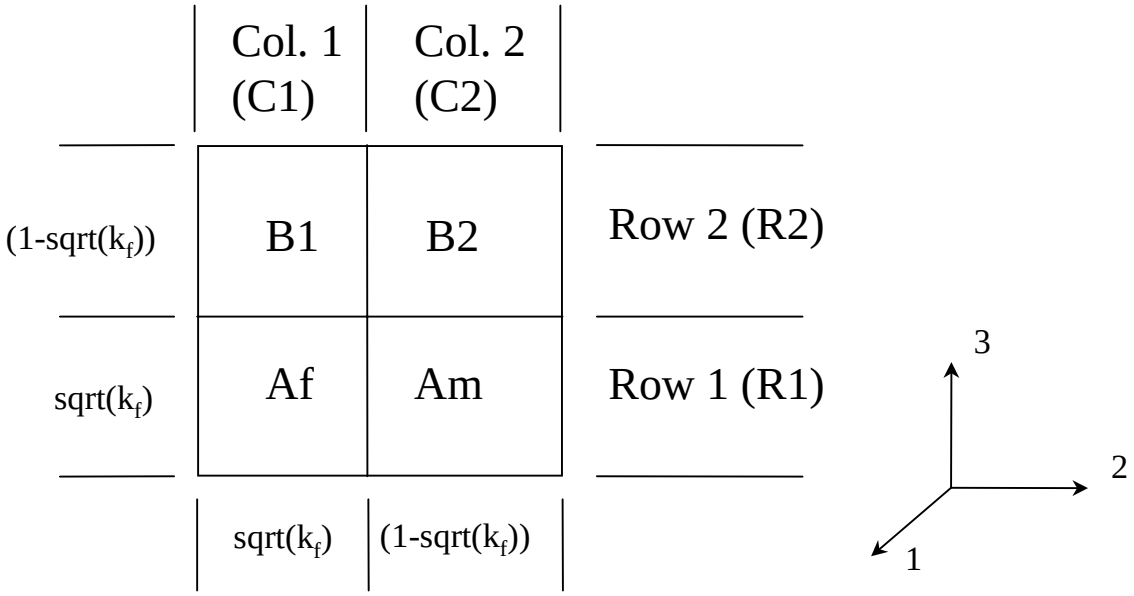

k_f=Fiber Volume Fraction
Af=Fiber Subregion
Am,B1,B2=Matrix Subregions

Figure 4.1: Geometry and Layout of Composite Unit Cell Model

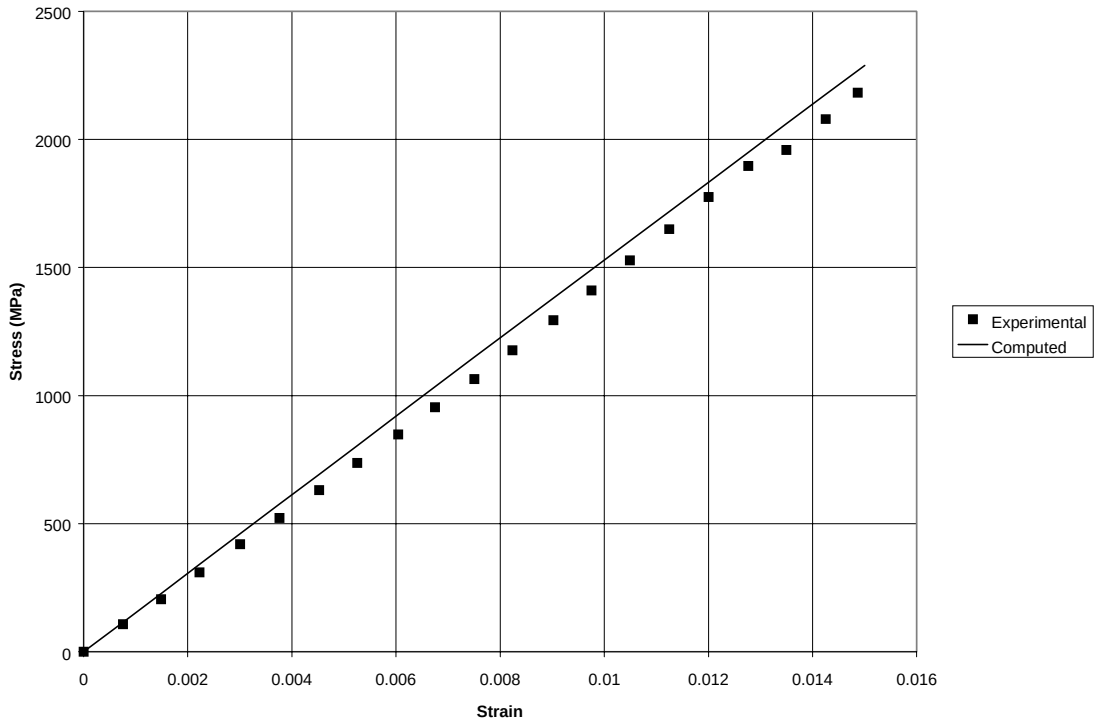

Figure 4.2: Model Predictions for [0°] IM7/977-2 Laminate

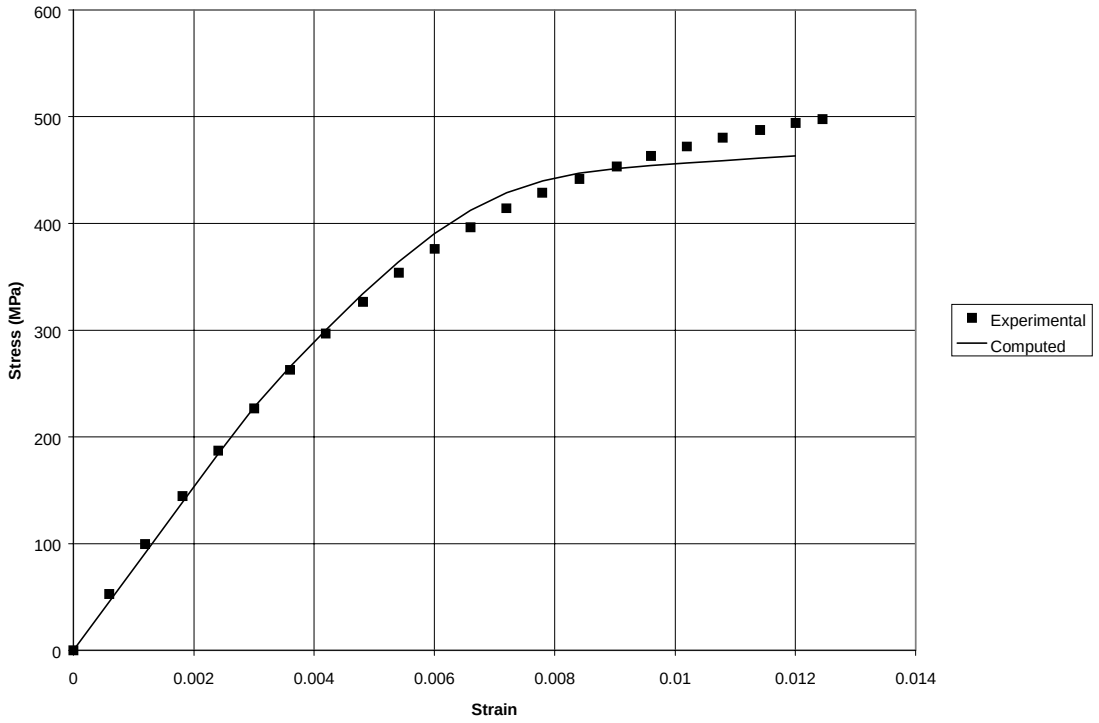

Figure 4.3: Model Correlations for [10°] IM7/977-2 Laminate

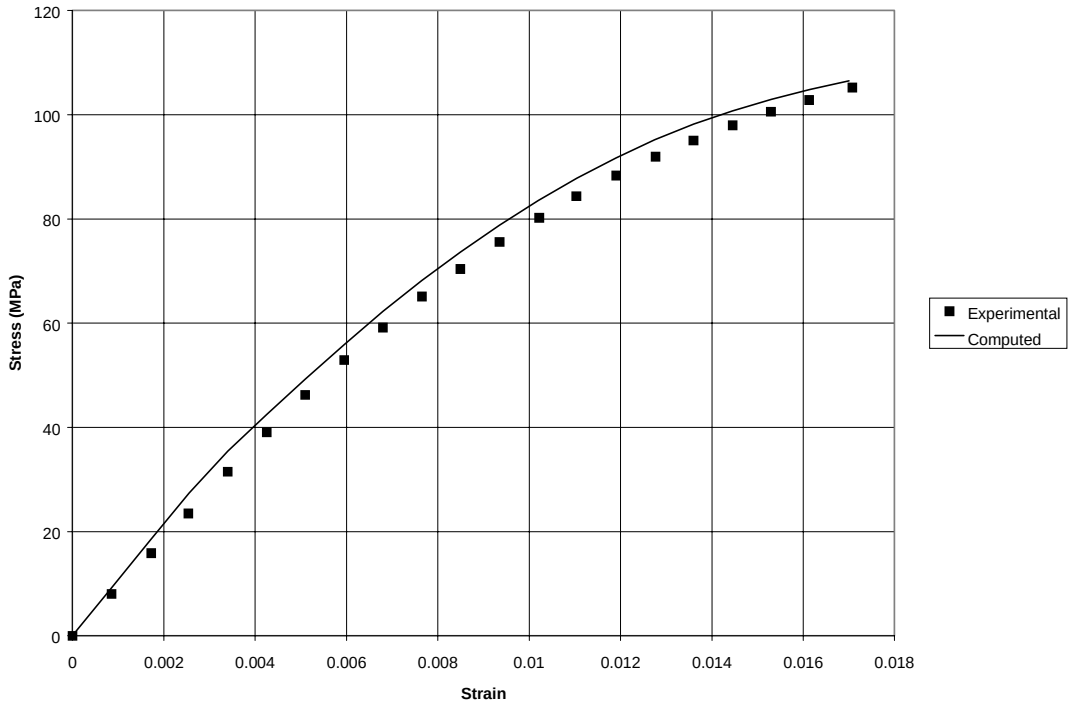

Figure 4.4: Model Predictions for [45°] IM7/977-2 Laminate

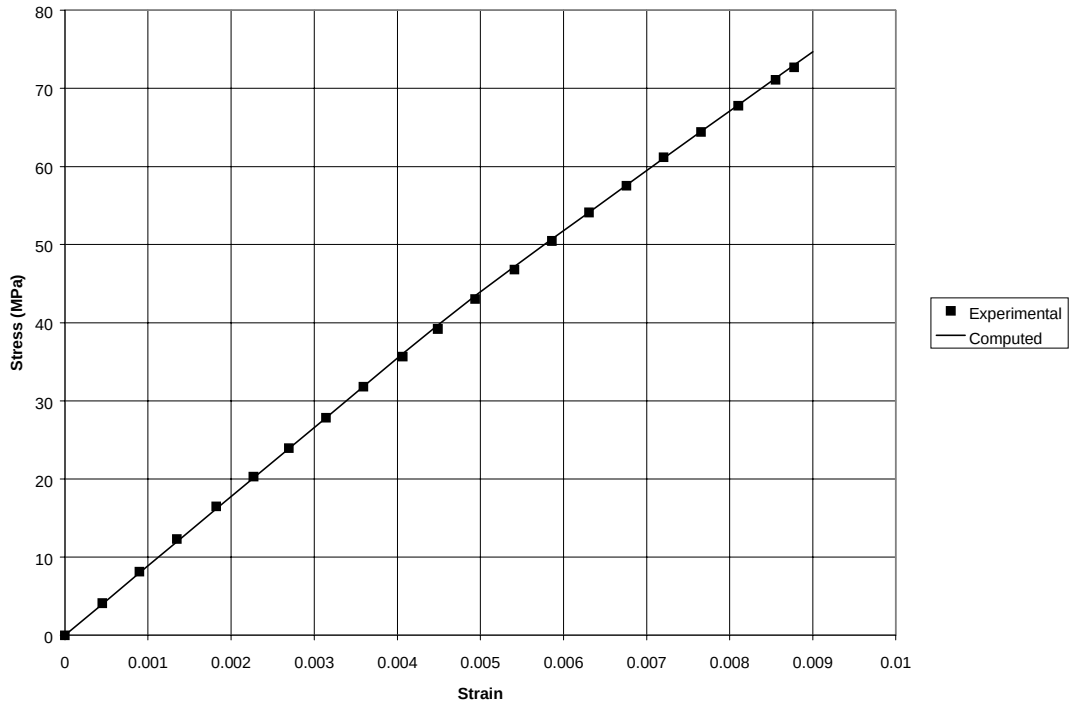

Figure 4.5: Model Predictions for [90°] IM7/977-2 Laminate

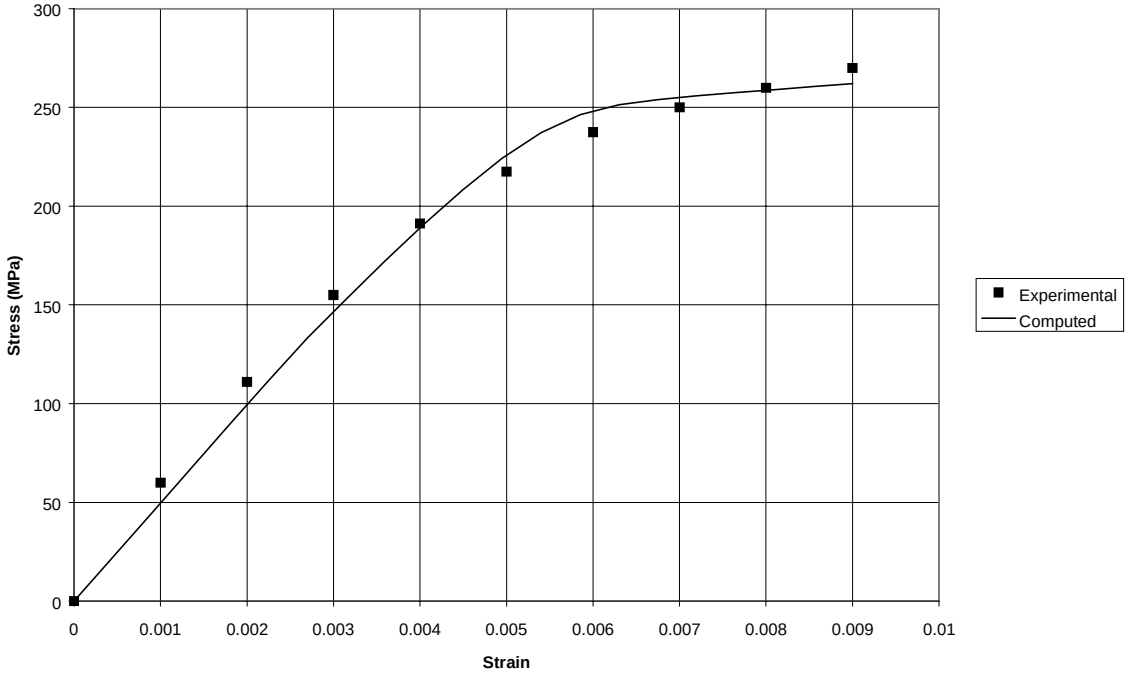

Figure 4.6: Model Correlations for [14°] AS4/PEEK Laminate at Strain Rate of $1x10^{-5}$ /sec

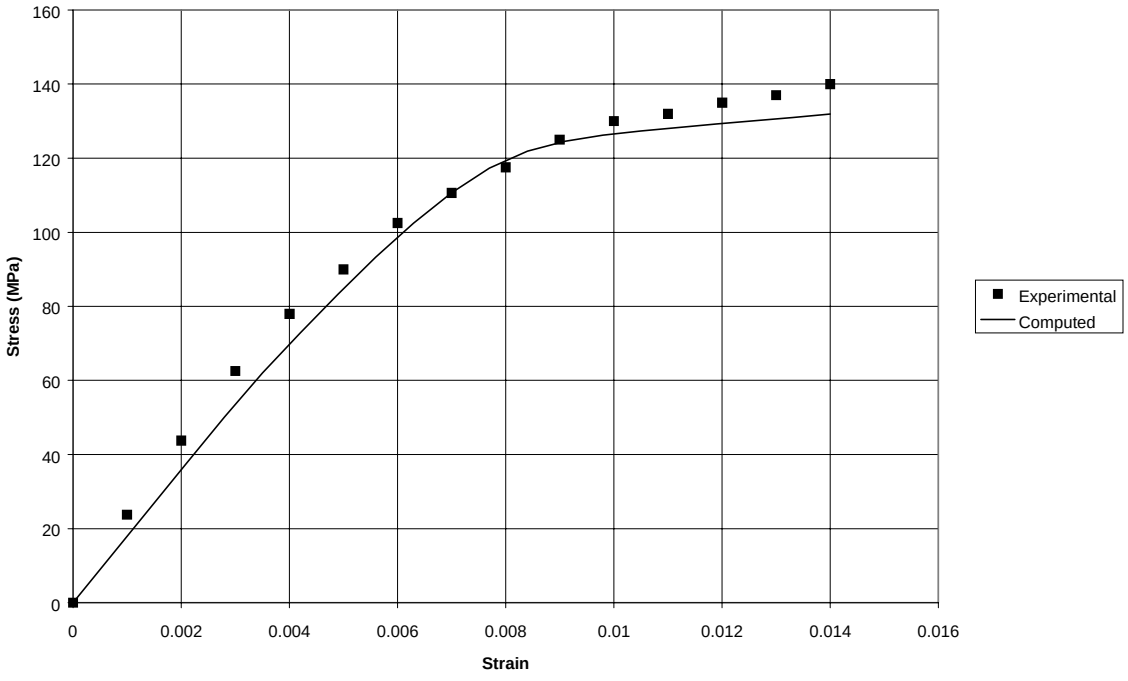

Figure 4.7: Model Predictions for [30°] AS4/PEEK Laminate at Strain Rate of $1x10^{-5}$ /sec

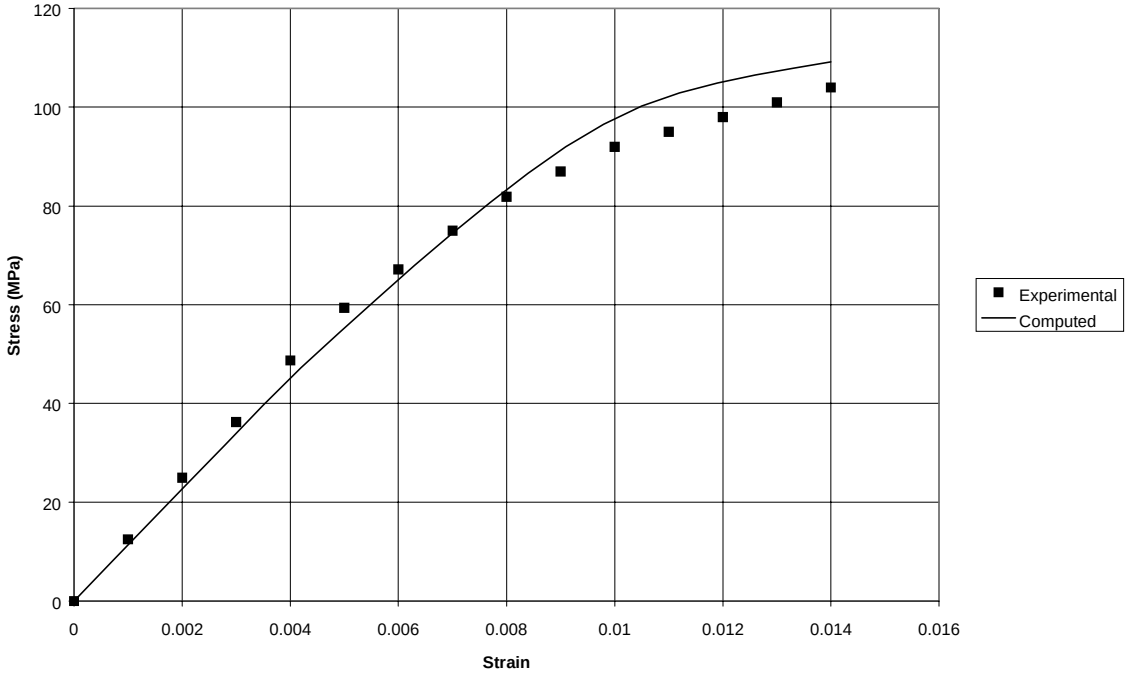

Figure 4.8: Model Predictions for [45°] AS4/PEEK Laminate at Strain Rate of $1x10^{-5}$ /sec

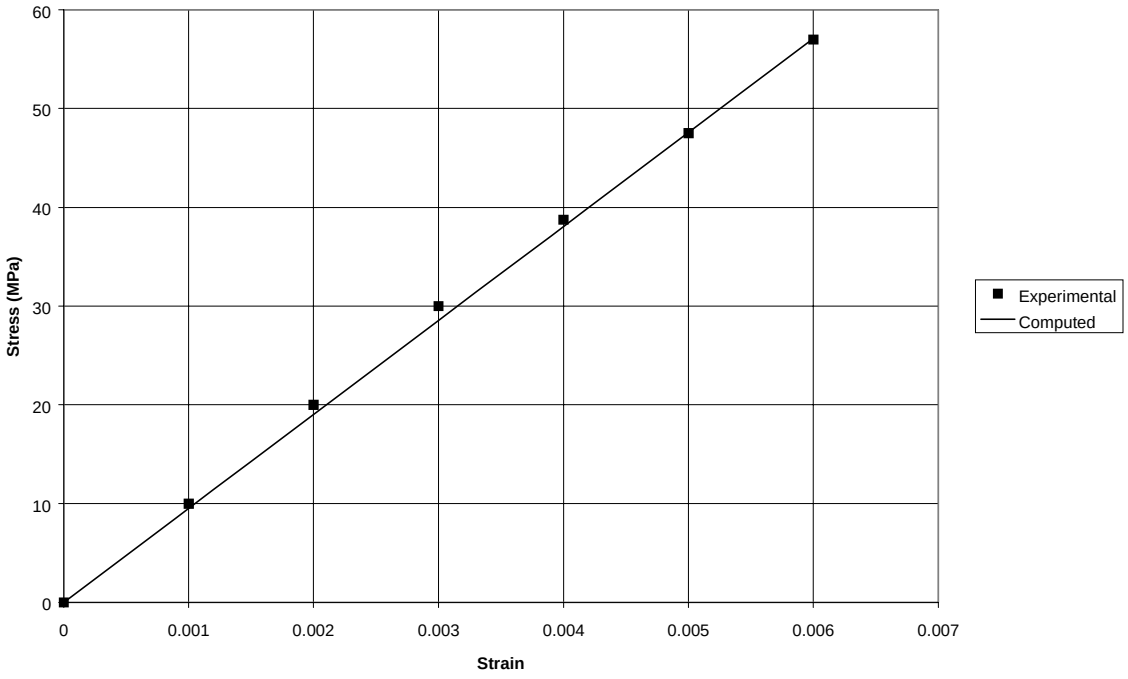

Figure 4.9: Model Predictions for [90°] AS4/PEEK Laminate at Strain Rate of $1x10^{-5}$ /sec

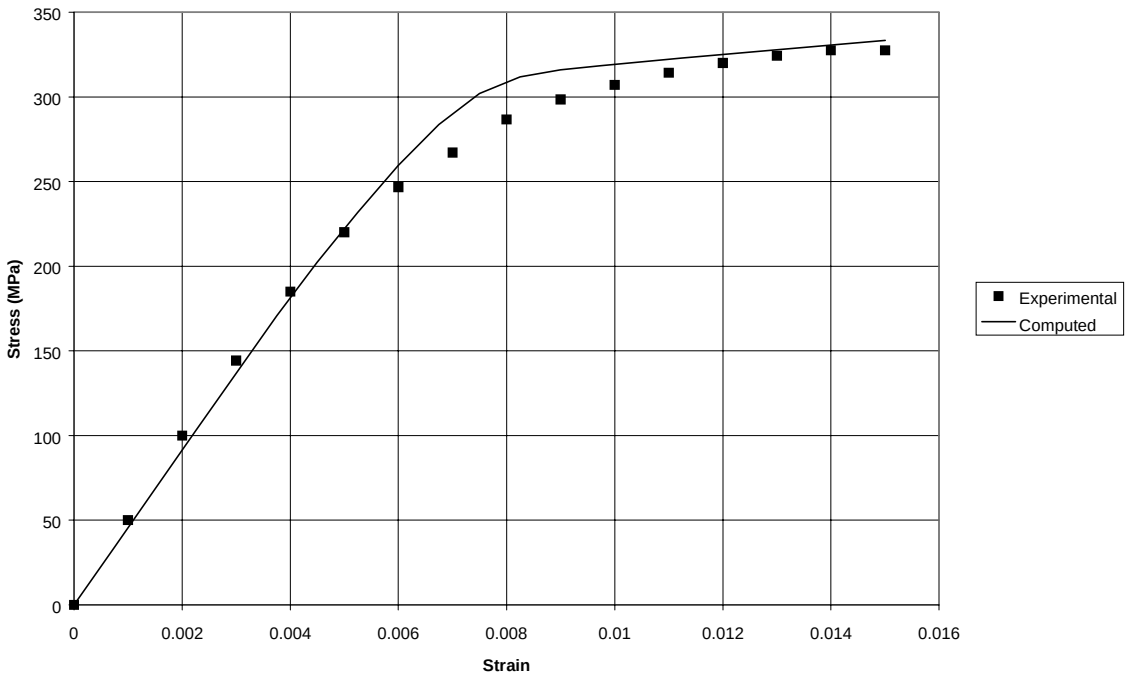

Figure 4.10: Model Correlations for [15°] AS4/PEEK Laminate
at Strain Rate of 0.1 /sec

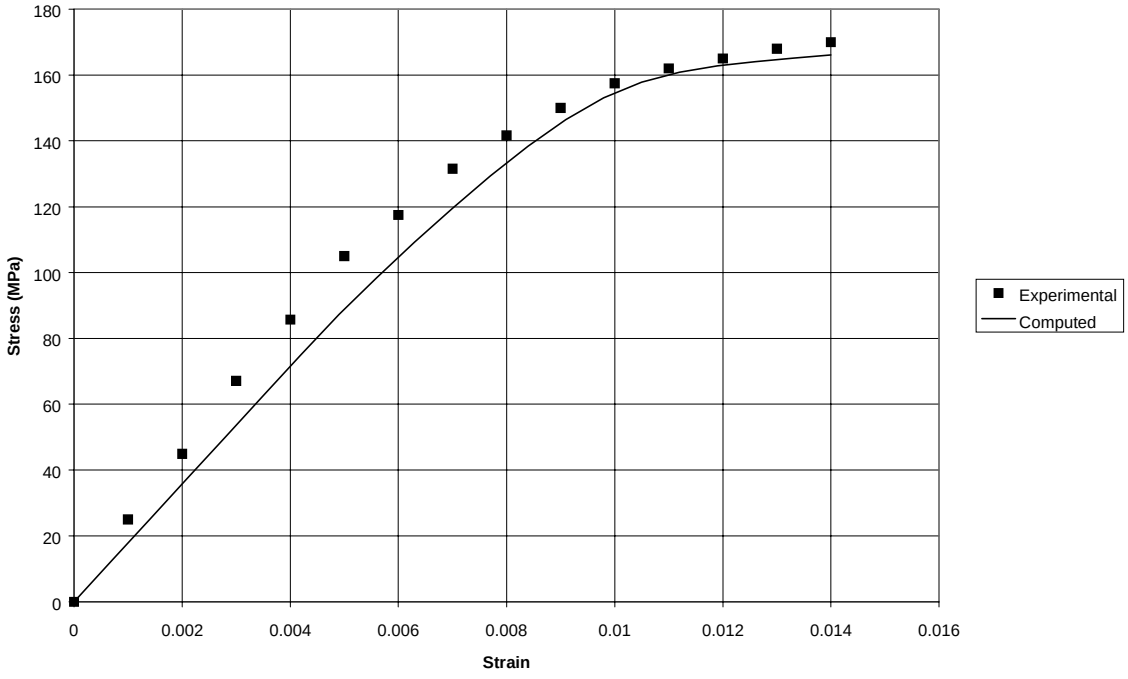

Figure 4.11: Model Predictions for [30°] AS4/PEEK Laminate
at Strain Rate of 0.1 /sec

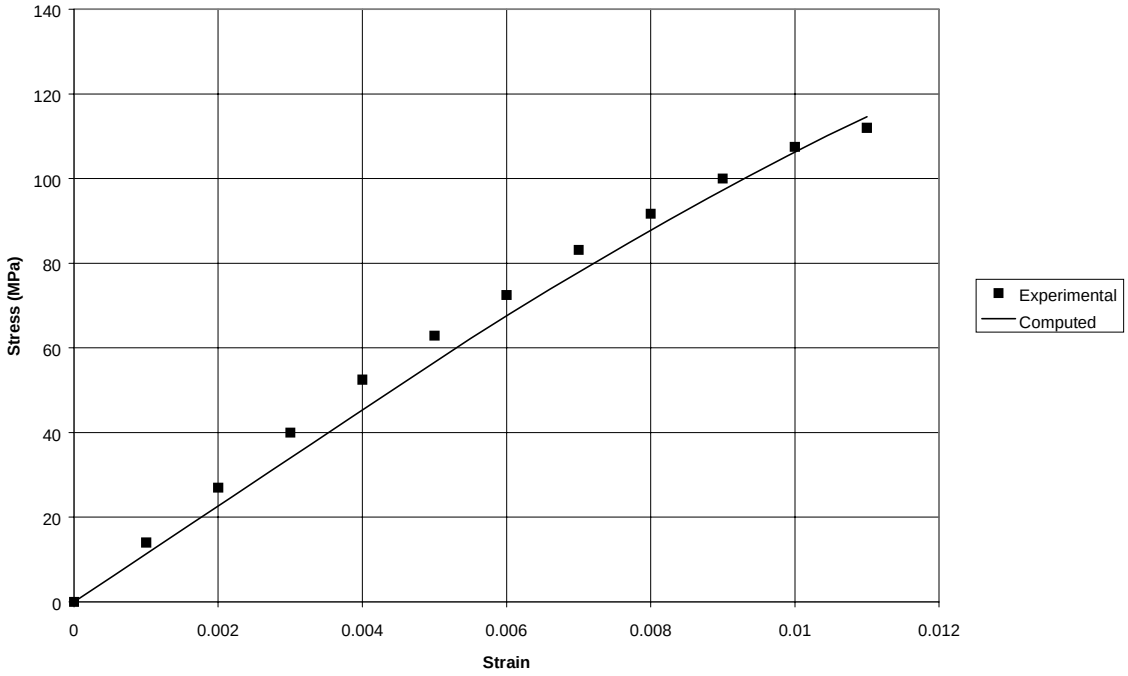

Figure 4.12: Model Predictions for [45°] AS4/PEEK Laminate
at Strain Rate of 0.1 /sec

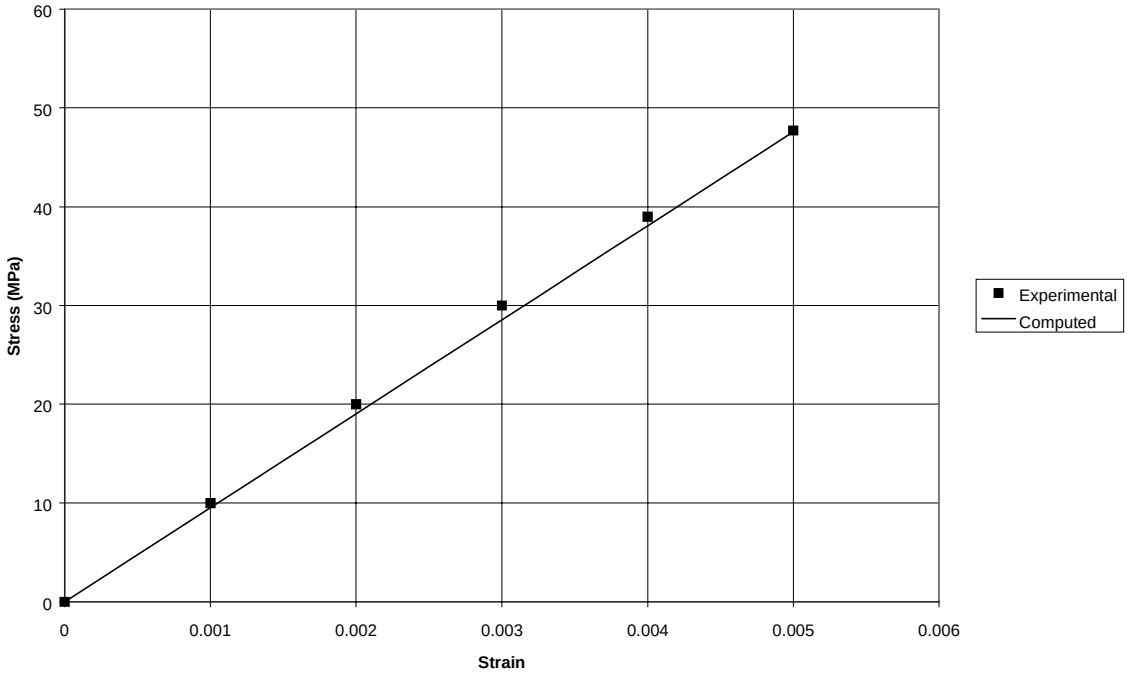

Figure 4.13: Model Predictions for [90°] AS4/PEEK Laminate
at Strain Rate of 0.1 /sec

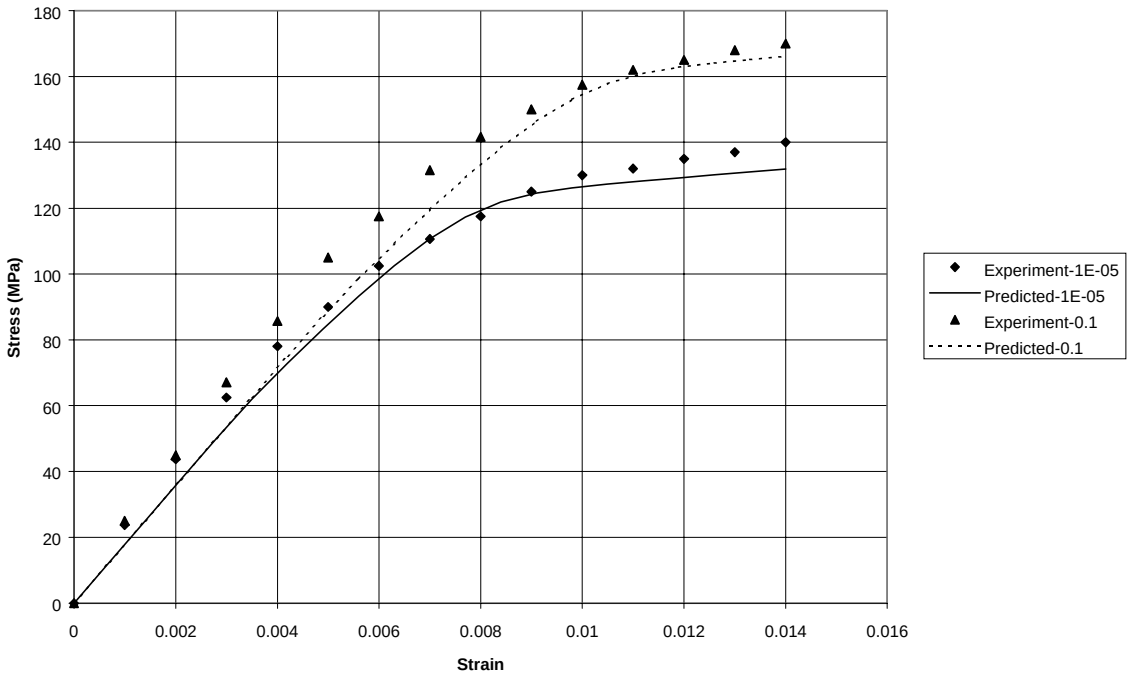

Figure 4.14: Prediction of Strain Rate Dependence of [30°] AS4/PEEK Laminate.

CHAPTER 5
PLY STRENGTH MODEL

The implementation of a ply failure model into the micromechanics equations developed in the last chapter will be presented next. An overview of the methodology used to predict ply ultimate strength will be given. The Hashin failure criterion, which was used in this study, will be described in detail. The ultimate strengths for the representative polymer matrix composites analyzed in the previous chapter will be predicted for a variety of fiber orientations and strain rates.

5.1 Overview

In order to develop structural level penetration and failure models that can be applied to high strain rate impact applications, ply level failure needs to be accurately predicted. As discussed in the background section of this report, previous researchers have developed a variety of ply level failure models. For this work, ply level failure due to local failure mechanisms was predicted based on macroscopic stresses and strengths. In particular, the Hashin failure model [50] was utilized in this work. As discussed earlier, some researchers such as Pecknold and Rahman [59] have utilized constituent level stresses to predict ply failure based on local failure mechanisms. However, for this study, ply level strength data were more readily available and considered to be more reliable than constituent level strength data. Nonetheless, in considering the ultimate future application of the ply strength models, the ability to account for and predict local failure mechanisms in at least an approximate manner was desired.

Since only ply level failure based on simple tensile tests was considered at this time, property degradation models were not utilized. For structural level modeling, the ability to only degrade certain material properties based on the local ply failure mechanisms would be desirable to provide improved simulation of stress transfer mechanisms. Furthermore, in implementing the model into a finite element code, a gradual degradation of the material properties might improve the stability of the finite element analysis. Since the failure model utilized in this study predicted failure based on approximations of local failure mechanisms, the eventual incorporation of property degradation models would be possible.

5.2 Hashin Failure Criteria

For this work, the Hashin failure criteria were utilized [50]. These criteria predicted ply level failure based on local mechanisms using macroscopic stresses and strengths. These criteria were based on stresses and strengths in the principal axes of the material, so appropriate transformations [24] were carried out to convert stresses from the structural axis system to the principal material axis system. Since the composites analyzed in this study were only subject to in plane loading and the out-of-plane stresses were found to be relatively small, the plane stress approximation to the Hashin model was utilized. However, in the future study of impact problems, where the out-of-plane stresses will be significant, three-dimensional versions of the criterion are available and will be used [50].

The Hashin criteria were based on quadratic combinations of stresses and strengths. Quadratic equations were chosen in order to provide the best approximation to the failure surface while still allowing for a relatively simple model [50]. Ply failure based on fiber tensile failure, fiber compressive failure, matrix tensile failure and matrix compressive failure was predicted separately. In each of the separate criteria, failure was considered to have occurred if the value of the expression is greater than one (1). For the purposes of this study, once failure in any of the failure modes was detected, total composite failure was considered to have occurred. In actuality, particularly for matrix dominated failure modes, the composite could withstand load after the "failure" load has occurred. However, for the simple uniaxial off-axis laminate configurations examined in this study, final composite failure was assumed to occur shortly after initial matrix cracking takes place, therefore only the initial failure load was predicted.

Failure criteria for each of the local failure modes were as follows. In each of the expressions, σ_{ij} was the macroscopic stress component, X_T was the ply tensile strength in the longitudinal (fiber) direction, and X_C was the compressive strength in the longitudinal direction. Furthermore, Y_T was the tensile strength in the transverse direction (perpendicular to the fiber in the plane of the composite), Y_C was the compressive strength in the transverse direction, and X_S was the ply in-plane shear strength. Failure was assumed to occur when the value of the strength expression became greater than or equal to one (1). Tensile fiber failure was predicted by using the following expression:

$$\left(\frac{\sigma_{11}}{X_T}\right)^2 + \left(\frac{\sigma_{12}}{X_S}\right)^2 = 1 \tag{5.1}$$

Compressive fiber failure was predicted using the following equation. Shear stresses were not included in the failure criterion since Hashin was unsure whether shear stresses increased or decreased the compressive strength. Therefore, the effects of shear stresses were neglected [50].

$$\frac{|\sigma_{11}|}{X_C} = 1 \tag{5.2}$$

Tensile matrix failure was predicted using the following expression:

$$\left(\frac{\sigma_{22}}{Y_T}\right)^2 + \left(\frac{\sigma_{12}}{X_S}\right)^2 = 1 \tag{5.3}$$

Compressive matrix failure was predicted as follows:

$$\left(\frac{\sigma_{22}}{2X_S}\right)^2 + \left[\left(\frac{Y_C}{2X_S}\right)^2 - 1\right]\frac{\sigma_{22}}{Y_C} + \left(\frac{\sigma_{12}}{X_S}\right)^2 = 1 \tag{5.4}$$

5.3 Verification Analyses

In order to verify the capabilities of the failure criteria as implemented into the composite micromechanics equations, the IM7/977-2 and AS4/PEEK composites considered in the last chapter were analyzed. The ply failure stresses were predicted for various fiber orientation angles and strain rates.

5.3.1 IM7/977-2 Composite

To verify the ply strength model, the IM7/977-2 composite considered in the last chapter was analyzed. For the IM7/977-2 system, the longitudinal tensile strength was 2300 MPa [67], the longitudinal compressive strength was 900 MPa [80], the transverse tensile strength was 73 MPa [67] and the shear strength was 85 MPa [67]. Due to a lack of data, the transverse compressive strength was assumed to be twice the transverse tensile strength. To compute the in-plane shear strength, the failure stress of a $[\pm 45°]_s$ laminate was divided by two (2), which is a standard procedure for determining shear strength [78]. The predicted and experimental [67] failure strength values for [10°] and [45°] laminates for the IM7/977-2 material system are shown in Table 5.1. Note that the experimental values of the failure stresses likely have some scatter, but the statistical data were not available. For both laminates considered, failure was predicted to be due to tensile matrix failure. The "failure stress" stated in Table 5.1 and all remaining tables was the longitudinal stress in the structural axis system (along the loading direction) at which failure was predicted to occur. However, all of the stress components were used in applying the Hashin failure criteria.

As can be seen in Table 5.1, for both fiber orientations the predicted failure stresses compared favorably to the experimental values, and most likely fell within the experimental scatter. These results indicated that the presented failure criteria produced accurate results for a variety of fiber orientations. However, more strength tests should be conducted over a wider range of strain rates to fully verify the model.

5.3.2 AS4/PEEK Composite

The ply strengths of the AS4/PEEK composite studied in the last chapter were also predicted. For this material, only quasi-static strength data were available. Ply shear strength data that provided an acceptable correlation with the available experimental results were not available. Furthermore, transverse stresses predicted using the deformation model for off-axis composite layers (such as [30°] and [45°] laminates) were greater than the transverse strengths indicated by the Weeks and Sun [25] data shown in Figures 4.9 and 4.13. Therefore, these values were not used for the transverse strengths.

Figures 4.9 and 4.13 indicated that the transverse modulus did not appear to vary with strain rate for this material, indicating that the transverse strengths were also rate independent. For a carbon fiber reinforced polymer matrix composite, longitudinal strengths have been found to be rate independent [7]. Therefore, for this study, the longitudinal and transverse strengths for the AS4/PEEK system were assumed to be rate independent. However, as can be seen from Figures 4.6-4.8 and Figures 4.10-4.12, for off-axis fiber orientations the strengths appeared to be rate dependent. Therefore, for this study, the shear strength was assumed to be rate dependent and the cause of the rate dependence seen in the strengths of the off-axis laminates.

For the AS4/PEEK material, a longitudinal tensile strength of 2070 MPa was used [81], and the transverse tensile strength was set to 83 MPa [81]. The longitudinal compressive strength was set equal to one-half of the longitudinal tensile strength, and the transverse compressive strength was again assumed equal to twice the transverse tensile strength, based on representative composite data [78]. The shear strength values were computed by correlating results from the [15°] laminates (Figures 4.6 and 4.8). From this information, the shear strength for a strain rate of $1x10^{-5}$ /sec was determined to be 63 MPa, and the shear strength for a strain rate of 0.1 /sec was determined to be 88 MPa. All of these strength values likely had some scatter, but the statistical data were not available.

Failure stresses were predicted for the [30°] and [45°] laminates for strain rates of $1x10^{-5}$ /sec and 0.1 /sec. The predicted and experimental results for a strain rate of $1x10^{-5}$ /sec are shown in Table 5.2, and the results for a strain rate of 0.1 /sec are shown in Table 5.3. In all cases, failure was predicted to be due to tensile matrix failure.

For both strain rates and both fiber orientations considered, the comparison between the predicted and experimental values was quite good and most likely within the experimental scatter. The results indicated that the failure criteria were able to predict ply failure for a variety of fiber orientations and strain rates. The results for AS4/PEEK also indicated that even when some approximations were required in determining the ply failure stresses, reasonable results could still be obtained.

5.4 Summary

The Hashin failure criteria were implemented into the composite micromechanics equations in order to predict the ply failure stresses in polymer matrix composites. The failure criteria predicted ply ultimate strengths by using quadratic combinations of macroscopic stresses and ply strengths to approximate local failure mechanisms. Equations were available to predict ply failure based on fiber tensile or compressive failure, or matrix tensile or compressive failure. Verification studies were conducted using two representative polymer matrix composites. The results for the IM7/977-2 system showed that if good macroscopic strength data can be obtained, ply ultimate strengths could be reasonably predicted with no approximations required. The results for the AS4/PEEK material, on the other hand, demonstrated that even if some approximations in the ply failure strengths were required, reasonable results could still be obtained. The AS4/PEEK calculations also provided preliminary indications that the rate dependence of ply strengths can be predicted. However, final application of the Hashin model will require developing expressions for determining the transverse and shear strengths as a function of strain rate. Strength tests conducted over a wide range of strain rates will help to accomplish this goal. The predictions for both material systems showed that the ply ultimate strength could be accurately determined for a variety of fiber orientation angles.

Table 5.1
Failure Stress Predictions for IM7/977-2 Laminate

	Predicted Failure Stress (MPa)	Experimental Failure Stress (MPa)
[10°] Laminate	480	500
[45°] Laminate	100	105

Table 5.2
Failure Stress Predictions for AS4/PEEK at Strain Rate of $1x10^{-5}$ /sec

	Predicted Failure Stress (MPa)	Experimental Failure Stress (MPa)
[30°] Laminate	130	140
[45°] Laminate	98	104

Table 5.3
Failure Stress Predictions for AS4/PEEK at Strain Rate of 0.1 /sec

	Predicted Failure Stress (MPa)	Experimental Failure Stress (MPa)
[30°] Laminate	165	170
[45°] Laminate	114	112

CHAPTER 6
FINITE ELEMENT IMPLEMENTATION

The polymer constitutive equations and the composite micromechanics model described in earlier chapters were implemented into LS-DYNA, a commercially available transient dynamic finite element code. In this chapter, an overview of LS-DYNA and the user defined material option will be given. The transformation of the polymer constitutive equations and the composite micromechanics model into an incremental form will be described. Verification studies conducted using the PEEK thermoplastic and the AS4/PEEK composite discussed in previous chapters will be presented.

6.1 Overview

In order to simulate the impact response of a composite structure, the ultimate long term goal of this research, finite element methods are required. With that goal in mind, the matrix constitutive equations and the composite micromechanics model described in previous chapters were implemented into LS-DYNA, a commercially available transient dynamic finite element code [82]. LS-DYNA uses explicit central difference integration methods to integrate the rate equations.

LS-DYNA had several material options for the analysis of composite materials. However, all of these models were for strain rate independent material response. Furthermore, only limited abilities to model nonlinearities in shear were present in the models, based on the Chang and Chang model [52,53].

LS-DYNA had a user defined material option that allowed users to implement material models that were not included with the finite element package. To use this option, a FORTRAN subroutine would be created which could then be linked to the finite element code. In the subroutine, strain increments for the current time step were passed in from the main program. Stresses and other history variables (such as state variables) from previous time steps were also available to the subroutine. From this information, the user defined material subroutine computed the stress increments, total stresses, and values of the history variables at the end of the current time increment.

6.2 Incremental Form of Polymer Constitutive Equations

To implement the polymer constitutive model discussed earlier into an LS-DYNA user defined material subroutine, the equations were converted into an incremental format. Specifically, Equations (3.7), (3.19) and (3.20) were adjusted so that increments in inelastic strain, internal stress and effective inelastic strain were computed instead of their corresponding rates. Rocca and Sherwood [62] implemented a version of the Ramaswamy-Stouffer constitutive equations into LS-DYNA to analyze the rate dependent inelastic deformation of polycarbonate. Their methodology was used as the basis for implementing the constitutive model described in this report. Rocca and Sherwood designed their user designed material subroutine to be used with plane stress shell elements. The same plane stress assumptions were used in the model implementation discussed here to maintain consistency with the implementation of the composite

micromechanics equations discussed later in this report. Maintaining the plane stress assumption for the polymer constitutive equations facilitated verification of the model.

To convert the flow equation (Equation (3.7)) into an incremental form, the rate equation was multiplied by the time increment Δt of the current time step to compute the inelastic strain increment $\Delta\varepsilon_{ij}^{I}$. The resulting equation was as follows:

$$\Delta\varepsilon_{ij}^{I} = D_o \exp\left[-\frac{1}{2}\left(\frac{Z_o^2}{3K_2}\right)^n\right] * \frac{S_{ij} - \Omega_{ij}}{\sqrt{K_2}} * \Delta t \tag{6.1}$$

where all of the terms were as defined earlier. Note that the total value of the deviatoric stress components and the internal stress components were used instead of the stress increments, and were the values from the previous time step. Equations (3.19) and (3.20) were modified to compute the increment in internal stress, $\Delta\Omega_{ij}$, and the increment in effective inelastic strain, $\Delta\varepsilon_e^I$. The following equations resulted:

$$\Delta\Omega_{ij} = \frac{2}{3} q\Omega_m \Delta\varepsilon_{ij}^{I} - q\Omega_{ij}\Delta\varepsilon_e^{I} \tag{6.2}$$

$$\Delta\varepsilon_e^{I} = \sqrt{\frac{2}{3}\Delta\varepsilon_{ij}^{I}\Delta\varepsilon_{ij}^{I}} \tag{6.3}$$

and all the terms in the equations were as defined earlier. In Equation (6.2), the total value of the back stress from the previous time increment was used in computing the stress increment for the current time step.

By examining Equations (6.1)-(6.3), one can notice that in many respects the transformation of the rate equations into an incremental format was carried out by applying forward Euler numerical integration methods [65]. While very simple equations resulted from this process, the forward Euler method would not be as accurate as other methods, particularly for stiff differential equations. As will be discussed in the analysis section of this chapter, using this simple approximation to integrate the rate equations lead to some discrepancies in the numerical results.

6.3 Numerical Implementation of Polymer Constitutive Equations

The incremental form of the polymer constitutive equations was incorporated into LS-DYNA through the use of a user defined material subroutine. As a first step, only the polymer constitutive equations were implemented and tested. The composite micromechanics equations were added once the constitutive model was verified to be programmed in correctly.

In the user defined subroutine, the stresses, deviatoric stresses and internal stresses from the previous time step, along with the strain increment for the current time step, were passed into the routine. The material properties were also read in from the LS-DYNA input file. The inelastic strain components for the current time step were computed by taking the inelastic strain rate determined in the previous time step, and multiplying it by the current time increment, as

suggested by Equation (6.1). The effective inelastic strain increment was computed using Equation (6.3).

For the shell element formulation, the through-the-thickness strain increment $\Delta\varepsilon_{33}$ was computed using the following expression:

$$\Delta\varepsilon_{33} = \frac{-\nu}{1-\nu}\left(\Delta\varepsilon_{11}^{E} + \Delta\varepsilon_{22}^{E}\right) + \Delta\varepsilon_{33}^{I} \tag{6.4}$$

where ν was the Poisson's ratio and $\Delta\varepsilon_{ij}^{E}$ was the elastic component of the strain increment. From this information, the mean and deviatoric strain increments were computed using standard definitions [24]. The elastic component of the deviatoric strain increment was determined by assuming that the inelastic portion of the deviatoric strain increment was equal to the inelastic strain increment [62]. This assumption neglected volume effects, which might be significant for the polymers considered in this study. Once the strain increments were computed, the stress increments and the deviatoric stress increments were calculated. The total stresses and total deviatoric stresses for the current time step were computed by adding the stress increments to the total stresses from the previous time step.

The internal stress increment was computed using Equation (6.2), and this value was added to the total internal stress from the previous time step to determine the total internal stress for the current time step. Equations (3.7) and (3.9-3.18) were used to compute the inelastic strain rate components for the current time step. The inelastic strain rates, deviatoric stresses and internal stresses were then stored in history variables to be used in future time steps.

6.4 Verification Analyses for Polymer Constitutive Equations

To test the implementation of the polymer constitutive equations, the tensile response of the PEEK material analyzed in previous chapters was computed. The elastic and inelastic material properties for PEEK are given in Table 3.2. The tensile stress-strain curves at constant strain rates of 0.1 /sec and 1.0 /sec were simulated using LS-DYNA. While these strain rates were slightly above the strain rate range for which the material was characterized, they were considered to be low enough for the material constants to still be valid. However, LS-DYNA was designed to be utilized for high strain rate applications, and sometimes had stability and convergence problems at lower strain rates [82]. The strain rates used for these analyses were chosen to be high enough to hopefully minimize these difficulties, but low enough to ensure validity of the material constants. The relatively low strain rates used for the analyses could still be a cause for any discrepancies in the computed results, as the integrator might not work well for low strain rates.

For the finite element model, four noded shell elements were used in a square mesh, ten elements on a side as is shown in Figure 6.1. Each side of the model was 20 mm long. The left hand side of the model was clamped, and a constantly increasing specified displacement was applied to the right hand side of the model. These boundary conditions were chosen in order to simulate a constant strain rate tensile test. The displacements applied at each time were computed by taking the constant strain rate, multiplying it by the current time to obtain total strain, and multiplying this value by the total length of the model to compute an average displacement. The finite element model was designed to simulate the behavior of the polymer at an infinitesimal material point. A model of this type was used instead of attempting to model the

actual specimen in order to facilitate comparison of the finite element results to the results computed using stand alone computer codes. A mesh convergence study showed that the mesh was adequate. To generate a stress-strain curve, results were read in from several elements at the center of model, in order to avoid edge effects.

Stress-strain curves computed at a strain rate of 0.1 /sec are shown in Figure 6.2, and tensile curves computed at a strain rate of 1.0 /sec are shown in Figure 6.3. In the figures, results computed using LS-DYNA (labeled "Finite Element" in the figures) were compared to results computed using the stand-alone computer code described in Chapter 3 (labeled "Analytical" in the figures). Note, however, that since the strain rates considered here were higher than those examined in the earlier analyses, the computed stresses were higher than those shown in Figures 3.6-3.8. Since all of the elements in the center of the finite element model had approximately equal stresses, only one curve is shown for the finite element results.

As can be seen in the figures, for both strain rates the finite element results compared reasonably well to the results computed using the stand-alone computer code. The nonlinearity and rate dependence of the tensile curves was captured by the finite element analysis. The finite element computations predicted somewhat higher stresses than the stand-alone code, particularly in the inelastic range. There were two possible causes for this discrepancy. First of all, as mentioned earlier the conversion of the constitutive equations to an incremental form used forward Euler types of approximations, which were less accurate than other types of integration methods, particularly for the stiff equations used here. In addition, the strain rates at which the analyses were conducted were significantly lower than is usually recommended for an LS-DYNA analysis. These factors most likely combined to cause the discrepancies seen in the analyses. As will be discussed in a later section of this report, these effects were most likely even more significant when the polymer constitutive equations were implemented into the composite micromechanics. Further discussion of the causes of the discrepancies will be presented in the section describing the verification analyses for the LS-DYNA implementation of the composite micromechanics equations.

6.5 Incremental Form of Composite Micromechanics Equations

The general format of the micromechanics equations as implemented into LS-DYNA were the same as discussed in Chapter 4. However, one difference was that in the user defined material subroutine stress increments were computed in each subcell using strain increments and inelastic strain increments. This is different from the stand-alone code described earlier, in which total stresses were computed based on total strains and total inelastic strains. Furthermore, for the LS-DYNA implementation a plane stress condition was assumed on the macroscopic unit cell level, and shell elements were used in the finite element analyses. The plane stress condition was assumed since the use of shell elements in LS-DYNA simplified the analysis of laminated composite material as compared to using solid elements. However, within the subcells of the composite unit cell, a full three-dimensional stress state was still permitted. The macroscopic through-the-thickness strain increment, $\Delta\varepsilon_{33}$, was computed using the following expression [36]:

$$\Delta\varepsilon_{33} = \frac{-C_{13}}{C_{33}}\left(\Delta\varepsilon_{11} - \Delta\varepsilon_{11}^{I}\right) - \frac{C_{23}}{C_{33}}\left(\Delta\varepsilon_{22} - \Delta\varepsilon_{22}^{I}\right) + \Delta\varepsilon_{33}^{I} \tag{6.5}$$

where $\Delta\varepsilon_{ij}$ was the strain increment, $\Delta\varepsilon_{ij}^{I}$ was the effective inelastic strain increment, and C_{ij} represented terms in the macroscopic elastic stiffness matrix. The relationship between the elastic stiffness matrix components and engineering constants such as modulus and Poisson's ratio was found in standard texts such as [36,47]. The effective inelastic strain increment was determined by multiplying the effective inelastic strain rate by the value of the time increment Δt, similar to what was described in Equation 6.1.

6.6 Numerical Implementation of Composite Micromechanics Equations

The incremental form of the composite micromechanics equations was once again implemented into LS-DYNA through the use of a user defined material subroutine. In the user defined routine, the macroscopic strain increments for the current time step, and the stresses and internal stresses for each subcell from the previous time step, were passed into the routine, along with the material properties. The through-the-thickness strain increment was computed using Equation 6.5. The inelastic strain increments were computed by multiplying the inelastic strain rates by the value of the time increment.

The stress increments and total stresses for each subcell were computed using the composite micromechanics equations, and the total stresses for the unit cell were determined using the uniform stress and uniform strain assumptions described earlier. The inelastic strain rate and internal stress for each subcell was determined using the incremental form of the polymer constitutive equations. The effective inelastic strain rates for the unit cell were calculated using Equations (4.59)-(4.64). The inelastic strain rates, internal stresses and total stresses for each subcell were stored in history variables for use in future time steps.

6.7 Verification Analyses for Composite Micromechanics Equations

The implementation of the composite micromechanics equations was tested by analyzing the AS4/PEEK composite considered in Chapter 4. Unidirectional composites with fiber orientations of [15°], [30°], [45°] and [90°] were once again considered. A constant strain rate of 0.1 /sec was applied to the finite element model. This strain rate was once again significantly lower than was usually recommended for an LS-DYNA analysis. However, this strain rate was within the range for which the PEEK material was characterized, and there were experimental data available at this strain rate. The material properties of the AS-4 fibers are given in Table 4.1, and the elastic and inelastic properties of the PEEK thermoplastic are once again given in Table 3.2.

The finite element model shown in Figure 6.1 was once again used. The boundary conditions described in the analysis of the pure PEEK material were applied to the model. An important point to note is that for the off-axis fiber orientation angles, the boundary conditions did not truly represent the periodicity conditions required to simulate the deformation response of a material point. However, periodic boundary conditions would have been overly difficult to apply to the model. The fiber orientation angle was specified in the shell element definition of the LS-DYNA input deck. To generate the stress-strain curves, results were read in from elements 45-47 and 55-57 of the model (see Figure 6.1). These elements, near the center of the model, were chosen in order to minimize edge effects and to minimize to the greatest extent possible the effects of the boundary conditions.

The computed stress-strain curves are shown in Figures 6.4-6.7. In each figure, results predicted by the finite element analyses were compared to the experimental values obtained by Weeks and Sun [25]. For the [30°] and [45°] laminates, the predicted finite element results varied significantly from element to element, even in the center of the model. This variation was most likely due to the nature of the approximate boundary conditions that were applied. Therefore, results from several elements were plotted in the figures. The elements that were used to generate each curve were listed in the legend of each figure. The results from the elements that are not plotted fell within the bounds given by the plotted curves. The actual tensile response, if proper boundary conditions were applied, would most likely have fallen within the bounds of the plotted curves.

As can be seen in the figures, for all of the fiber orientations the elastic portion of the deformation response was predicted quite well by the finite element analyses. However, the stresses in the inelastic range were overpredicted when compared to the experimental values. Furthermore, as can be seen in the results for the [15°] and [30°] laminates, once saturation was about to occur, the finite element results became somewhat unstable, with the total stresses beginning to rise with increasing strain.

There were several possible causes for the discrepancies seen in the predictions of the inelastic stresses. First of all, the fact that the applied boundary conditions did not truly represent proper periodic boundary condition most likely affected the results. For the off-axis fiber orientations, the response of the finite element model was not truly representative of the response of an infinitesimal material point. In addition, since the value of the material constant β was determined empirically, some modification of this value might be required.

More significant explanations for the discrepancies between the experimental and predicted results, however, related to the nature of the incremental formulation of the polymer constitutive equations. As discussed earlier, in the analyses of the pure PEEK thermoplastic the inelastic stresses were somewhat overpredicted. The reasons for those discrepancies were hypothesized to be due to both the low strain rate which was used for the analysis and the method used to integrate the rate equations in the polymer constitutive model. Furthermore, in the analyses of the pure PEEK material, an essentially uniaxial stress state was applied to the material. For the composite, on the other hand, the polymer was in a fully multiaxial stress state, which might have magnified any discrepancies and instabilities in the analysis.

To further explore the effects of the integration method used on the rate equations in the polymer constitutive model, the implementation of the equations was revised. Specifically, each time step was broken down into ten equally spaced “substeps” within the user defined material subroutine. The Euler integration was then carried out for each “substep” in the analysis. By reducing the size of the time step over which each integration was performed, the accuracy of the computations should improve. Specifically, the methodology described in Section 6.6 was again utilized. However, each calculation was carried out ten times for each time step, using time and strain increments equal to one-tenth of the time and strain increments passed into the routine.

Finite element analyses were carried out on the [15°] and [30°] AS4/PEEK laminates at a strain rate of 0.1 /sec using the revised equation formulation, and the results are shown in Figures 6.8 and 6.9. By comparing Figure 6.8 to Figure 6.4, and by comparing Figure 6.9 to Figure 6.5, the observation can be made that revising the method used to integrate the polymer constitutive equations improved the results both qualitatively and quantitatively. These results indicated that the method used to integrate the rate equations in the finite element implementation could significantly affect the results. However, since the revised algorithm significantly increased the

execution time of the analysis, more sophisticated integration methods need to be implemented in the future. However, by further refining the integration methods and using higher strain rates in the analyses, the discrepancies between the predicted and experimental results should be significantly reduced.

6.8 Summary

The polymer constitutive equations and the composite micromechanics model have been implemented into the explicit finite element code LS-DYNA. The analytical equations described in previous chapters were converted into an incremental format. Verification studies were conducted on the PEEK thermoplastic and the AS4/PEEK composite studied in previous chapters. The stresses predicted in the inelastic range of the deformation response were somewhat overpredicted compared to experimental results and results computed using stand-alone computer codes. Possible explanations for the discrepancies were identified and discussed. The method used to integrate the rate equations was found to have a significant effect on the accuracy of the results. Future work will concentrate on improving the integration methods used in converting the rate equations into an incremental form. In addition, methods of improving the boundary conditions applied when studying off-axis composite laminates will be considered. Furthermore, once high strain rate data are obtained, characterization studies and analyses will be conducted using this data. Since LS-DYNA was designed to be used at higher strain rates, analyses conducted at high strain should compare more favorably to the experimental data.

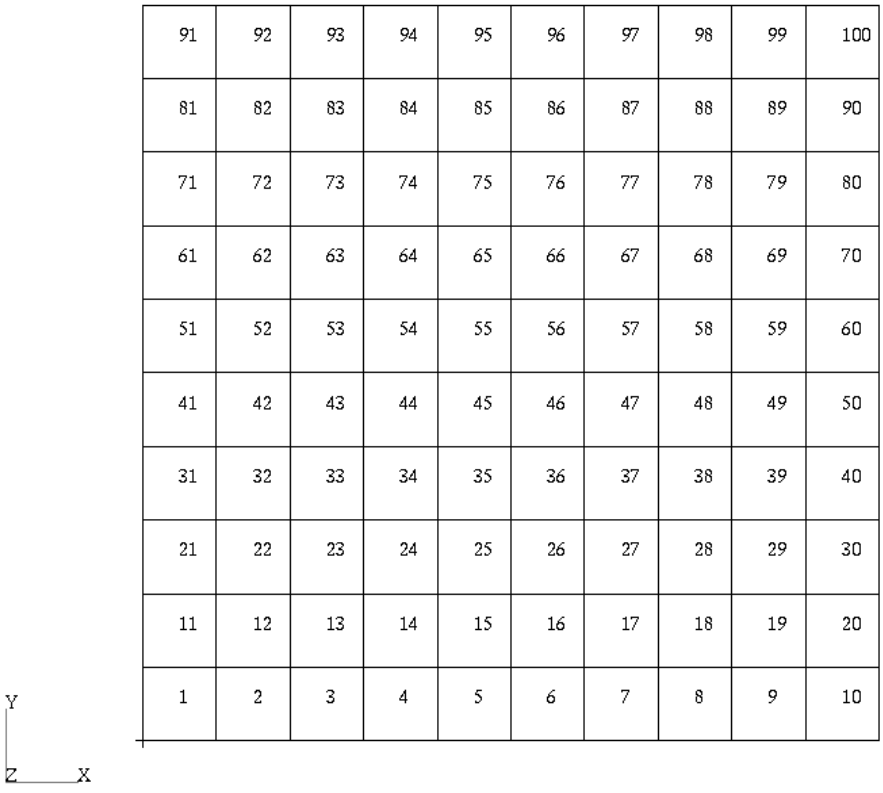

Figure 6.1: Finite Element Model Used for Verification Analyses

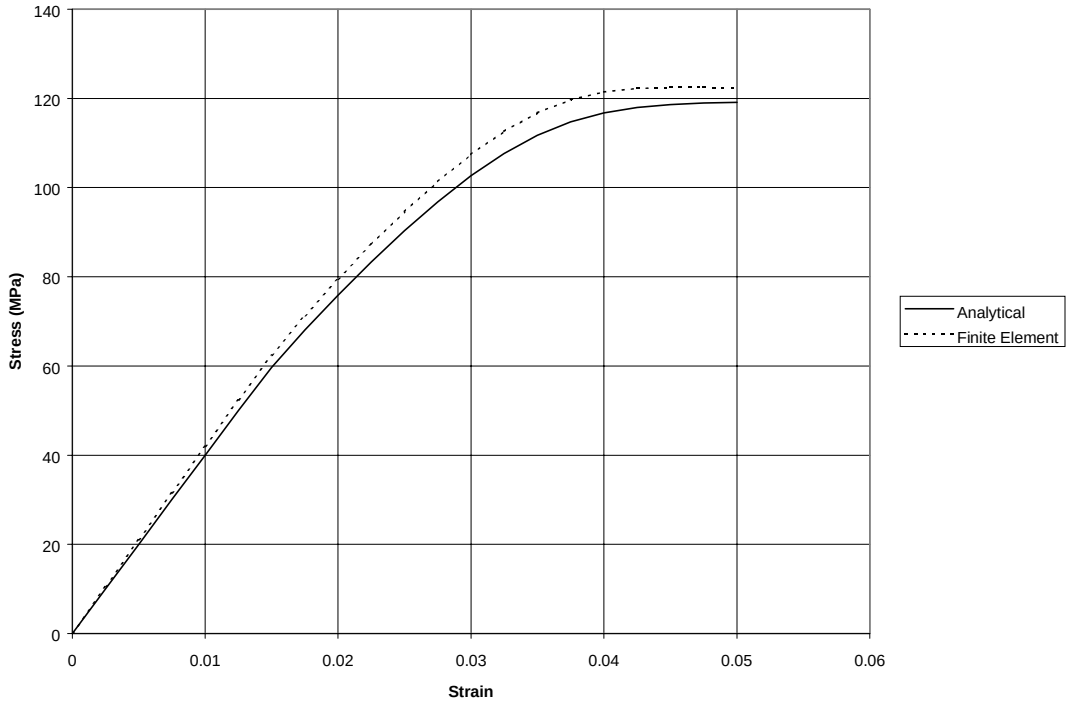

Figure 6.2: Finite Element Predictions for PEEK at Strain Rate of 0.1 /sec

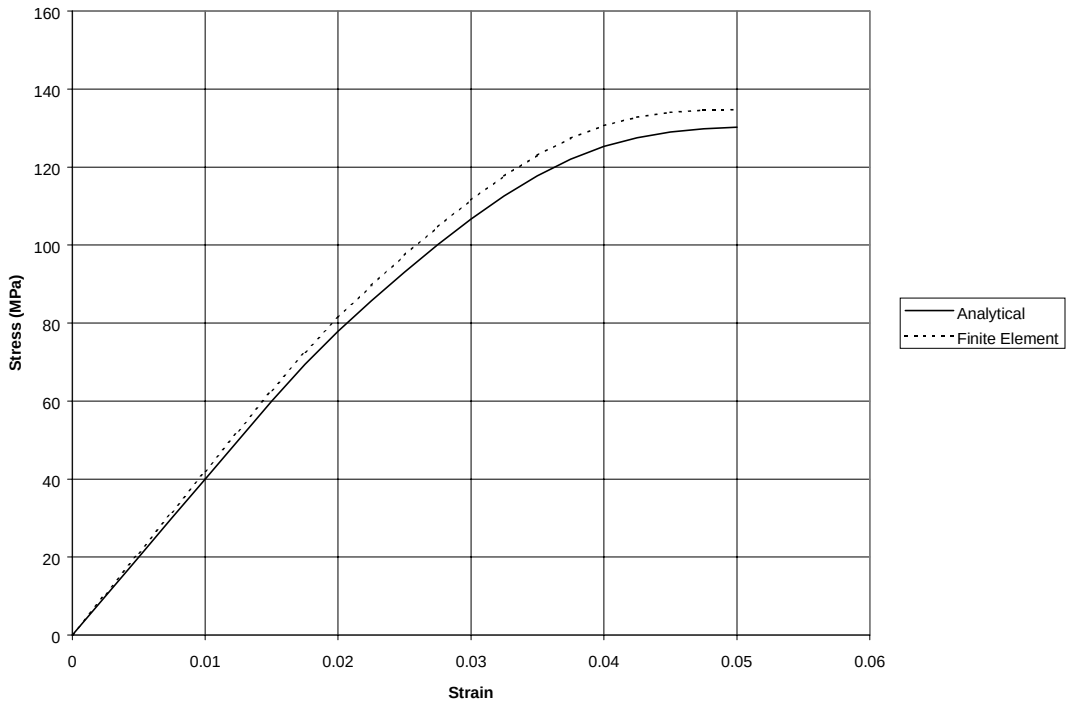

Figure 6.3: Finite Element Predictions for PEEK at Strain Rate of 1.0 /sec

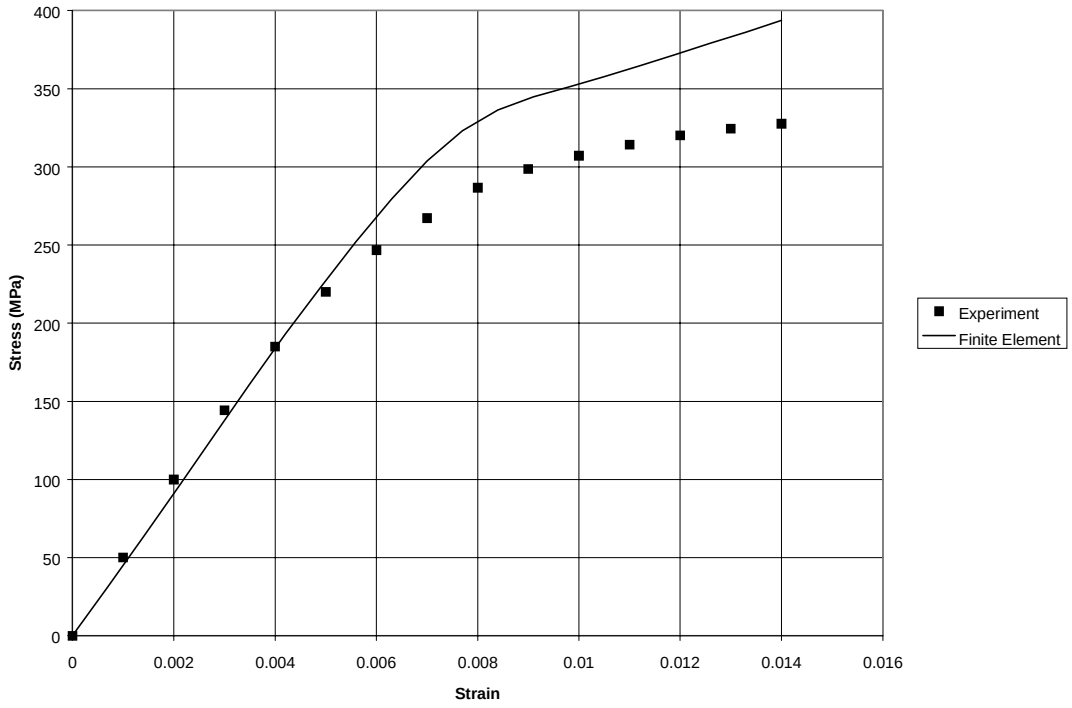

Figure 6.4: Finite Element Predictions for AS4/PEEK [15°] Laminate at Strain Rate of 0.1 /sec

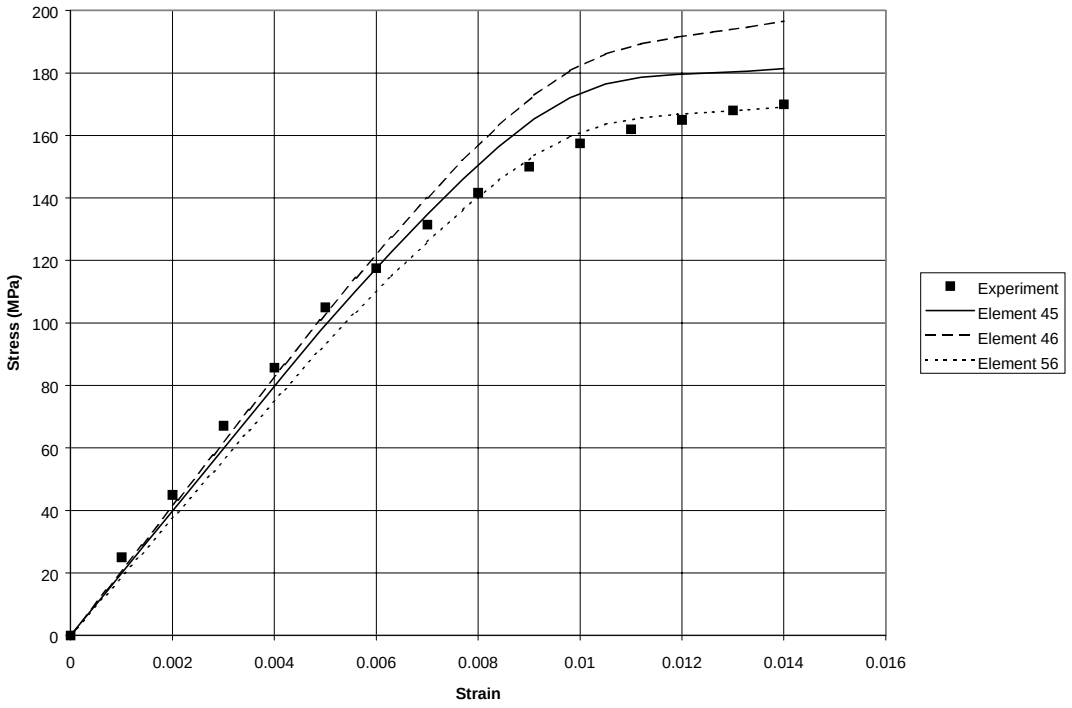

Figure 6.5: Finite Element Predictions for AS4/PEEK [30°] Laminate at Strain Rate of 0.1 /sec

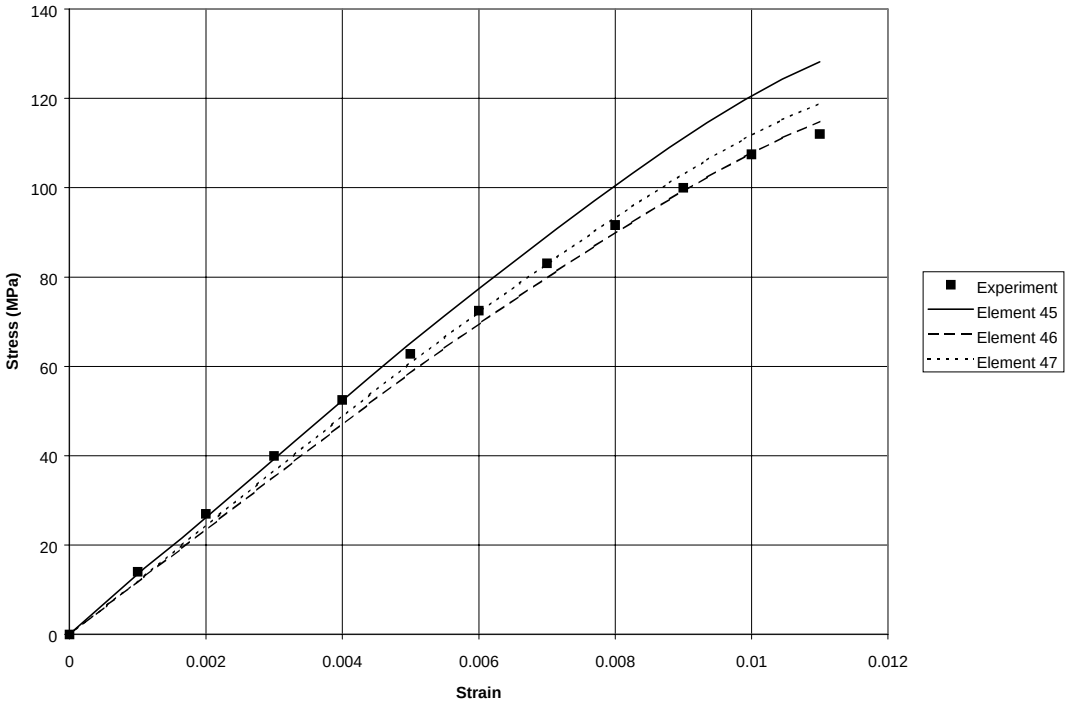

Figure 6.6: Finite Element Predictions for AS4/PEEK [45°] Laminate at Strain Rate of 0.1 /sec

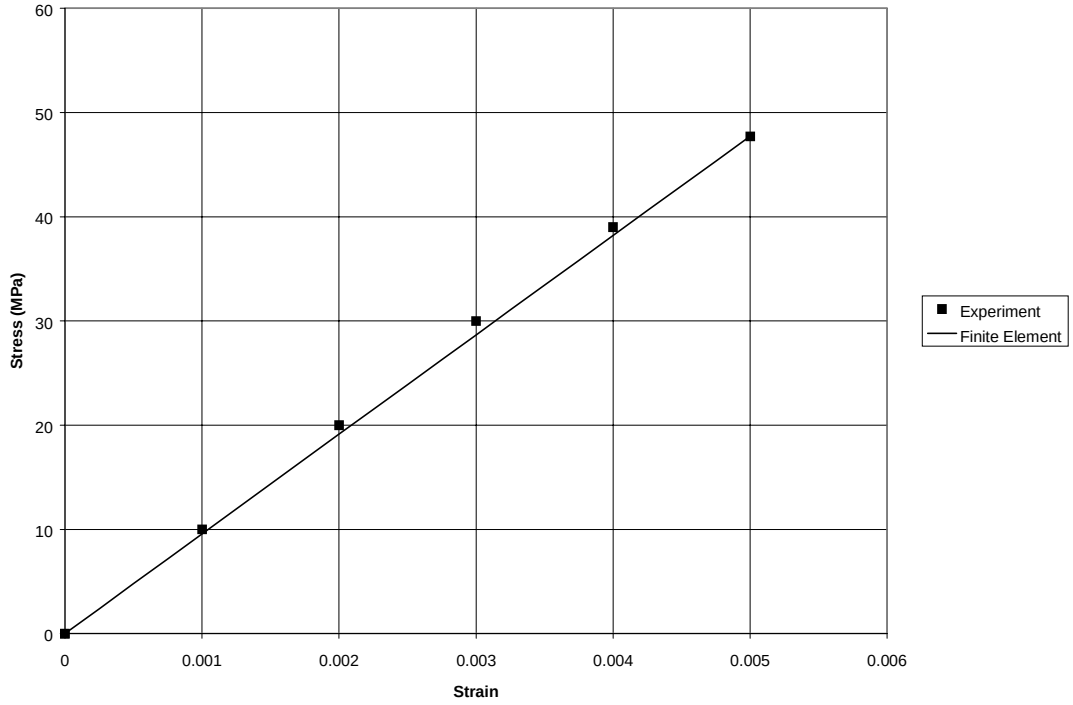

Figure 6.7: Finite Element Predictions for AS4/PEEK [90°] Laminate at Strain Rate of 0.1 /sec

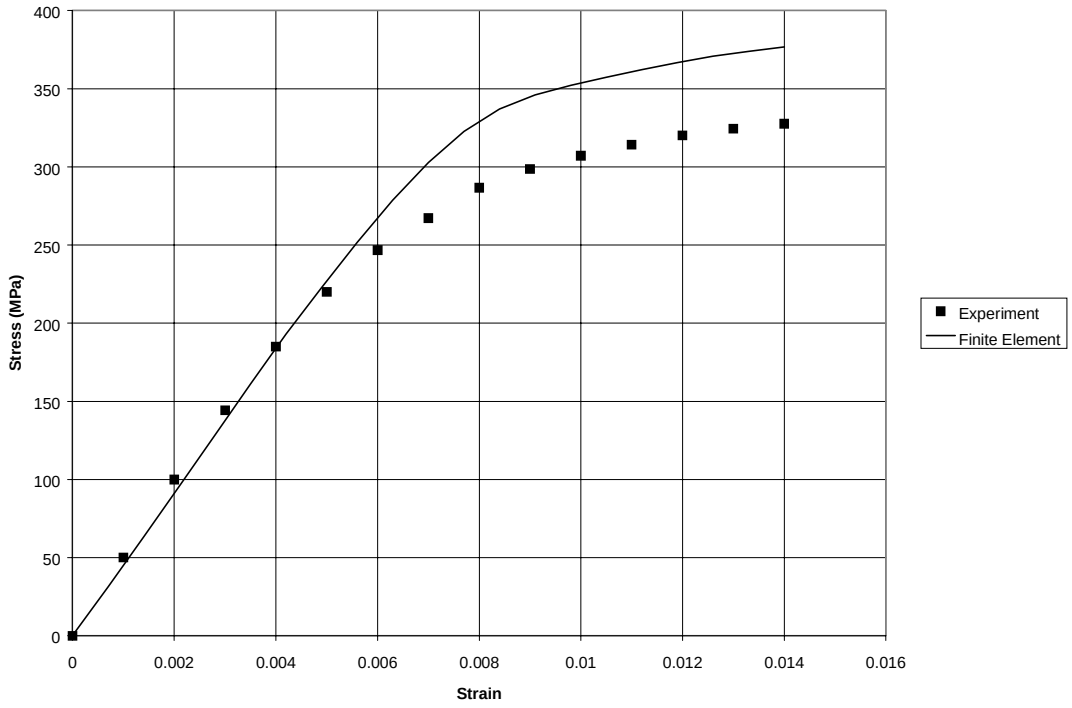

Figure 6.8: Finite Element Predictions for AS4/PEEK [15°] Laminate at Strain Rate of 0.1 /sec with Revised Equation Formulation

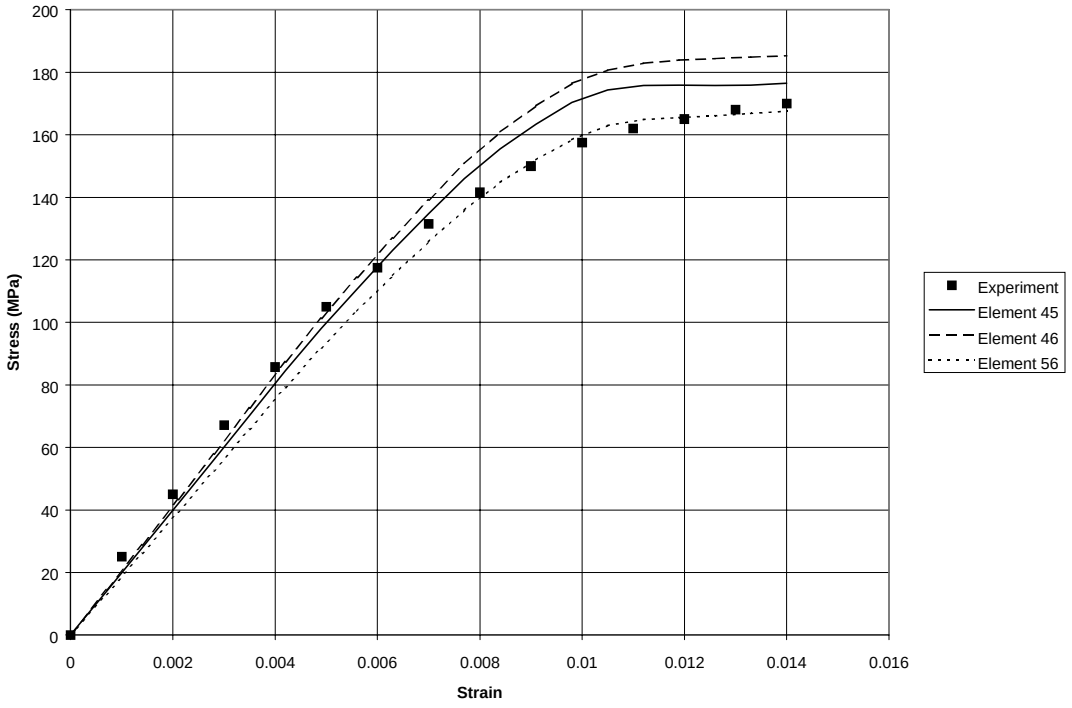

Figure 6.9: Finite Element Predictions for AS4/PEEK [30°] Laminate at Strain Rate of 0.1 /sec with Revised Equation Formulation

CHAPTER 7
SUMMARY AND CONCLUSIONS

A rate dependent deformation and strength model for polymer matrix composites has been developed which accounts for material nonlinearities. The deformation model has also been implemented into a transient dynamic finite element code. The goal of this research was to develop preliminary models that would provide insight into the analytical methods required to conduct detailed simulations of polymer matrix composites subject to high strain rate impact. In this chapter, a general summary of the work presented in this report will be given, along with a discussion of future work.

7.1 Summary

Rate dependent, inelastic constitutive equations based on the Ramaswamy-Stouffer state variable equations were formulated and implemented numerically to model the nonlinear deformation of ductile, crystalline (or semi-crystalline) polymers. While the Ramaswamy-Stouffer equations were originally developed to simulate the response of metals above about one-half of the melting temperature, appropriate modifications were made to the model in order to analyze the response of polymers. For example, the effects of hydrostatic pressure on the inelastic response were accounted for by modifying the effective stress definition in the flow law. Specifically, the shear terms in the effective stress were modified to model the effect of hydrostatic stresses on the deformation response. Correlation studies were conducted using two representative polymeric materials, Fiberite 977-2 and PEEK, and good correlation between the computed deformation response and experimental values was obtained.

A mechanics of materials based micromechanics technique was developed and numerically implemented to predict the effective deformation response of a composite with a nonlinear, rate dependent matrix constituent. The effective response of the composite was computed based on the response of the individual constituents. The fibers were assumed to be linearly elastic, and the polymer matrix was analyzed using the constitutive equations described above. To formulate the micromechanics equations, uniform stress and uniform strain assumptions were applied to a composite unit cell. The effective stresses in the composite unit cell were computed given the effective strains. Constituent level stresses in the fiber and matrix were also calculated, along with the effective inelastic strains. Verification studies were conducted using two polymer matrix composites, IM7/977-2 and AS4/PEEK. Analyses were conducted on these materials for a variety of fiber orientations and strain rates. The predicted results compared well to experimentally obtained stress-strain curves.

To predict the ultimate strength of a composite ply, which is a necessary step in the development of full failure and penetration models for a polymer matrix composite under high strain rate impact, the Hashin failure criteria were implemented into the composite micromechanics equations. In the Hashin criteria, local failure mechanisms such as fiber failure or matrix cracking were approximated based on ply level stresses and strengths. Ply ultimate strengths were predicted for the two composites considered in the earlier analyses, and the results were compared to experiment. Even though some approximations were required in determining the ply strengths for the AS4/PEEK material, for both materials the comparison between the

predicted ply strengths and the experimental values were very good for a variety of fiber orientations and strain rates.

The polymer constitutive equations and the composite micromechanics deformation model were implemented into LS-DYNA, a transient dynamic explicit finite element code. The user defined material subroutine option was used in implementing the equations into LS-DYNA. To conform to the requirements of LS-DYNA, the equations were converted into an incremental format. Given strain increments, increments in stress, internal stress and inelastic strain were computed. The implementation of the deformation model was carried out by analyzing the PEEK thermoplastic and AS4/PEEK composite considered earlier. The results computed for the pure polymer by finite element analysis compared reasonably well to stress-strain curves computed using a stand-alone computer code, with some overprediction of the stresses in the inelastic range of the deformation response. The stress-strain curves generated by finite element analysis for the AS4/PEEK composite compared quite well to experimental values in the elastic range. In the inelastic range, the stresses were generally overpredicted, and the analysis displayed some instability after "saturation" was reached. Further analyses indicated that the integration method used to implement the incremental form of the polymer constitutive equations likely was a significant cause of the discrepancies, as refining the integration technique led to improvements in the calculation of the inelastic stresses. The low strain rates at which the analyses were carried out most likely also contributed to inaccuracies in the finite element calculations.

7.2 Future Work

As mentioned earlier, the overall goal of this research was to develop preliminary deformation and strength models that would provide insight into the analytical methods required to conduct detailed simulations of polymer matrix composites subject to high strain rate impact. As a result of this study, several areas of research were indicated as future steps in accomplishing the overall goal. First of all, the polymer constitutive equations will be revised in order to represent the physical mechanisms more accurately, particularly the dependence of the deformation response on the hydrostatic stress. Furthermore, the equations will be modified so that the deformation during unloading can be predicted by the model. The constitutive model will also be extended into the large deformation domain. Finally, more sophisticated integration methods will be utilized in the numerical implementation of the model in order to improve the robustness of the calculations.

A lamination theory will be incorporated into the composite micromechanics equations, to allow for the analysis of full composite laminates. The model will also be modified to allow for the analysis of woven composites, as these types of composites are more likely to be used in fan containment applications. Finally, the micromechanics will also be extended into the large deformation regime.

The ply strength model will be extended to allow for the full penetration and failure analysis of composite laminates. A property degradation model will also be incorporated into the failure calculations in order to allow for the gradual reduction of material properties during impact penetration. In addition, the developed methods will also be modified to allow for the analysis of woven composites.

All of the modifications mentioned above will be implemented into LS-DYNA through modification of the user defined material subroutine. Furthermore, the methods used to develop incremental forms of the constitutive equations will be modified in order to improve the stability and accuracy of the finite element calculations. The developed penetration and failure models will also be implemented into LS-DYNA as part of this process.

High strain rate Hopkinson bar tests will be conducted on representative materials, and the constitutive equations will be characterized and validated for high strain rate conditions. High strain rate impact tests will then be conducted on laminated and woven polymer matrix composites. The impact tests will then be simulated using finite element analyses. The ultimate goal of this research is to be able to accurately simulate the high strain rate impact of polymer matrix composites. Once this goal is accomplished, new and improved design tools will thus be available which can help engineers design structures subject to high rate loading such as aircraft engine fan containment systems.

REFERENCES

1. Harding, J. and Welsh, L.M., "A Tensile Testing Technique for Fiber Reinforced Composites at Impact Rates of Strain", Journal of Materials Science, Vol. 18, pp. 1810–1826, 1983.

2. Staab, G.H. and Gilat, A., "High Strain Rate Response of Angle-Ply Glass/Epoxy Laminates", Journal of Composite Materials, Vol. 29, pp. 1308–1320, 1995.

3. Choe, G.H., Finch, W.W. Jr., and Vinson, J.R., "Compression Testing of Composite Materials at High Strain Rates", Proceedings of the Fourth Japan-U.S. Conference on Composite Materials, Technomic Publishing Co., Lancaster, PA, pp. 82–91, 1988.

4. Nicholas, T., "Material Behavior at High Strain Rates", Impact Dynamics, J. Zukas, T. Nicholas, H. Swift, L. Greszczuk, and D. Curran, eds., Krieger Publishing Co., Malabar, FL, pp. 277–332, 1992.

5. Harding, J., "The High Speed Punching Behavior of Woven-Roving Glass-Reinforced Composites", Proceedings of the Conference on Mechanical Properties at High Rates of Strain, Inst. Phys. Conf. Ser. No. 47, Institute of Physics, Bristol, England, pp. 318–330, 1979.

6. Daniel, I.M., Hsiao, H.M., and Cordes, R.D., "Dynamic Response of Carbon/Epoxy Composites", High Strain Rate Effects on Polymer, Metal and Ceramic Matrix Composites and Other Advanced Materials, AD–Vol. 48, Y.D.S. Rajapakse and J.R. Vinson, eds., ASME, pp. 167–177, 1995.

7. Daniel, I.M., Hamilton, W.G., and LaBedz, R.H., "Strain Rate Characterization of Unidirectional Graphite/Epoxy Composite", Composite Materials: Testing and Design (Sixth Conference), ASTM STP 787, I.M. Daniel, ed., American Society of Testing and Materials, pp. 393–413, 1982.

8. Al-Salehi, F.A.R., Al-Hassani, S.T.S., and Hinton, M.J., "An Experimental Investigation into the Strength of Angle Ply GRP Tubes under High Rates of Loading", Journal of Composite Materials, Vol. 23, pp. 288–305, 1989.

9. Groves, S.E., Sanchez, R.J., Lyon, R.E., and Brown, A.E., "High Strain Rate Effects for Composite Materials", Composite Materials: Testing and Design (Eleventh Volume), ASTM STP 1206, E.T. Camponeschi, Jr., ed., American Society of Testing and Materials, pp. 162–176, 1993.

10. Rosen, S.L., Fundamental Principals of Polymer Materials, John Wiley and Sons, New York, 1982.

11. Cessna, L.C. Jr. and Sternstein, S.S., "Viscoelasticity and Plasticity Considerations in the Fracture of Glasslike High Polymers", Fundamental Phenomena in the Material Sciences, 4, Fracture of Metals, Polymers and Glasses, L.J. Broutman, J.J. Duga, and J.J. Gilman, eds., Plenum Press, New York, pp. 45, 1967.

12. Miller, E., Introduction to Plastics and Composites, Marcel Dekker, Inc., New York, 1996.

13. Ward, I.M., Mechanical Properties of Solid Polymers, John Wiley and Sons, New York, 1983.

14. Amoedo, J., "Rate-Dependent Constitutive Equations and Process Modeling of Polymer Materials", PhD Dissertation, Rensselaer Polytechnic Institute, Troy, New York, 1990.

15. Boyce, M.C., Parks, D.M., and Argon, A.S., "Large Inelastic Deformation of Glassy Polymers. Part I: Rate Dependent Constitutive Model", Mechanics of Materials, Vol. 7, pp. 15–33, 1988.

16. Hasan, O.A. and Boyce, M.C., "A Constitutive Model for the Nonlinear Viscoelastic Viscoplastic Behavior of Glassy Polymers", Polymer Engineering & Science, Vol. 35, pp. 331–344, 1995.

17. Qian, Z. and Liu, S., "Unified Constitutive Modeling from Viscoelasticity and Viscoplasticity of Polymer Matrix Composites", Proceedings of the American Society of Composites Twelfth Technical Conference, R.F. Gibson and G.M. Newaz, eds., Technomic Publishing Co., Lancaster, PA, pp. 165–174, 1997.

18. Bordonaro, C.M., "Rate Dependent Mechanical Behavior of High Strength Plastics: Experiment and Modeling", PhD Dissertation, Rensselaer Polytechnic Institute, Troy, New York, 1995.

19. Krempl, E., McMahon, J.J., and Yao, D., "Viscoplasticity Based on Overstress with a Differential Growth Law for the Equilibrium Stress", Mechanics of Materials, Vol. 5, pp. 35, 1986.

20. Valisetty, R.R. and Teply, J.L., "Overall Instantaneous Viscoplastic Properties of Composites", Journal of Composite Materials, Vol. 26, pp. 1708–1724, 1992.

21. Zhang, C. and Moore, I.D., "Nonlinear Mechanical Response of High Density Polyethylene. Part II: Uniaxial Constitutive Model", Polymer Engineering & Science, Vol. 37, pp. 414–420, 1997.

22. Ward, I.M. and Hadley, D.W., An Introduction to the Mechanical Properties of Solid Polymers, John Wiley and Sons, New York, 1993.

23. Ward, I.M., "Review: The Yield Behavior of Polymers", Journal of Materials Science, Vol. 6, pp. 1397–1417, 1971.

24. Stouffer, D.C. and Dame, L.T., Inelastic Deformation of Metals. Models, Mechanical Properties and Metallurgy, John Wiley and Sons, New York, 1996.

25. Weeks, C.A. and Sun, C.T., "Nonlinear Rate Dependence of Thick-Section Composite Laminates", High Strain Rate Effects on Polymer, Metal and Ceramic Matrix Composites and Other Advanced Materials, AD–Vol. 48, Y.D.S. Rajapakse and J.R. Vinson, eds., ASME, pp. 81–95, 1995.

26. Yoon, K.J. and Sun, C.T., "Characterization of Elastic-Viscoplastic Properties of an AS4/PEEK Thermoplastic Composite", Journal of Composite Materials, Vol. 25, pp. 1277–1296, 1991.

27. Gates, T.S. and Sun, C.T., "Elastic/Viscoplastic Constitutive Model for Fiber Reinforced Thermoplastic Composites", AIAA Journal, Vol. 29, pp. 457–463, 1991.

28. Thiruppukuzhi, S.V. and Sun, C.T., "A Viscoplasticity Model for High Strain Rate Characterization of Polymeric Composites", Proceedings of the American Society of Composites Twelfth Technical Conference, R.F. Gibson and G.M. Newaz, eds., Technomic Publishing Co., Lancaster, PA, pp. 450–459, 1997.

29. Espinosa, H.D., Lu, H.C., Dwivedi, S.K., and Zavattieri, P.D., "A Finite Deformation Anisotropic Plasticity Model for Fiber Reinforced Composites", Proceedings of the American Society of Composites Twelfth Technical Conference, R.F. Gibson and G.M. Newaz, eds., Technomic Publishing Co., Lancaster, PA, pp. 429–441, 1997.

30. O'Donoghue, P.E., Anderson, C.E. Jr., Friesenhahn, G.J., and Parr, C.H., "A Constitutive Formulation for Anisotropic Materials Suitable for Wave Propagation Computer Programs", Journal of Composite Materials, Vol. 26, pp. 1860–1884, 1992.

31. Tay, T.E., Ang, H.G., and Shim, V.P.W., "An Empirical Strain Rate-Dependent Constitutive Relationship for Glass-Fibre Reinforced Epoxy and Pure Epoxy", Composite Structures, Vol. 33, pp. 201–210, 1995.

32. Aboudi, J., Mechanics of Composite Materials: A Unified Micromechanical Approach, Elsevier, New York, 1991.

33. Agarwal, B.D. and Broutman, L.J., Analysis and Performance of Fiber Composites, John Wiley and Sons, New York, 1990.

34. Gibson, R.F., Principles of Composite Material Mechanics, Mc-Graw Hill, New York, 1994.

35. Christensen, R.M., Mechanics of Composite Materials, John Wiley & Sons, New York, 1979.

36. Hyer, M.W., Stress Analysis of Fiber-Reinforced Composite Materials, Mc-Graw Hill, New York, 1998.

37. Murthy, P.L.N. and Chamis, C.C., "Integrated Composite Analyzer (ICAN): Users and Programmers Manual", NASA TP–2515, National Aeronautics and Space Administration, 1986.

38. Benveniste, Y., "A New Approach to the Application of Mori-Tanaka's Theory in Composite Materials", Mechanics of Materials, Vol. 6, pp. 147–157, 1987.

39. Goldberg, R.K. and Hopkins, D.A., "Application of the Boundary Element Method to the Micromechanical Analysis of Composite Materials", Computers and Structures, Vol. 56, pp. 721–731, 1995.

40. Lerch, B.A., Melis, M.E., and Tong, M., "Experimental and Analytical Analysis of Stress-Strain Behavior in a $[90°/0°]_{2s}$ SiC/Ti-15-3 Laminate", NASA TM–104470, National Aeronautics and Space Administration, 1991.

41. Walker, K.P., Jordan, E.H., and Freed, A.D., "Equivalence of Green's Function and the Fourier Series Representation of Composites with Periodic Microstructure", Micromechanics and Inhomogeneity-The Toshira Mura 65^{th} Anniversary Volume, G.J. Weng, M. Taya and H. Abé, eds., Springer, New York, pp. 535–558, 1990.

42. Walker, K.P., Freed, A.D., and Jordan, E.H., "Microstress Analysis of Periodic Composite", Composites Engineering, Vol. 1, pp. 29–40, 1991.

43. Espinosa, H.D., Emore, G., and Xu, Y., "High Strain Rate Behavior of Composites with Continuous Fibers", High Strain Rate Effects on Polymer, Metal and Ceramic Matrix Composites and Other Advanced Materials, AD-Vol. 48, Y.D.S. Rajapakse and J.R. Vinson, eds., ASME, pp. 7–18 1995.

44. Clements, B.E., Johnson, J.N., and Hixson, R.S., "Stress Waves in Composite Materials", Physical Review E, Vol. 54, pp. 6876–6888, 1996.

45. Aidun, J.R. and Addessio, F.L., "An Enhanced Cell Model with Nonlinear Elasticity", Journal of Composite Materials, Vol. 30, pp. 248–280, 1996.

46. Nahas, M.N., "Survey of Failure and Post-Failure Theories of Laminated Fiber-Reinforced Composites", Journal of Composite Technology and Research, Vol. 8, pp. 138–153, 1986.

47. Herakovich, C.T., Mechanics of Fibrous Composites, John Wiley and Sons, New York, 1998.

48. Reddy, J.N., and Pandey, A.K., "A First-Ply Failure Analysis of Composite Laminates", Computers and Structures, Vol. 25, pp. 371–393, 1987.

49. Sun, C.T. and Quinn, B.J., "Evaluation of Failure Criteria Using Off-Axis Laminate Specimens", Proceedings of the American Society for Composites Ninth Technical Conference, T.-W. Chou and J.R. Vinson, eds., Technomic Publishing Co., Lancaster, PA, 1994.

50. Hashin, Z., "Failure Criteria for Unidirectional Fiber Composites", Journal of Applied Mechanics, Vol. 47, pp. 329–334, 1980.

51. Chang, F.-K., Scott, R.A., and Springer, G.S., "Failure Strength of Nonlinearly Elastic Composite Laminates Containing a Pin Loaded Hole", Journal of Composite Materials, Vol. 18, pp. 464–477, 1984.

52. Chang, F.-K. and Chang, K.-Y., "Post-Failure Analysis of Bolted Composite Joints in Tension or Shear-Out Mode Failure", Journal of Composite Materials, Vol. 21, pp. 809–833, 1987.

53. Chang, F.K. and Chang, K.-Y., "A Progressive Damage Model for Laminated Composites Containing Stress Concentrations", Journal of Composite Materials, Vol. 21, pp. 834–855, 1987.

54. Yen, C.-F., "Analysis of Impact Damage Progression in Composite Structures", Proceedings of the 5th International LS-DYNA Users Conference, Southfield, MI, 1998.

55. Banerjee, R., "Numerical Simulation of Impact Damage in Composite Laminates", Proceedings of the American Society for Composites Seventh Technical Conference, H.T. Hahn, ed., Technomic Publishing Co., Lancaster, PA, 1992.

56. Rotem, A., "Prediction of Laminate Failure with the Rotem Failure Criterion", Composites Science and Technology, Vol. 58, pp. 1083–1094, 1998.

57. Tabiei, A., Yiang, Y., and Simitses, G.J., "Compressive Behavior of Moderately Thick Plates with Progressive Damage", Mechanics of Composite Materials and Structures, Vol. 4, pp. 281–295, 1997.

58. Langlie, S. and Cheng, W., "Numerical Simulation of High Velocity Impact on Fiber-Reinforced Composites", ASME Pressure Vessels and Piping Division (Publication) PVP., ASME, Vol. 159, pp. 51–64, 1989.

59. Pecknold, D.A. and Rahman, S., "Application of a New Micromechanics-Based Homogenization Technique for Nonlinear Compression of Thick-Section Laminates", Compression Response of Composite Structures, ASTM STP 1185, S.E. Groves and A.L. Highsmith, eds., American Society for Testing and Materials, pp. 34–54, 1994.

60. Saleeb, A.F. and Arnold, S.M., "A General Reversible Hereditary Constitutive Model: Part I-Theoretical Developments", NASA TM–107493, National Aeronautics and Space Administration, 1997.

61. Bodner, S.R., "Review of a Unified Elastic-Viscoplastic Theory", Unified Constitutive Equations for Creep and Plasticity, A.K. Miller, ed., Elsevier, Barking, Essex, England, 1987.

62. Rocca, D.P. and Sherwood, J.A., "Impact of Steel Projectiles into Thin Polycarbonate Lenses using a Unified State Variable Constitutive Model with Failure in LS-DYNA", Proceedings of the 5th International LS-DYNA Users Conference, Southfield, MI, 1998.

63. Stouffer, D.C. and Bodner, S.R., "A Relationship Between Theory and Experiment for a State Variable Constitutive Equation", Mechanical Testing for Deformation Model Development, ASTM STP 765, R.W. Rohde and J.C. Swearengen, eds., American Society of Testing and Materials, pp. 239–250, 1982.

64. Walker, K.P., "Research and Development Program for Nonlinear Structural Modeling with Advanced Time-Temperature Dependent Constitutive Relationships", NASA CR–165533, National Aeronautics and Space Administration, 1981.

65. Kreyszig, E., Advanced Engineering Mathematics, 7th Edition, John Wiley and Sons, New York, 1992.

66. Almen, G.R., Byrens, R.M., MacKenzie, P.D., Maskell, R.K, McGrail, P.T., and Sefton, M.S., "977 - A Family of New Toughened Epoxy Resins", 34th International SAMPE Symposium, pp. 259–270, 1989.

67. Gieseke, B., Private Communication, Cincinnati Testing Laboratories, Inc., 1997.

68. Bordonaro, C.M. and Krempl, E., "The Rate-Dependent Mechanical Behavior of Plastics: A Comparison Between 6/6 Nylon, Polyetherimide and Polyetheretherketone", Use of Plastics and Plastic Composites: Materials and Mechanics Issues, MD–Vol. 46, V.K. Stokes, ed., ASME, pp. 43–56, 1993.

69. Arnold, S.M., Pindera, M.-J., and Wilt, T.E., "Influence of Fiber Architecture on the Elastic and Inelastic Response of Metal Matrix Composites", NASA TM–106705. National Aeronautics and Space Administration, 1995.

70. Sun, C.T. and Chen, J.-L., "A Micromechanical Model for Plastic Behavior of Fiber Composites", Composites Science and Technology, Vol. 40, pp. 115–129, 1991.

71. Robertson, D.D. and Mall, S., "Micromechanical Relations for Fiber-Reinforced Composites Using the Free Transverse Shear Approach", Journal of Composites Technology and Research, Vol. 15, pp. 181–192, 1993.

72. Robertson, D.D. and Mall, S., "Micromechanical Analysis for Thermoviscoplastic Behavior of Unidirectional Fiber Composites", Composites Science and Technology, Vol. 50, pp. 483–496, 1994.

73. Robertson, D.D. and Mall, S., “A Non-Linear Micromechanics-Based Analysis of Metal-Matrix Composite Laminates”, Composites Science and Technology, Vol. 52, pp. 319–331, 1994.

74. Pindera, M.-J. and Bednarcyk, B.A., “An efficient implementation of the generalized method of cells for unidirectional, multi-phased composites with complex microstructures”, Composites: Part B, Vol. 30, pp. 87–105, 1999.

75. Paley, M. and Aboudi, J., “Micromechanical Analysis of Composites by the Generalized Method of Cells Model”, Mechanics of Materials, Vol. 14, pp. 127–139, 1992.

76. MathSoft, Inc., “MATHCAD, Version 6.0, User’s Guide”, MathSoft, Inc., 1995

77. Gates, T.S., Chen, J.-L., and Sun, C.T., “Micromechanical Characterization of Nonlinear Behavior of Advanced Polymer Matrix Composites”, Composite Materials: Testing and Design (Twelfth Volume), ASTM STP 1274, R.B. Deo and C.R. Saff, eds., American Society of Testing and Materials, pp. 295–319, 1996.

78. Daniel, I.M. and Ishai, O., Engineering Mechanics of Composite Materials. Oxford University Press, New York, 1994.

79. Murthy, P.L.N., Ginty, C.A., and Sanfeliz, J.G., “Second Generation Integrated Composite Analyzer (ICAN) Computer Code”, NASA TP–3290, National Aeronautics and Space Administration, 1993.

80. Smith, D.L. and Dow, M.B., “Properties of Three Graphite/Toughened Epoxy Resin Composites”, NASA TP–3102, 1991.

81. Coquill, S.L. and Adams, D.F., “Mechanical Properties of Several Neat Polymer Matrix Materials and Unidirectional Carbon Fiber-Reinforced Composites”, NASA CR–18105, 1989.

82. Livermore Software Technology Company, “LS-DYNA User’s Manual, Version 940”, Livermore Software Technology Company, Livermore, CA, 1997.

REPORT DOCUMENTATION PAGE

Form Approved
OMB No. 0704-0188

1. AGENCY USE ONLY (*Leave blank*)	2. REPORT DATE	3. REPORT TYPE AND DATES COVERED
	December 1999	Technical Memorandum

4. TITLE AND SUBTITLE

Strain Rate Dependent Deformation and Strength Modeling of a Polymer Matrix Composite Utilizing a Micromechanics Approach

5. FUNDING NUMBERS

WU–523–24–13–00

6. AUTHOR(S)

Robert K. Goldberg

7. PERFORMING ORGANIZATION NAME(S) AND ADDRESS(ES)

National Aeronautics and Space Administration
John H. Glenn Research Center at Lewis Field
Cleveland, Ohio 44135–3191

8. PERFORMING ORGANIZATION REPORT NUMBER

E–12046

9. SPONSORING/MONITORING AGENCY NAME(S) AND ADDRESS(ES)

National Aeronautics and Space Administration
Washington, DC 20546–0001

10. SPONSORING/MONITORING AGENCY REPORT NUMBER

NASA TM—1999-209768

11. SUPPLEMENTARY NOTES

This report was submitted as a dissertation in partial fulfillment of the requirements for the degree Doctor of Philosophy to the College of Engineering, University of Cincinnati, Cincinnati, Ohio, 1999. Responsible person, Robert K. Goldberg, organization code 5920, (216) 433–3330.

12a. DISTRIBUTION/AVAILABILITY STATEMENT

Unclassified - Unlimited
Subject Category: 24 Distribution: Nonstandard

This publication is available from the NASA Center for AeroSpace Information, (301) 621–0390.

12b. DISTRIBUTION CODE

13. ABSTRACT ***(Maximum 200 words)***

Potential gas turbine applications will expose polymer matrix composites to very high strain rate loading conditions, requiring an ability to understand and predict the material behavior under extreme conditions. Specifically, analytical methods designed for these applications must have the capability of properly capturing the strain rate sensitivities and nonlinearities that are present in the material response. The Ramaswamy-Stouffer constitutive equations, originally developed to analyze the viscoplastic deformation of metals, have been modified to simulate the nonlinear deformation response of ductile, crystalline polymers. The constitutive model is characterized and correlated for two representative ductile polymers, Fiberite 977–2 and PEEK, and the computed results correlate well with experimental values. The polymer constitutive equations are implemented in a mechanics of materials based composite micromechanics model to predict the nonlinear, rate dependent deformation response of a composite ply. Uniform stress and uniform strain assumptions are applied to compute the effective stresses of a composite unit cell from the applied strains. The micromechanics equations are successfully verified for two polymer matrix composites, IM7/977–2 and AS4/PEEK. The ultimate strength of a composite ply is predicted with the Hashin failure criteria that were implemented in the composite micromechanics model. The failure stresses of the two composite material systems are accurately predicted for a variety of fiber orientations and strain rates. The composite deformation model is implemented in LS-DYNA, a commercially available transient dynamic explicit finite element code. The matrix constitutive equations are converted into an incremental form, and the model is implemented into LS-DYNA through the use of a user defined material subroutine. The deformation response of a bulk polymer and a polymer matrix composite are predicted by finite element analyses. The results compare reasonably well to experimental values, with some discrepancies. The discrepancies are at least partially caused by the method used to integrate the rate equations in the polymer constitutive model.

14. SUBJECT TERMS	15. NUMBER OF PAGES
Composite materials; Impact; Micromechanics; Viscoplasticity; Strain rate; Strength	87
	16. PRICE CODE: A05

17. SECURITY CLASSIFICATION OF REPORT	18. SECURITY CLASSIFICATION OF THIS PAGE	19. SECURITY CLASSIFICATION OF ABSTRACT	20. LIMITATION OF ABSTRACT
Unclassified	Unclassified	Unclassified	